Adaptive Implementation of Turbo Multi-User Detection Architectures

by

Salah Awad Al-iesawi

A thesis submitted to the School of Electrical Electronic & Computer Engineering

in partial fulfilment of the requirements for the degree of

Doctor of Philosophy

Faculty of Science, Agriculture and Engineering

Newcastle University, April 2012

Abstract

MULTI-access techniques have been adopted widely for communications in underwater acoustic channels, which present many challenges to the development of reliable and practical systems. In such an environment, the unpredictable and complex ocean conditions cause the acoustic waves to be affected by many factors such as limited bandwidth, large propagation losses, time variations and long latency, which limit the usefulness of such techniques. Additionally, multiple access interference (MAI) signals and poor estimation of the unknown channel parameters in the presence of limited training sequences are two of the major problems that degrade the performance of such technologies.

In this thesis, two different single-element multi-access schemes, interleave division multiple access (IDMA) and code division multiple access (CDMA), employing decision feedback equalization (DFE) and soft Rake-based architectures, are proposed for multi-user underwater communication applications. By using either multiplexing pilots or continuous pilots, these adaptive turbo architectures with carrier phase tracking are jointly optimized based on the minimum mean square error (MMSE) criterion and adapted iteratively by exchanging soft information in terms of Log-Likelihood Ratio (LLR) estimates with the single-user's channel decoders. The soft-Rake receivers utilize developed channel estimation and the detection is implemented using parallel interference cancellation (PIC) to remove MAI effects between users.

These architectures are investigated and applied to simulated data and data obtained from realistic underwater communication trials using off-line processing of signals acquired during sea-trials in the North Sea. The results of different scenarios demonstrate the penalty in performance as the fading induces irreducible error rates that increase with channel delay spread and emphasize the benefits of using coherent direct adaptive receivers in such reverberant channels. The convergence behaviour of the detectors is evaluated using EXIT chart analyses and issues such as the adaptation parameters and their effects on the performance are also investigated. However, in some cases the receivers with partial knowledge of the interleavers' patterns or codes can still achieve performance comparable to those with full knowledge. Furthermore, the thesis describes implementation issues of these algorithms using digital signal processors (DSPs), such as computational complexity and provides valuable guidelines for the design of real time underwater communication systems.

Acknowledgements

I would like to express my gratitude to my supervisors Dr. Charalampos Tsimenidis, Prof. Bayan Sharif and Dr. Martin Johnston for giving me the opportunity and support to complete this research. For all their valuable comments, hints, and suggestions that inspired this work remarkable I wish to express my appreciation. They have always taught me to aim for the best and I have grown to respect them; not only for their great intuition and intellect, but also, for the dedication they show to their students.

My gratitude is also extended to the School of Electrical, Electronic and Computer Engineering for giving me the opportunity to undertake this memorable learning experience. I would also like to thank my friends Mohammed, Muayad, Emad, Chintan Shah, Ammar and many others for being a lively and entertaining part of the journey. I also thank many other people, the football team and community group, who made life enjoyable at Newcastle City. I will really miss this part of my life.

I dedicate this research to my home country (IRAQ) for supporting me financially. Last but not least I would like to dedicate this work to my family and my parents, who have supported me throughout my life. I thank **Allah** for all that and all the things that have happened to me in my life.

Salah A. Al-iesawi
April 2012

Declaration

I declare that this thesis is my own work and it has not been previously submitted, either by me or by anyone else, for a degree or diploma at any educational institute, school or university. To the best of my knowledge, this thesis does not contain any previously published work, except where another person's work used has been cited and included in the list of references.

Salah A. Al-iesawi

Contents

List of Tables

List of Figures

List of Abbreviations and Symbols

List of Abbreviations

ALE	Address Latch Enable
ALU	Arithmetic Logic Unit
APP	*A Posteriori* Probability
AUV	Autonomous Underwater Vehicle
BCJR	Bahl-Cocke-Jelinek-Raviv
BPF	Bandpass Filter
BPSK	Binary Phase Shift Keying
CBC	Chip-by-Chip
CE	Channel Estimation
CIR	Channel Impulse Response
CPU	Central Processing Unit
CSI	Channel State Information

DAI	Digital Audio Interface
DEC	Decoder
DFE	Decision Feedback Equalization
DM	Data Memory
DMA	Direct Memory Access
DS-CDMA	Direct-Sequence Code Division Multiple Access
DSP	Digital Signal Processor
ENC	Encoder
EXIT	EXtrinsic Information Transfer
FB	Feedback
FDMA	Frequency Division Multiple Access
FF	Feedforward
FIR	Finite Impulse Response
FPGA	Field Programmable Gate Arrays
IC	Interference Cancellation
IDMA	Interleave Division Multiple Access
iid	Independent and identically distributed
ISI	Intersymbol Interference
LFSR	Linear Feedback Shift Register
LLR	Log-Likelihood Ratio
LLRC	Log Likelihood Ratio Combining
LMS	Least Mean Square

LPF	Lowpass Filters
MAI	Multiple Access Interference
MAP	Maximum *A posteriori* Probability
ML	Maximum Likelihood
MMSE	Minimum Mean Square Error
MRC	Maximal Ratio Combining
MUD	Multi-User Detection
NLMS	Normalised Least Mean Squares
NSC	Non-Systematic Convolutional
PBC	Peak Basis Correlation
PCG	Precision Clock Generators
PDA	Probability Data Association
PDF	Probability Density Function
PDP	Power Delay Profile
PIC	Parallel Interference Cancellation
PLL	Phase-Locked Loop
PM	Program Memory
PN	Pseudorandom
PP	Parallel Port
PS	Program Sequencer
RF	Radio Frequency
SHARC	Super Harvard Architecture

SIC	Successive Interference Cancellation
SIMD	Single Instruction and Multiple Data
SNR	Signal to Noise Ratio
SSS	Spread Spectrum System
T-MUD	Turbo Multiuser Detection
TDD	Time-division duplexing
TDL	Tapped Delay Line
TDMA	Time Division Multiple Access
TR	Time Reversal
UACs	Underwater Acoustic Channels
UWC	Underwater Communication
UWNs	Underwater Networks
VLSI	Very Large Scale Integration

List of Symbols

$(.)^H$	Hermitian transpose operator
η_k	Distortion term
$\hat{\phi}(n)$	A phase correction parameter
μ_f	Step-size for the FF filter
$\mathbf{u}_b(n)$	Contents of the FB equalizer during the n-th transmitted symbol
$\mathbf{u}_f(n)$	Contents of the FF equalizer during the n-th transmitted symbol
$x_k(n)$	n-th chip transmitted by user k

$(.)^*$	Conjugate operation
$\hat{\mathbf{w}}_b(n)$	Tap-weight vectors of the FB filters
$\hat{\mathbf{w}}_f(n)$	Tap-weight vectors of the FF filter
μ	Adaptation constant
μ_b	Step-size for the FB filter
$\phi_p(t)$	Joint effects of phase distortion
$\phi_p(t)$	Phase of the p-th arriving path
σ^2	Noise variance
$\mathbf{c}_k$	Coded bits sequence
$\mathbf{R}$	Correlation matrix
$\mathbf{r}(n)$	Received signal vector at n-th bit
$\mathbf{s}_k$	Spreading vector of the k-th user
Im{.}	Imaginary part
$\tilde{y}(n)$	Reconstructed MAI transmitted signal
$\varepsilon(n)$	Phase error measurement
a	Positive adaptation constant
A_k	Transmitted signal amplitude of the kth user
B	Signal bandwidth
B_d	Doppler spread
c	Sound velocity in m/s
$d^{I_k}(m)$	mth coded chip bits for the in-phase data streams
$d^{Q_k}(m)$	mth coded chip bits for the quadrature-phase data streams

D_k	Deinterleaver of the k-th user
d_k	Information bits of kth user
DS	Despreader
$E[.]$	Expectation operator
f_c	Carrier frequency
$h(t)$	Channel impulse response
$h_p(t)$	Magnitude of the p-th arriving path
I_k	Interleaver of the k-th user
I_L	An identity matrix with dimension L
J_{min}	Cost function corresponding to the optimal filter weights
K	Total number of users
L	Spreading length
$L_{dec}[x_k(n)]$	*A priori* information
$L_m[x_k(n)]$	Extrinsic LLRs of $x_k(n)$
M	Order of the FIR filter
M_b	Taps of the FB filter
M_f	Taps of the FF filter
N_b	Length of the information bits
P	Total number of paths
$p(t)$	Pulse shape function of the transmitted waveform
R	Channel coding rate
r	Received signal

s_k	Spreading sequence of kth user
T_c	Chip duration
$t_r(n)$	Training sequence
T_s	Symbol duration
u_h	Wave height
$Var[.]$	Variance operator
$w(t)$	Additive White Gaussian Noise (AWGN)
$y(t-\tau_p)$	Transmitted signal delayed by τ_p
$z(t)$	Bandpass received signal

CHAPTER 1

Introduction

1.1 Motivations

IN the last two decades, with the ongoing integration of electronic circuits and growing computational power, digital systems have brought great advances in the research and development of underwater acoustic technology. Such systems are of increasing interest in a wide variety of applications, such as navigation and surveillance in military, speech transmission and control of sensing equipment in deep sea fishing and environmental monitoring. For all these applications the principal function is to achieve reliable communication between various remote instruments both in point-to-point links and in network scenarios. Unfortunately, the long intersymbol interference (ISI) and the dynamic nature of the underwater acoustic channels (UACs) makes it fundamentally much more difficult than most of the radio channels.

However, in the network environment, the performance is in addition affected by the multiple-access interference (MAI) from other acoustic modems. Consequently, the performance of such network depends on the receiver's ability to work in the presence of severe interference. Research in this field has developed various system architectures for the mitigation ISI/MAI signals, and such architectures have been considered as a natural extension in the development of physical-layer systems.

1.2 Limitations and Challenges

The UAC is one of the most difficult media for data transmission, and developing reliable communications systems for this environment has proved to be very challenging. In such channels, the significant multipath phenomenon results in time spread or severe ISI, and this can extend to over 100s of transmitted symbols causing frequency selective fading and signal distortion. On the other hand, the slow propagation speed of sound introduces large Doppler spread or shifts, which causes interference among different frequency components of the signal. This problem is severe especially if significant motion, directional or random, is involved between the transmitter and the receiver. In contrast to mobile cellular communications, where a Doppler shift will cause only a rotation of the phase constellation, a Doppler shift in UACs will additionally cause compression or expansion of the received signal depending on the direction of the relative movement. Additionally, ambient and man made noise in combination with considerable propagation loss reduces the input signal-to-noise ra-

tio (SNR). Therefore, these channel characteristics restrict the range and bandwidth efficiency of underwater networks (UWNs) and consequently, the bit rate of underwater communication is severely limited [1, 2].

However, the propagation medium has strong effects on the performance and deployment of UWNs, where the severity of these characteristics depends on depth, type of water and weather conditions which seriously affect any underwater transmissions. To compensate for the resulting signal distortion, adaptive systems capable of fast tracking must be employed [3]. The situation is further worsened if multiple users are present simultaneously in both time and frequency. Therefore, designing a UWN that maximizes throughput and reliability while minimizing the power consumption becomes a very difficult task [4]. We next discuss various multiple-access architectures that have been used in underwater environments.

1.3 Multiple Access Architectures

The most commonly used techniques that allocate the channel resources to multiple users are frequency division multiple access (FDMA), time division multiple access (TDMA) and code division multiple access (CDMA). Unlike the FDMA and TDMA systems in Fig. 1.1, that divide the spectrum into different frequency bands or time slots, CDMA approach overlaps every signal on the same carrier frequency by means of a unique code which is independent of the data signal. Therefore, users in CDMA are recognized by different spreading codes; in contrast, they are separated by orthogonal time slots in TDMA, or by orthogonal frequency bands in FDMA.

The low available bandwidth of the UAC restricts the usefulness of FDMA technologies. In order to establish high rate communication between several users, the users must share the same frequency band. Further, the extended and variable propagation delay in UACs precludes the effective use of TDMA in which each time slot would be dedicated to a single user. These constraints lead to a network scenario in which communications from multiple users occur simultaneously [2]. An attractive approach is to use spread spectrum systems (SSSs), which utilize spreading codes or different interleaver patterns to differentiate between users and additionally improve immunity against multipath effects. Direct-sequence code division multiple access (DS-CDMA) or CDMA is the most popular technology of SSS. However, introducing SSSs in UWNs allows asynchronous communications at low input SNRs at the

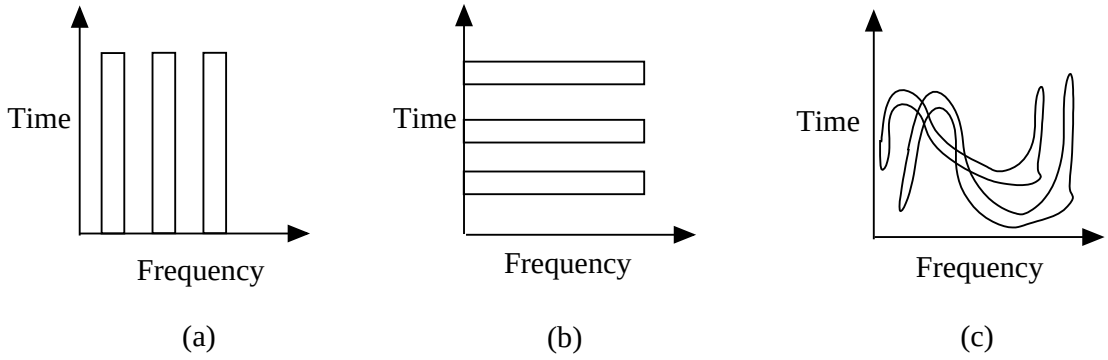

Figure 1.1: Multiple access Architectures : (a) FDMA, (b) TDMA, (c) CDMA.

expense of tracking performance and reduced data throughput in an already bandwidth limited channel. CDMA networks consist of a number of nodes and are formed by establishing two way acoustic links between various instruments. With decentralized networks, the receiver detects only the desired user's signal using knowledge of its spreading code. In contrast, communication in a centralized network scenario between the distributed nodes takes place through a central station. Therefore, the receiver is capable of detecting the data sequences from all active users in the network using knowledge of all users' codes. Hence, any node can be assigned the role of a base station, which can be used to establish a link between the central stations through a separate acoustic channel. However, many interesting spread spectrum applications may consider transmission in the same bandwidth, e.g. communication with several buoys, divers and unmanned underwater vehicles [5].

In this thesis, the objective of proposed multiuser techniques is to overcome the challenges and performance limitations induced by the highly UACs and additionally improve the bandwidth efficiency as much as possible. Towards this goal, two promising turbo receivers, a multiuser architecture with Rake reception and decision feedback equalization (DFE) based multiuser architecture are investigated. For each architecture, adaptive chip-rate equalization and synchronization are then performed. In such a way, it is possible to update the receiver parameters at the chip rate, which may be necessary for rapidly time-varying channels.

1.4 Literature Review

Based on the philosophy of code-spread CDMA [6] and chip interleaved CDMA [7], the interleave division multiple access (IDMA) and its generalization called multi-layer IDMA were developed by [8] and hence inherited many advantages of CDMA. Unlike CDMA, which uses user-specific spreading codes, IDMA employs user specific chip-interleavers, and exploits full bandwidth expansion for coding. These features facilitate chip-based detection strategies and maintain good performance with far lower complexity than the CDMA scheme proposed in [9]. In addition, multi-layer IDMA offers a high degree of adaptivity and can be considered as a joint modulation, channel coding and multiple access scheme [10]. The associated chip-by-chip IDMA algorithm is essentially a low-cost iterative cancellation technique to remove jointly both MAI and ISI. It has been shown in [8] that the algorithm can achieve near single user performance for systems with equal power control. The computational complexity of the algorithm is very low and independent of K. Therefore, these meritorious properties provided the motivation to investigate the performance of such turbo chip detectors for real channel conditions.

1.4.1 Channel Estimation Based T-MUD Architectures

T-MUDs are widely used in CDMA and IDMA systems as an attractive solution to overcome the channel impairments and MAI between users. Previous work on T-MUDs, e.g. [8] and [9], are based on the assumption that the receiver has perfect channel estimation (CE). Unfortunately, for doubly selective channels, as in UACs, proper CE becomes very difficult at low SNRs and imperfect CE can significantly degrade performance. In the context of single-user systems, the iterative soft feedback CE concept with turbo equalization of [11] was used by [12] to generate extended training symbols. The results have demonstrated performance improvement and reliable communication compared to a reference non-iterative DFE receiver. Moreover, iterative CE can provide a significant performance gain compared to the case when pilot symbols are used in a one-shot approach to estimate the channel. The use of data-multiplexed pilots was first proposed in [13] for equalizer adaptation in downlink CDMA systems and later extended in [14] to incorporate chip-fractional sampling. In [15] and [16], CE methods, MMSE and recursive least squares (RLS) algorithms,

are proposed for frequency selective fading channels. In [17] and [18], the linear equalizer combined with separate CE has been proposed and its development in [19] has investigated the impact of sparse CE on the equalization of phase coherent communication signals. Long code CDMA with orthogonal signalling has been the subject of study in [20], where the maximum likelihood (ML) CE was employed over time varying channels. By utilising pilot and traffic channels, a CE method for CDMA has been investigated in [21]. However, the limited capability of most these algorithms with time-multiplexing pilots may preclude their use in highly Doppler channels.

The use of continuous pilot aided CE was first proposed in [22], where the placement of pilot sequences were reported to significantly affect the system performance. The sequence incurs energy loss without expanding bandwidth and can be superimposed with the transmitted signal in order to measure the real and imaginary parts of the unknown channel. The sequence and energy level is known at the receiver, therefore it is possible to track the time varying channels and compensate for channel effects. For IDMA systems, different CE schemes are studied in [23] and [24], where data and training are superimposed to allow the CE and detection to be done at the same time instant. While semi-blind maximal ratio combining (MRC) CE algorithm using continuous pilot is presented in [25]. These algorithms outperform the time-multiplexing algorithms but with high complexity due to inversion of a matrix growing linearly with the number of chips per user.

1.4.2 Direct Adaptation Based T-MUD Architectures

As the channel dispersion increases, the errors in the estimated coefficients have a significant impact on the performance of Rake based receivers, where performance is limited by both MAI and ISI [26] and exhibits an error floor as reported in [27,28] due to degraded CE. Therefore, direct adaptation techniques that do not need explicit CE are more suited for such channels. The effects of ISI can be further reduced using direct adaptation of the DFE coefficients [29]. The DFE has been also successfully applied to direct SSS in [30], and the authors in [1] demonstrated the ability of DFE to achieve real-time operation and to exploit diversity offered by the multipath channel.

In addition, the receivers with symbol rate adaptation as required in SSS may not perform satisfactory in dynamic UACs, where the channel parameters' variations over symbol duration are not negligible. Therefore, it is desirable for the receiver algorithm to be able to adapt its coefficients more frequently than a symbol interval, thus offering the possibility to track unknown channel variations associated with large Doppler spreads [31]. In [3] and [32], the authors explored the use of a DFE to cancel ISI in CDMA systems, and as the symbols are relatively long, a symbol DFE is not able to track rapidly varying channels. For such channels, a chip hypothesis feedback decisions can help track the channel at the chip rate rather than the symbol rate. In [3], at the cost of increased complexity, chip level equalization in conjunction with a multichannel combiner has proven to be one of the most attractive receivers for CDMA. Two types of decision-feedback receiver are proposed based on symbol decision feedback and chip hypothesis feedback principles, and their operation in a realistic underwater acoustic system has achieved excellent results, demonstrating the possibility of supporting multiple users in a highly distorted underwater channel.

1.4.3 Analysis of T-MUDs

The task of deriving analytical expressions for turbo architectures is more complicated when the CE is involved in the turbo process. Therefore, the performance of turbo multiuser architectures is usually studied via time consuming closed-loop simulations. These simulations require a large number of frames to give meaningful results. However, it is desirable to use other approaches to better understand the operation of such architectures, especially the convergence behaviour of the turbo process. In low SNR regions, the behaviour of turbo receivers is difficult to analyse with the conventional BER chart, and the EXIT charts analysis in [33] is very useful in such regions. For the case of a known time invariant channel, the analysis is used to analyze the performance of turbo equalization in [34,35]. The benefit of using such charts to analyse iterative receivers designed for CDMA systems are presented in [36].

1.4.4 Recent Developments in UWC Systems

A review of the developments in underwater communication (UWC) and the recent advances in cancellation approaches for underwater systems were investigated in [37] and [38], respectively. Linear turbo equalizers and their practical applications in UWCs are investigated in [39, 40]. These receivers provided a good trade-off between complexity and performance for long UACs, which usually demand high computational cost. Previous work in multiuser UWC has also asserted the feasibility of coherent detection in the presence of other users. Implementation of multiuser detection strategies for coherent UWCs has been applied in [41]. In [38], the multichannel combiner is used to estimate and remove the interference signal. Based on the principles of joint channel equalization and MAI cancellation, both decentralized equalizers and their centralized equivalents are studied in [42]. In these receivers, the crossover feedback is used to cancel out the MAI effects between users by utilizing the information of the users' training sequence. In the case of CDMA networks, the bandwidth expansion not only provide immunity against multipath components, but may also take advantage of the multipath diversity by utilizing Rake filters at the receiver. In [43], CDMA systems over time-dispersive channels have been investigated, and their implementation with a Rake receiver and space diversity techniques are studied in [38]. In the presence of large time-delay spread and other channel impairments, by assuming perfect channel information, different multiple-access schemes in [44] have been tested for UWCs using simulated results. These schemes have yet to be fully studied especially for real UACs. However, the focus in most these papers was on the adaptive schemes with low complexity applicable for digital signal processors' (DSPs) implementations over long ISI channels, and multiuser modems that can operate in a network environment to meet the emerging demand for different underwater applications.

1.5 Research Contributions and Publications

This thesis examines two distinct low complexity T-MUDs for IDMA and CDMA over multipath channels. The network of interest is the cellular type of shallow water networks with single-sensor reception, addressing the transmission link between two central stations. In addition, one may also think of a multicode transmission

in CDMA [45], or a multilayer IDMA [23], where a single user is allocated several spreading codes or interleaver sequences in order to achieve higher data rates. The contributions have appeared in journals [46,47] and conference papers [48–55]. These contributions can be also summarised as follows:

- The main originality of the thesis holds in the consideration of IDMA detection methods and continuous pilots that have been rarely studied and tested in underwater environments.

- Adaptive CE with hard/soft estimation for T-MUDs is proposed using two different training pilots, time-multiplexing and continuous pilots. Based on the MMSE criterion, the adaptive algorithms are jointly optimized with carrier phase tracking and adapted iteratively to track the channel coefficients.

- With full/partial knowledge, turbo DFE-IC detector using different training methods is proposed based on the principles of direct adaptive equalization techniques. Compared to traditional Rake IDMA, the proposed scheme decouples the equalization and chip detection processes, which leads to lower complexity suited to downlink receivers.

- Since IDMA is a variation of CDMA but with long random chip interleavers, IDMA detection methods are introduced to the CDMA systems to improve system performance. Making comparisons with other work, T-MUDs of two CDMA forms using IDMA detection methods on realistic channels, are the main contributions of the proposed CDMA receivers.

- The convergence behaviour of T-MUDs is also evaluated using extrinsic information transfer (EXIT) charts. Key issues such as computational complexity are also discussed as well as the details about the hardware structures such as DSP typically used in such systems.

1.6 Thesis Outline

This thesis is divided into six Chapters, where Chapters 1 and 2 contain material of introductory and theoretical background, while Chapters 3-5 contain our major research contributions. In Chapter 2, the principles of propagation in multipath channels and the physical characteristics of the UACs are introduced to clarify the limitations and difficulties of such environment. Moreover, a brief overview of the T-MUDs is presented along with the key features of IDMA/CDMA systems. Chapter 3 is devoted to the proposed CE with Rake reception based T-MUDs. Adaptive estimation issues and carrier phase tracking of both theoretical and practical interest are also discussed. In Chapter 4, a novel DFE-IC architecture based T-MUDs is presented based on MMSE criterion. Then, the Chapter provides the principles of EXIT charts, where imperfect CE is given to the receivers. To assess the performance of the proposed techniques, extensive results of multiplexing and continuous pilots based estimation are provided using both simulation and experimental results in Chapter 5. The signal design and experimental setup are also outlined in Chapter 5, along with the impacts of different systems parameters. Then, we examine the computational cost requirements of the proposed algorithms on the ADSP-21364 processor. The hardware architecture of the processor is also given. Finally, the conclusions along with the contributions from the thesis are presented in Chapter 6, followed by a set of possible future research directions.

CHAPTER 2

Fundamental Concepts

2.1 Introduction

THIS chapter briefly reviews the UACs characteristics and the difficulties it imposes on communication signals. The chapter begins with an introduction to the propagation model and channel physics. Then, the impact of channel characteristics on the transmitted data is discussed and the differences from the terrestrial transmission are highlighted.

In addition, the chapter provides the multiuser architectures for CDMA and IDMA systems. The CDMA transmission model is presented along with the fundamental benefits of the system. Emphasis is placed on the description of optimum and suboptimum turbo CDMA architectures, and some of them will be referenced for comparison in terms of complexity in later chapters. An IDMA system with BPSK modulation is also described in this chapter. The mathematical representation of the correlation function of user-specific interleavers is also discussed along with the chip-by-chip (CBC) IDMA receiver architecture. Some insights and differences of the IDMA from other techniques will be presented and finally conclusions are drawn.

2.2 Channel Characteristics and Limitation

The acoustic signal experiences reflections from the surface and bottom as well as refraction within the water column. As illustrated in Fig. 2.1, the acoustic wave propagates along many paths from a source to a receiver. By nature, the sea surface is a time varying and randomly rough interface. Rays scattered from the surface experience a great deal of fluctuation such as variations in amplitude and propagation time as well as arrival angle. Consequently, surface rays are the dominant factor to the dynamics of the rapidly varying channel. The direct and bottom scattered arrivals usually have little surface fluctuations and are more stable. Channel physics such as scattering by bubbles and attenuation may all contribute to changes of the channel [56].

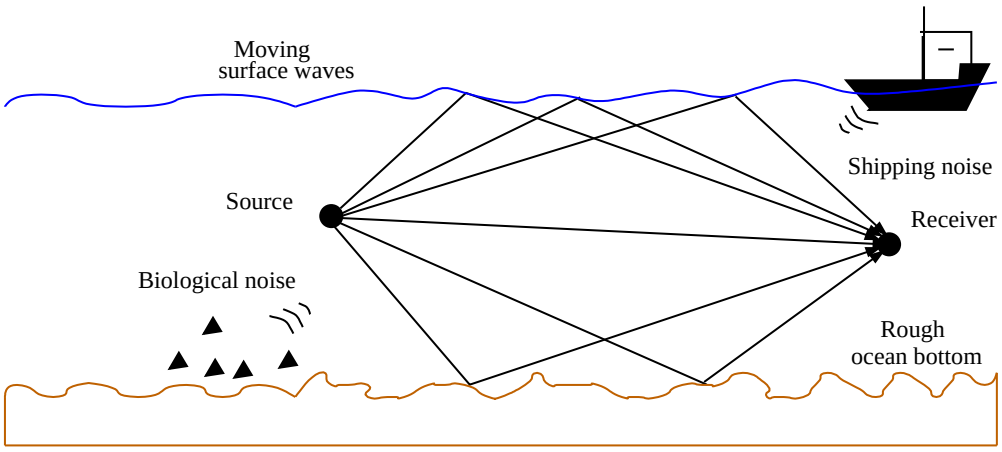

Figure 2.1: Multipath propagation structure of UACs

2.2.1 Band-limited Channel

The available bandwidth of the UAC is severely limited by the transmission loss (i.e., large scale fading). The dominant factors affecting transmission loss are spreading loss, absorption loss, and scattering loss at the sea surface and sea floor. The spreading phenomenon is caused when the signal intensity weakens and the sound expands over a larger volume. Combining the spreading loss and the absorption effects, the total signal attenuation can be expressed as [57]

$$10 \log \Lambda(r_r, f) = \kappa.10 \log r_r + r_r.10 \log \Lambda_a(f), \tag{2.1}$$

where the first term is the spreading term that defines the geometry of the propagation (i.e., κ= 1 is cylindrical, $\kappa = 2$ is spherical, and $\kappa = 1.5$ is practical spreading) and the second term represents the absorption factor that models the conversion of sound energy into heat, and can be approximated as [57, 58]

$$10 \log \Lambda_a(f) = \begin{cases} 0.11(\frac{f^2}{1+f^2}) + 44(\frac{f^2}{4100+f}) + 2.75.10^{-4}(f^2+0.003), & f >= 0.4 \\ 0.002 + 0.11(\frac{f}{1+f}) + 0.011f, & f < 0.4 \end{cases} \tag{2.2}$$

where the $\Lambda_a(f)$ is the attenuation factor in dB/km, f is the signal frequency and r_r is the distance in km.

While the spreading term increases with distance and is independent of the sound frequency, the absorption of sound by the water is highly dependent on frequency. This dependence severely limits the available bandwidth, which is in practice also limited by the transducer bandwidth. Therefore, the bandwidth increases at shorter distances and it is limited at longer distances, e.g. at 100 km the available bandwidth is only about 1 kHz. Thus, this limitation implies the need for bandwidth-efficient modulation techniques [59].

2.2.2 Non-Gaussian Noise Channel

In UACs, the noise consists of site specific noise and ambient noise. Unlike the ambient noise that exists in the background of the sea, site specific noise is present only in certain places in warm waters. There are many sources of ambient noise in the ocean and the noise nature depends strongly on its source. The common sea surface noise sources include passing ships, breaking waves, rain and turbulence. With these different sources, the total ambient noise level can vary widely. The ambient noise level $N_L(f)$ is a function of f and the following formula gives the power spectral density in dB re 1 μPa per Hz of the four major components [57]

$$N_L(f) = \begin{cases} 17 - 30\log(f), & \text{Turbulence noise} \\ 50 + 7.5{u_c}^{1/2} + 20\log(f) - 40\log(f + 0.4), & \text{Surface noise} \\ -15 + 20\log(f), & \text{Thermal noise} \\ 40 + 20(s_h - 0.5) + 26\log(f) - 60\log(f + 0.03), & \text{Shipping noise} \end{cases} \tag{2.3}$$

where $0 < s_h < 1$ is the shipping density and the wind speed u_c in m/s. Although, the ambient noise is often approximated as Gaussian and is not white, the site specific noise often contains significant non-Gaussian components [59].

Since the ambient noise decreases significantly over the frequency range, it can be used as a limit for determining the lowest frequency of the transmission bandwidth. At different frequencies, each component impacts the noise spectrum differently. Additional noise sources will probably contribute to the noise level in shallow water channels. This level experiences a large dynamic range, which varies significantly between the different seasons, the time of day, depth, location and weather. Therefore, this noisy channel has characteristics difficult to represent statistically.

2.2.3 Multipath Fading Channel

In RF channels, a number of models such as Rayleigh fading for the probability distribution and Jakes model for the power spectral density of the fading process are well accepted and even standardized. In UACs, there has been no consensus among researchers on a statistical characterization model applicable to such mediums. Experimental results suggest that some channels may as well be characterized as deterministic, while others seem to exhibit Rice or Rayleigh fading [59].

In general, the multipath fading channel is modelled using a tapped delay line (TDL) channel model as shown in Fig. 2.2. Then, the received baseband signal can be written as

$$r(t) = \sum_{p=0}^{P-1} h_p(t) y(t - \tau_p) + w(t), \tag{2.4}$$

where P is the number of paths, $w(t)$ is the additive noise and $y(t - \tau_p)$ denotes the transmitted signal delayed by τ_p. The channel impulse response (CIR) $h(t)$ is implemented as a time-varying linear filter with complex-baseband response given by [60]

$$h(t) = \sum_{p=0}^{P-1} h_p(t - \tau_p) e^{j\phi_p(t)}, \tag{2.5}$$

where $h_p(t)$ and $\phi_p(t)$ are the magnitude and phase of the p-th arriving path, respectively. However, due to the large scale fading increasing with both range and frequency, the channel is characterized by a limited channel bandwidth. Small scale fading in the channel is a result of the time spreading of the transmitted signal and time variability of the channel $h(t)$. Time variability is the inherent change in the dynamic nature of the propagation channel or changes that occur because of the relative motion between the source and receiver. Inherent variations occur on very long time scales and do not impact the instantaneous signal levels (e.g., monthly changes in temperature). In contrast, the changes that occur on short time scales (e.g., changes induced by surface waves) affect the signal and cause the displacement of the reflection point, resulting in both scattering of the signal and Doppler spreading due to the changing path length. Therefore, the channel exhibits both time and frequency dispersive fading which are caused by the Doppler and delay spreads.

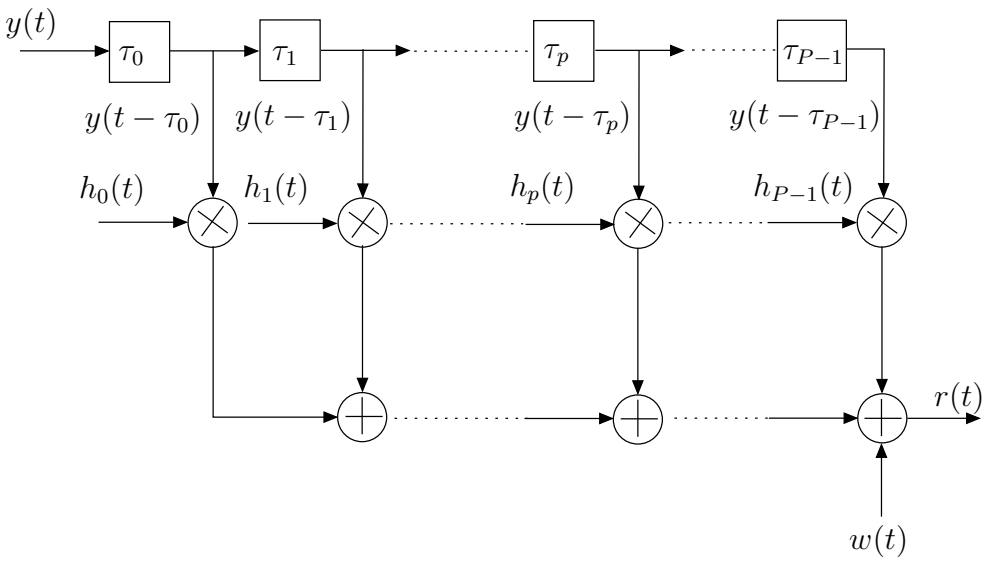

Figure 2.2: Tapped delay-line multipath model

2.2.3.1 Time spreading

Time spreading arises when the transmitted signal with multiple time-shifted and time-scaled versions arrive at the receiver. In UACs, these versions result from reflections, refraction and scatterers of the transmitted signal within the ocean. The phase and random amplitude of these arrivals, which are directly related to the acoustic velocity structure and the channel geometry, cause variations in the received signal. However, the ISI effect in such channels is the most dominant distortion source and the transmission is referred to as wideband. In shallow water channels, where the transmission range is larger than the water depth, the excessive delay spread is usually in the order of tens or even hundreds of milliseconds, which results in frequency selective signal distortion and severe ISI. Thus, the coherent receiver in such long ISI channels is much more complex than those in RF channels.

2.2.3.2 Frequency spreading

The dynamic nature of the channel and the relative transmitter/receiver movement results in propagation paths that are different from moment to moment, therefore, the CIR changes over time. If the channel was constant and there was no significant motion in the transmitter and receiver, the channel would appear time invariant. However, time variations in the channel will result in Doppler spreading and the band

of frequencies over which the Doppler spectrum is essentially non-zero is referred to as the Doppler spread B_d of the channel.

In UACs, the dominant factors resulting in Doppler spread are sea surface roughness and transmitter/receiver motion. If there is no motion, then the B_d due to wind effects at the sea surface can be written as [61]

$$B_d = 4/u_c[1 + \frac{4\pi f_c \cos(\theta_1)}{c}]u_h, \tag{2.6}$$

where f_c is the carrier frequency, θ_1 is the incident angle in degrees and the wave height u_h of the surface waves is given by $u_h = 0.005u_c^{1.5}$. However, B_d can vary greatly, but in relatively low sea states and without a moving source/receiver, B_d of less than 10 Hz is not untypical. Furthermore, the non-negligible transmitter/receiver motion causes an increase (or decrease) in the propagation path between the transmitter and receiver. Consequently, it induces a corresponding time expansion (or compression) of the received signal. This occurs through the Doppler shift effect, which causes frequency shifting as well as additional frequency spreading. This effect is proportional to the v/c ratio of the transmitter/receiver velocity to the sound speed. Because c=1500 m/s is very low compared to the speed of electromagnetic waves, motion induced Doppler distortion of an acoustic signal can be extreme. Assuming a centre frequency of 15 kHz, the Doppler shift associated with a velocity of 1 m/s is approximately 10 Hz. Such a phase distortion of a channel can cause severe tracking problems with many adaptive algorithms [59]. For more discussion about this type of Doppler spread see [62].

2.2.3.3 Doubly spread channels

The CIR that exhibits both time and Doppler spread, such as the shallow UAC, can be characterized as doubly spread channels. Both delay and Doppler spread are forms of dispersion, and there is a close connection between channels exhibiting delay spread and channels exhibiting Doppler spread. However, the channel can be characterized in terms of the product $B_d\tau_{rms}$, which is known as the spread factor of the channel. If $B_d\tau_{rms} < 1$, then the channel is said to be under-spread in which the channel can be estimated reliably and used to aid the receiver in demodulating the signal. In contrast, the CE is extremely difficult and high data error rates occur if $B_d\tau_{rms} > 1$, which is considered as an overspread channel. However, in the UAC, a normalized

Table 2.1: Differences between underwater and terrestrial networks

Parameters	Terrestrial	Underwater
Signal type	electromagnetic	acoustic
Speed	3×10^8 m/s	1500 m/s
Propagation delay	low	high
Required power	low	more important
Attenuation	low	high

Doppler spread of less than 10^{-3} is needed for coherent detection and the receiver has to be designed with signal processing techniques that take this fact into account [63].

2.2.4 Terrestrial Channels versus UACs

In most RF channels, for which CDMA receivers have been developed, the delay spread of the channel is in the order of a few chip intervals only, such that the induced ISI can be neglected. While a UAC is often tens of chip intervals, which at moderate processing gains causes non negligible ISI. The channel fluctuates significantly in the time it takes to propagate and such a situation makes it difficult to implement the modulation or detection algorithms that require knowledge of the channel. In addition, the available bandwidth of UAC is severely limited and depends on transmission range and frequency, whereas the sound propagation is five orders less than in air. Motion of just one metre has a significant effect on multiple access techniques that need accurate timing of the received signal.

However, the ratio of Doppler to f_c is in the order of 10^{-3}-10^{-4} in UACs, while the ratio in RF channels is in the order of 10^{-7}-10^{-9}. Further, the narrowband assumptions used in RF channels rarely apply to UACs. Some of these differences, both in terms of propagation aspects and in terms of the required energy costs, are outlined in Table 2.1 [63, 64]. It should be pointed out that the UACs combine the worst aspects of RF channels, and coherent underwater systems are much more complex than those in RF systems. Therefore, most existing terrestrial techniques that are well established cannot work easily in water, and specific underwater extensions will be required.

2.3 Code Division Multiple Access (CDMA)

In recent years, CDMA has become one of the most common multiple access techniques. The transmitted signal in such architectures is spread over a frequency band much wider than the minimum bandwidth required to transmit the input data. The introduced redundancy plays a significant role in the CDMA design and allows for the utilisation of many interesting features such as flexibility in the support of multiple users, allocation of different data rates, robustness against fading or against jamming and enhanced security. However, CDMA performance is restricted by MAI from other interfering users and ISI caused by multipath fading. Numerous MUDs and equalization techniques have been previously considered to mitigate these types of interference. In the following subsections, the transmission model and the receiver structures of CDMA are presented.

2.3.1 Transmission Model

The structure of a CDMA transmitter with K users and binary phase shift keying (BPSK) as the modulation scheme is shown in Fig. 2.3. The information bits d_k of the kth user is spread by a unique sequence s_k with length L. By assigning different users different spreading codes, each user is mapped onto a unique code dimension in the system, which allows the transmission of data simultaneously over the same frequency band without significantly interfering with each other. Assuming that d_k and s_k are real values $\{1, -1\}$, the resulting received signal $r(t)$ after transmitting over a synchronous multiple access channel is defined as

$$r(t) = \sum_{k=1}^{K} x_k(t) + w(t), \tag{2.7}$$

where

$$x_k(t) = \sum_{n=-\infty}^{\infty} \sum_{l=1}^{L} h_k d_k(n) s_k(l) p(t - lT_c - nT_s), \tag{2.8}$$

is the signal of user k with symbol duration T_s, T_c is the chip duration, and $p(t)$ represents the pulse shape function of the transmitted waveform, which is non zero in the interval $[(l-1)T_c, lT_c)$ within the duration of the n-th transmitted symbol. The discrete-time representation of the above received signal can be expressed in vector

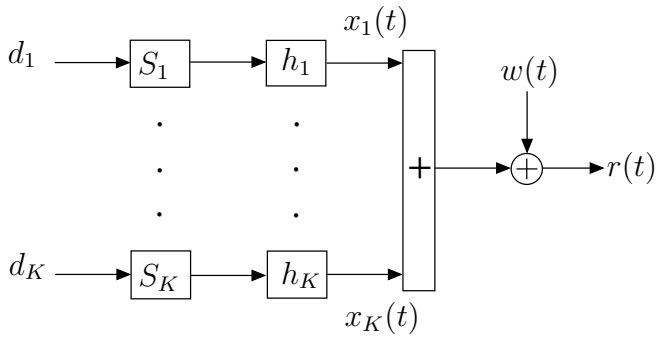

Figure 2.3: Transmitter architecture of CDMA system.

form as [7]

$$\mathbf{r}(n) = \sum_{k=1}^{K} h_k d_k(n)\mathbf{s}_k + \mathbf{w}(n), \quad n = -\infty, ... + \infty \tag{2.9}$$

where $\mathbf{s}_k = [s_k(1), s_k(2), ..., s_k(L)]^T$ represents the spreading vector of the k-th user, $\mathbf{r}(n) = [r_1(n), r_2(n), ..., r_L(n)]^T$ is the received signal vector at the n-th bit with dimension L, and $\mathbf{w}(n) = [w_1(n), w_2(n), ..., w_L(n)]^T$ is the Gaussian noise vector with covariance matrix $\sigma^2 I_L$ (I_L is an identity matrix with dimension L). By ignoring the time index n for brevity, the received signal can also be written in matrix form as

$$\mathbf{r} = \mathbf{SHd} + \mathbf{w}, \tag{2.10}$$

where $\mathbf{S} = [\mathbf{s}_1, \mathbf{s}_2 ... \mathbf{s}_K]$, $\mathbf{d} = [d_1, d_2 ... d_K]^T$, and $\mathbf{H} = \text{diag}(h_1, h_2, ..., h_K)$ represents a diagonal matrix. However, the transmitted signal occupies a bandwidth that equals the spread factor L multiplied by the bandwidth of the user data. This is illustrated in Fig. 2.4. In practice, the duration of the symbol interval is selected to be an integer number of the chip duration. That is

$$L = \frac{T_s}{T_c}. \tag{2.11}$$

2.3.1.1 Spreading and Scrambling Operations

In CDMA, the spreading sequence is used to scramble the signal in addition to the spreading. Thus, the spreading unit can be equivalently represented as a combination of a repetition operation followed by a scrambling unit. The relationship between spreading and scrambling is illustrated in Fig. 2.5. The spreading operation can

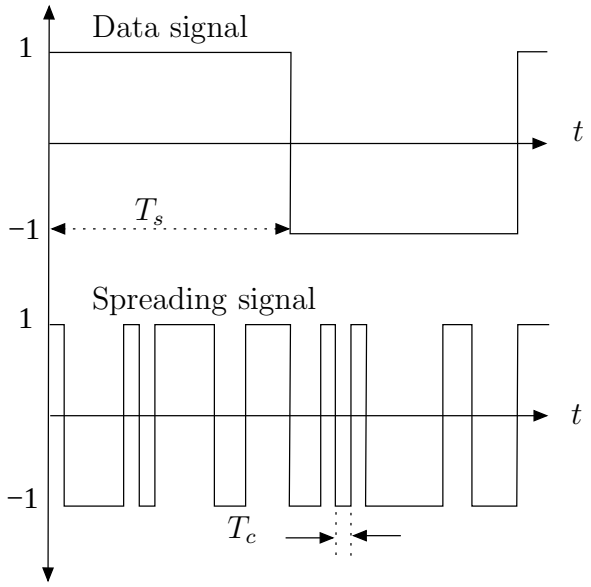

Figure 2.4: The relationship between a data signal and a 15-chip short spreading signal.

be achieved with an identical sequence for several users. The scrambling operation makes the signals from different users separable from each other without changing the signal bandwidth. The selection of good scrambling codes is important to the design of an efficient system, because correlation characteristics and length of the sequence establish a bound on the system capacity. Therefore, the number of users that can be supported is limited by the number of codes that can be generated. In general, these codes are supposed to be statistically independent, identically distributed random processes. Moreover, the sequence should have many characteristics such as very low correlation between time-shifted versions of the sequence and very low crosscorrelation with any other interference signals.

For ease of generation, a scrambling code is a pseudorandom noise (PN) sequence that can be generated with a fixed length of chips by mathematical rules. Statistically, it satisfies the requirements of randomness properties and can be classified as either short or long. In a short code, the sequence is the same for every data symbol period. In a long code, the sequence period is larger than the symbol period; therefore different portions of the sequence will be used to modulate the data symbols. In practice, the short code signatures exhibit high cross correlation peak values and they are only quasi-orthogonal. Thus the short sequences in CDMA systems are not statistically

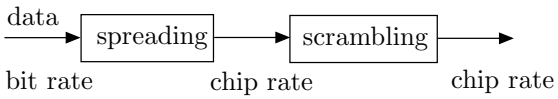

Figure 2.5: The relation between spreading and scrambling operations

independent. In contrast, the sequences with long periods behave more like Bernoulli sequences and can support more users than short sequences. The long code CDMA systems are sometimes called pseudorandom systems as compared to deterministic short code CDMA systems.

2.3.2 Receiver Architectures for CDMA

2.3.2.1 The Optimum Receiver

In the optimum receiver, the observation vector $\mathbf{y} = [y_1, y_2 ... y_K]^T$ with $y_k = \mathbf{s}_k^T \mathbf{r}$ represents the input to the decision algorithm that is used to approximate the desired decisions. Based on the MAP criterion, the log-likelihood ratio (LLR), L_k is calculated as [9, 65]

$$\begin{aligned} L_k &= \log \frac{\sum_{B^+} \exp(-(\mathbf{y}-\mathbf{RHd})^T (2\sigma^2 \mathbf{R})^{-1} (\mathbf{y}-\mathbf{RHd}) \prod_{k' \neq k} \Pr(d_{k'})}{\sum_{B^-} \exp(-(\mathbf{y}-\mathbf{RHd})^T (2\sigma^2 \mathbf{R})^{-1} (\mathbf{y}-\mathbf{RHd}) \prod_{k' \neq k} \Pr(d_{k'})} \\ &= \log \frac{\sum_{B^+} (\exp\left(2\mathbf{d}^T\mathbf{Hy} - \mathbf{d}^T\mathbf{HRHd})/(2\sigma^2)\right) \prod_{k' \neq k} \Pr(d_{k'})}{\sum_{B^-} (\exp\left(2\mathbf{d}^T\mathbf{Hy} - \mathbf{d}^T\mathbf{HRHd})/(2\sigma^2)\right) \prod_{k' \neq k} \Pr(d_{k'})}. \end{aligned} \tag{2.12}$$

where B^+ is all the combinations of $[d_1 = \pm 1, ..., d_{k-1} = \pm 1, d_k(n) = +1, d_{k+1} = \pm 1, ..., d_K = \pm 1]$, B^- is similarly defined and $\mathbf{R} = \mathbf{S}^T\mathbf{S}$ is the correlation matrix between K users. The optimum algorithm can be implemented by using the maximum likelihood (ML) detector [66], and when there is no *a priori* information, $\hat{\mathbf{d}}$ can be calculated as

$$\begin{aligned} \hat{d} &= \arg\{\max\{\exp(-(\mathbf{r}-\mathbf{SHd})^T (2\sigma^2 \mathbf{I}_S)^{-1} (\mathbf{r}-\mathbf{SHd}))\}\} \\ &= \arg\{\max\{2\mathbf{d}^T\mathbf{HS}^T\mathbf{r} - \mathbf{d}^T\mathbf{HRHd}\}\} \\ &= \arg\{\max\{2\mathbf{d}^T\mathbf{Hy} - \mathbf{d}^T\mathbf{HRHd}\}\}. \end{aligned} \tag{2.13}$$

Since all the combinations of $\mathbf{d}$ are included in the optimal detection, the related complexity grows exponentially with the number of users. However, there exist sub-

optimum receivers whose complexity growths only linearly with the number of users.

2.3.2.2 Suboptimum Receivers

The three typical suboptimum detectors, namely the single user detector, decorrelator and MMSE detector, employ a linear transformation of matched-filter output vectors [66]. Thus, these detectors can be written as

$$\hat{\mathbf{d}} = \mathbf{T}\mathbf{y}, \tag{2.14}$$

where

$$\mathbf{T} = \mathbf{I}, \tag{2.15}$$

for the single-user detector,

$$\mathbf{T} = \mathbf{R}^{-1}, \tag{2.16}$$

for the decorrelator detector and

$$\mathbf{T} = (\mathbf{R} + \sigma^2\mathbf{H}^{-2})^{-1}\mathbf{H}^{-1}, \tag{2.17}$$

for the MMSE detector. Then decisions are made on the output of (2.14). The decorrelator detector is optimal as the noise variance σ^2 goes to zero and it is designed to completely mitigate the MAI signal. Moreover, the decorrelator detector needs to know all the users' spreading sequences, and it has the advantage that knowledge of the received signal and channel state information (CSI) are not required. The MMSE detector estimates $\mathbf{R}^{-1}$ while considering the noise in the system. Therefore, the MMSE detector suppresses both the MAI and the background noise and it outperforms the other two detectors. Since matrix inversion is required in the decorrelator and linear MMSE detector, the corresponding complexity is in the order of K^2. However, the MMSE detector needs to know all spreading sequences as well as the CSI and to reduce these requirements, adaptive MMSE, blind MMSE and iterative detectors can be used.

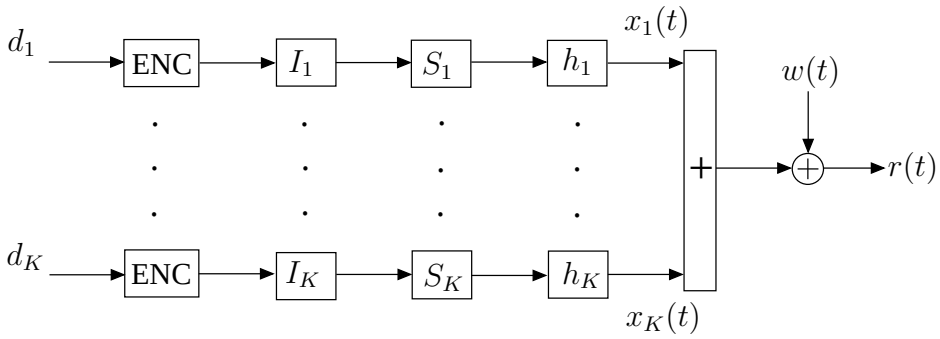

Figure 2.6: Transmitter architecture of coded CDMA system

2.3.2.3 Iterative Multiuser Receiver

Channel coding has become common for practical systems but the optimal architecture with coding is more complex than that for uncoded systems. In this case, T-MUDs are alternative solutions to improve the system performance at a relatively low computational cost. The block diagram of the coded CDMA transmitter is shown in Fig. 2.6. The information bits d_k of the k-th user are encoded by an encoder (ENC), then interleaved by an interleaver I_k to reduce the effects of error bursts at the input of each decoder. The interleaved coded bits are modulated with their own signature sequence s_k before being transmitted on a multiple access channel.

Fig. 2.7 shows the general T-MUD for the coded CDMA system. The two major functional modules, MUD and a bank of K single-user decoders (DECs), exchange information in terms of LLRs with the cooperation of the interleaver/deinterleaver blocks. The enhanced extrinsic information λ_k is fed back to the detector and appropriately used in the next iteration. Moreover, T-MUDs may utilize the extrinsic information feedback in different forms, where the optimal structure uses this information as *a priori* probabilities for each coded bit. In contrast, the MMSE detector uses them to estimate the mean and variance of each coded bit. However, by employing the instantaneous linear MMSE filtering, L_k is estimated as [9]

$$L_k = \frac{2h_k \mathbf{e}_k^T (\mathbf{V}_k + \sigma^2 \mathbf{R}^{-1})^{-1} (\mathbf{R}^{-1}\mathbf{y} - \mathbf{H}\mathbf{E}_k)}{1 - h_k^2 \mathbf{e}_k^T (\mathbf{V}_k + \sigma^2 \mathbf{R}^{-1})^{-1} \mathbf{e}_k}, \tag{2.18}$$

where $\mathbf{E}_k = [E_1, ..., E_{k-1}, 0, E_{K+1}, ..., E_K]^T$ with $E_k = tanh(\lambda_k/2)$ denoting the expectation of d_k, $\mathbf{V}_k = diag(h_1^2 Var_1, ..., h_{k-1}^2 Var_{k-1}, h_k^2, h_{k+1}^2 Var_{k+1}, ..., h_K^2 Var_K)$ with $Var_k = 1 - (E_k)^2$ as the variance of d_k, and $\mathbf{e}_k$ is a K dimensional vector of all zeros

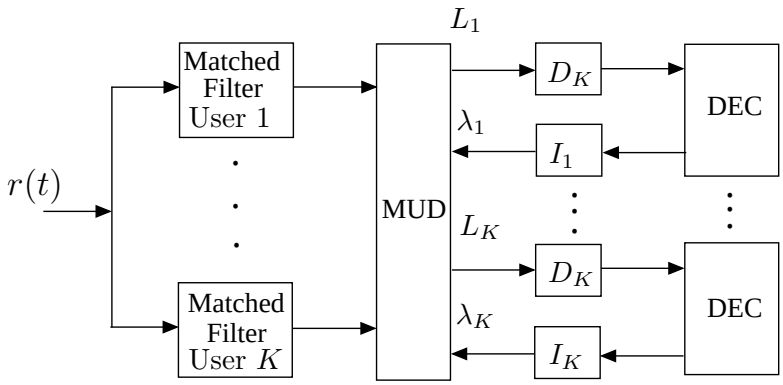

Figure 2.7: Turbo CDMA receiver

except for the k-th element.

2.4 Interleave Division Multiple Access (IDMA)

Multiuser architectures require some unique characteristic so that each user can be recognized from each other. For CDMA systems, the characteristic feature is to use user-specific signatures and the interleaver is usually employed to suppress channel impairments. However, as discussed in the previous sections, the high complexity of multiuser CDMA architectures restricts their practical implementation. This section describes the transmission and detection principles of IDMA systems, where the chip-level interleavers are the only means for user separation. The scheme allows low complexity detection techniques that are applicable to systems with large K in multipath channels. For simplicity, only iterative detection strategies for real channel conditions are considered, but the principle can be easily extended to complex signalling.

2.4.1 Transmitter Description and Signal Model

The transmitter structure with K simultaneous users of an IDMA system is depicted in Fig. 2.8. The input data sequence $\mathbf{d}_k$ of user k is encoded using an encoder, generating a coded sequence $\mathbf{c}_k$. The elements in $\mathbf{c}_k$ are then fed to a scrambling $\mathbf{s}$ with code $\{+1, -1, +1, -1, ...\}$ and length L. The chip sequence is permuted by a chip-level interleaver $I_k[.]$ before transmitting on a multiple access channel. These interleavers disperse the coded sequences so that the adjacent chips are approximately

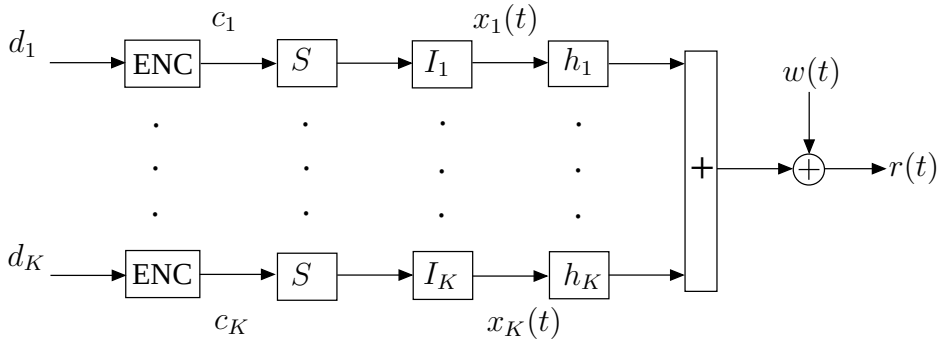

Figure 2.8: Transmitter architecture of coded IDMA system

uncorrelated. The transmitted signal due to the k-th user is defined as

$$x_k(t) = \sum_{n=-\infty}^{\infty} \sum_{l=1}^{L} I_k[c_k(n)s(l)]p(t - lT_c - nT), \tag{2.19}$$

and the received baseband signal from all users can be written as

$$r(t) = \sum_{k=1}^{K} x_k(t) \otimes h(t) + w(t), \tag{2.20}$$

where $h(t)$ is defined as in (2.5), and $\otimes$ denotes convolution operation. After chip-matched filtering and sampling at the chip rate, the signal at a time instant n can be represented as [7]

$$r(n) = \sum_{k=1}^{K} \sum_{p=0}^{P-1} h_{k,p} x_k(n - p) + w(n), \tag{2.21}$$

where $w(n)$ are samples of an AWGN process with zero-mean and variance σ^2. However, a common spreading sequence $\mathbf{s}$ can be used for all users and different interleavers patterns I_k are employed for user separation. This results in an IDMA scheme, which inherits many advantages from CDMA such as robustness against fading, dynamic channel sharing, mitigation of interference and asynchronous transmission.

2.4.2 The Role of Interleavers

Unlike turbo and turbo-like codes, where the task of a single interleaver is to decorrelate different sequences of bits, in IDMA a set of interleavers are used not only to

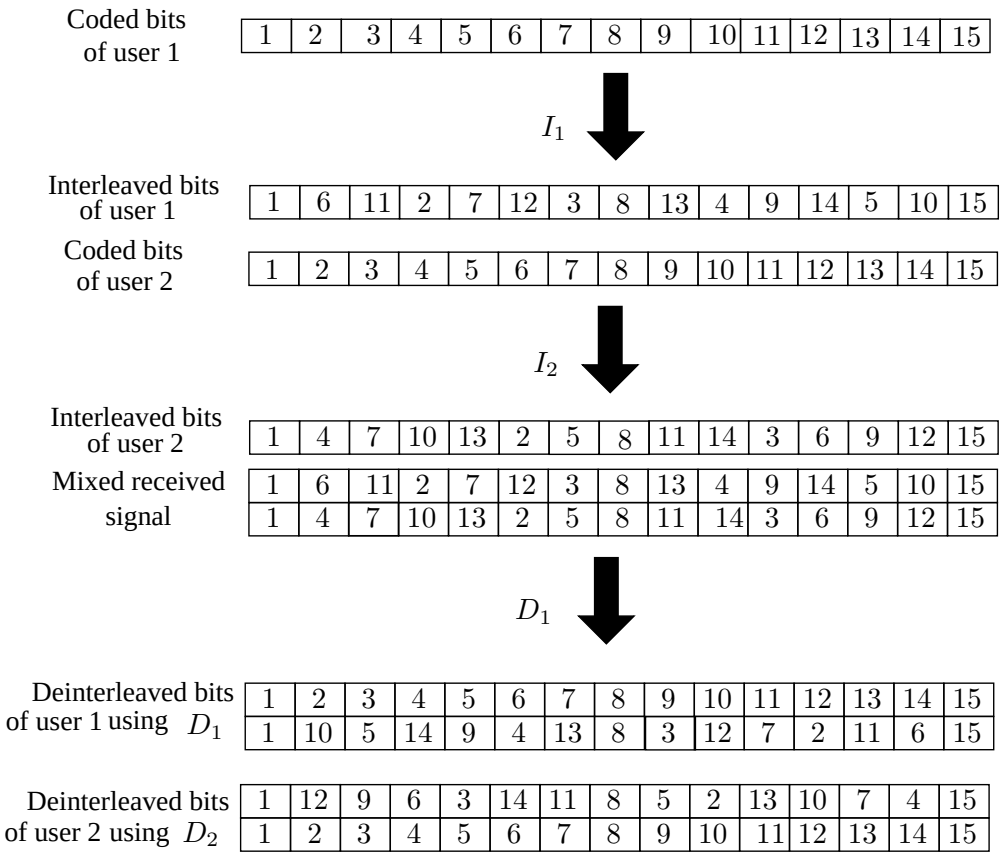

Figure 2.9: Users' separation using different deinterleavers

decorrelate different bit sequences, but also to decorrelate different users. Fig. 2.9 illustrates how the receiver separates different users by their unique interleaver patterns. The signal of user 1 after deinterleaver D_1 shifts back to its original order and can be decoded correctly, whereas the MAI from user 2 is of random order and thus acts as independent and non-correlated interference [67]. Moreover, the correlation between these interleavers determines how strongly interference from other users affects the decoding process of a specific user. Thus, it is important to design the interleavers in a way which reduces the crosscorrelation properties and maximize the minimum distance of the crossing interleaving. The correlation upper bound of interleavers and minimum spreading distance, which are usually used in the analysis of different interleavers, are discussed in the next section.

2.4.2.1 Correlation upper bound and spreading distance

An interleaver rearranges the ordering of a data sequence by means of a deterministic bijective mapping. Let $\mathbf{b}_k = [b_k(1), b_k(2), ..., b_k(N)]$, be a sequence of length N elements. An interleaver maps $\mathbf{b}_k$ onto a sequence $\mathbf{x}_k = [x_k(1), x_k(2), ..., x_k(N)]$ such that x_k is a permutation of the elements of b_k. Orthogonality implies no collision among interleavers and the two interleavers I_i and I_j are called orthogonal if

$$C^c(b_i(I_i), b_j(I_j)) = 0, \tag{2.22}$$

where the crosscorrelation C^c is the scalar product between two vectors b_i and b_j. Good correlation properties are obtained when the term C^c is close to 0 for $i \neq j$. However, evaluating the correlation C^c between two interleavers is very computationally expensive, since correlation is affected by the coded data length. Therefore, to analyze the correlation properties, the peak basis correlation (PBC) function in [68] can be used. Let the canonical basis $e_i = I_J$ and the generating set w_j be defined as

$$w_i(j) = \begin{bmatrix} 1 & -1 & \cdots & -1 \\ 1 & 1 & & \vdots \\ \vdots & & \ddots & -1 \\ 1 & \cdots & 1 & 1 \end{bmatrix}, i, j\, \varepsilon(1, 2..J) \tag{2.23}$$

The PBC between I_i and I_j is denoted by $C^c_{max}(I_i, I_j)$ and defined as

$$C^c_{max}(I_i, I_j) = \underset{w_j}{max} \sum_{i=1}^{J} \langle I_i(c(e_i)), I_j(c(w_j)) \rangle. \tag{2.24}$$

For all vectors of generating set w_j , there exists a maximum value $I(I_i, I_j)$ representing the correlation between I_i and I_j. In addition, the minimum distance (d_{min}) criterion for all the interleavers is defined as [69]

$$d_{min} = \min(d_s(k)), k\, \varepsilon(1, ..., K), \tag{2.25}$$

and

$$d_s(k) = \min |I_k(i) - I_k(i-1)|, i\, \varepsilon(2, ..., J), \tag{2.26}$$

where K is the total number of interleavers and $d_s(k)$ represents the minimum cross interleaving distance of the k-th interleaver.

2.4.2.2 Choice of Interleavers

Since multiple interleavers are key components for such systems, it is vital to choose good interleavers which are weakly correlated between different users. Despite this importance, usually interleavers are independently and randomly chosen. In this case, the interleaver indices requires a large a mount of memory to store when the number of users is large. There is also a potential risk that some interleavers may be highly correlated. However, there are a large number of papers on the interleaver design for IDMA systems.

Power interleavers in [70] use a master interleaver to generate a set of interleavers. This method lowers the memory requirements for storing interleaver patterns, and reduces the amount of bits to specify which interleavers are adopted. However, the generation of this family of interleavers is slow especially when the number of users is large. Nested interleavers can be obtained with a simple recursion method. Compared with random interleavers, these interleavers reduce the memory and bandwidth requirements. Orthogonal and PN interleavers utilize different primitive polynomials, so each user only needs to store its own primitive polynomial to generate its interleaving sequence. Obviously, this method is better than the nested and random interleavers [68]. However, when user number K becomes large, it is difficult to find enough primitive polynomials for PN interleavers, and systems have to tolerate generation time for nested interleavers.

2.4.3 Turbo CBC Receiver Architecture

The block diagram of the IDMA receiver is shown in Fig. 2.10. The receiver consists of a CBC MUD, K deinterleaver/interleaver pairs, K despreader/spreader pairs and a bank of K single-user decoders (DECs). The turbo process commences at the MUD, followed by the decorrelating and decoding operations, then back for the next iteration through the spreading and interleaving operations. For simplicity, single-path channels with real coefficients and BPSK modulation are first discussed. By removing the subscript p in $h_{k,p}$, and denoting the channel coefficient of the k-th user

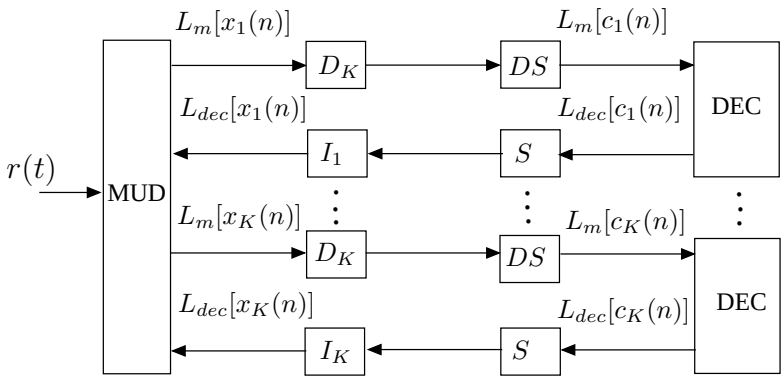

Figure 2.10: Turbo IDMA receiver

by h_k, (2.21) can be expressed as

$$r(n) = \sum_{k=1}^{K} h_k x_k(n) + w(n), \tag{2.27}$$

where $x_k(n)$ is the n-th chip transmitted by user k. In the following subsections, the functionality of the various IDMA components is discussed.

2.4.3.1 CBC Multiuser Detectors

The inputs to the MUD are the channel observation $\mathbf{r}$ and the *a priori* information $L_{dec}[x_k(n)]$. For a single-path channel, $x_k(n)$ is only related to $r(n)$, thus the corresponding *a posteriori* log-likelihood ratio (LLRs) based on the multiple access constraint of $x_k(n)$ can be expressed as

$$\log\left(\frac{\Pr(x_k(n)=+1|\mathbf{r})}{\Pr(x_k(n)=-1|\mathbf{r})}\right) = \underbrace{\log\left(\frac{p(r(n)|x_k(n)=+1)}{p(r(n)|x_k(n)=-1)}\right)}_{L_m[x_k(n)]} + \underbrace{\log\left(\frac{\Pr(x_k(n)=+1)}{\Pr(x_k(n)=-1)}\right)}_{L_{dec}[x_k(n)]}, \forall k, n \tag{2.28}$$

When the received signal $r(n)$ is subjected to noise with a Gaussian distribution, the probability density function $p(r(n)|x_1(n), ..., x_k(n))$ of the channel transition function be defined as

$$p(r(n)|x_1(n), ..., x_k(n)) = \frac{1}{\sqrt{2\pi\sigma^2}} \exp\left(\frac{-(r(n) - \sum_{k=1}^{K} h_k x_k(n))^2}{2\sigma^2}\right), \tag{2.29}$$

where σ^2 is the noise variance. According to Bayes' rule, the MAP estimate of the extrinsic LLRs $L_m[x_k(n)]$ is computed as

$$L_m[x_k(n)] = \log \frac{\sum_{X^+} p(r(n)|x_1(n), ..., x_k(n)) \prod_{k' \neq k} \Pr(x_{k'}(n))}{\sum_{X^-} p(r(n)|x_1(n), ..., x_k(n)) \prod_{k' \neq k} \Pr(x_{k'}(n))}, \tag{2.30}$$

where $Pr(x_k(n))$ is the *a priori* probability of $x_k(n)$, X^+ and X^- are the set of $[x_1(n), ..., x_k(n) = +1, ..., x_K(n)]$ and $[x_1(n), ..., x_k(n) = -1, ..., x_K(n)]$, respectively. However, this optimum approach is usually prohibitively complicated and its complexity increases exponentially with K. In the following, a suboptimal low complexity CBC approach [71] is discussed based on a Gaussian approach.

CBC detection provides a coarse estimation of $\{x_k(n), \forall n, k\}$. To maintain low complexity, the coding and spreading constraints are not considered in the MUD. For user k, (2.27) can be rewritten as

$$r(n) = h_k x_k(n) + \eta_k(n), \tag{2.31}$$

where

$$\eta_k(n) = \sum_{k'=1,\ k' \neq k}^{K} x_{k'}(n) + w(n), \tag{2.32}$$

is the distortion term with respect to $x_k(n)$. Assume that $x_k(n), \forall k$ are independent and identically distributed (i.i.d.) random variables. By applying the central limit theorem, η_k can be approximated as a Gaussian random variable with mean

$$E[\eta_k(n)] = \sum_{k'=1,\ k' \neq k}^{K} h_{k'} E[x_{k'}(n)], \tag{2.33}$$

and variance

$$Var[\eta_k(n)] = \sum_{k'=1,\ k' \neq k}^{K} h_{k'} Var[x_{k'}(n)] + \sigma^2, \tag{2.34}$$

where $E[x_{k'}(n)]$ and $Var[x_{k'}(n)]$ of a random variable $x_k(n)$ can be defined as [9]

$$\begin{aligned} E[x_k(n)] &= \frac{Pr[x_k(n) = +1] - Pr[x_k(n) = -1]}{Pr[x_k(n) = +1] + Pr[x_k(n) = -1]} \\ &= \frac{\exp\{x_k(n)\} - 1}{\exp\{x_k(n)\} + 1} = \tanh\{L_{dec}[x_k(n)]/2\}, \quad \forall k, n \end{aligned} \tag{2.35}$$

$$Var[x_k(n)] = 1 - \{E[x_k(n)]\}^2, \quad \forall k, n, \tag{2.36}$$

By applying the Gaussian approximation to (2.31), $L_m[x_k(n)]$ in (2.30) can be calculated as

$$\begin{aligned} L_m[x_k(n)] &= \log\left(\exp\left(-\frac{\{r(n) - E[\eta_k(n)] - h_k\}^2}{2Var[\eta_k(n)]}\right)\right) \\ &\quad - \log\left(\exp\left(-\frac{\{r(n) - E[\eta_k(n)] + h_k\}^2}{2Var[\eta_k(n)]}\right)\right) \\ &= 2h_k\frac{\{r(n) - E[\eta_k(n)]\}}{Var[\eta_k(n)]} = 2h_k\frac{\{r(n) - E[r(n)] + h_kE[x(n)]\}}{Var[r(n)] - |h_k|^2Var[x(n)]}, \end{aligned} \tag{2.37}$$

where

$$E[r(n)] = \sum_{k'} h_{k'}E[x_{k'}(n)], \tag{2.38}$$

$$Var[r(n)] = \sum_{k'}|h_{k'}|^2Var[x_{k'}(n)]+\sigma^2. \tag{2.39}$$

For the k-th user, the outputs $L_m[x_k(n)]$ of the MUD are deinterleaved to form the *a priori* LLRs, then transferred to the despreader and decoder for further refinement. The despreading and decoding operations will be explained in the following subsection.

2.4.3.2 Despreading and Decoding Operations

After user-specific deinterleaving, $\{L_m[x_k(D_k(n))], \forall n\}$ are assumed to be uncorrelated, which is approximately accurate due to interleaving. Then, the signal is integrated over the duration of one data symbol using the despreader (DS). By despreading the signal, the detector extracts the processing gain and performs the decorrelation process on each coded bit based on $L_m[x_k(D_k(n))]$ and the spreading constraint. The bit-level *a priori* LLR for the decoder can be computed as

$$L_m[c_k(n)] = \sum_{j=(n-1)L+1}^{nL} s(j)L_m[x_k(D_k(j))], \quad n = 1, ..., N_d \tag{2.40}$$

The decorrelated outputs $L_m[c_k(n)]$ from the k-th despreader are used to perform standard *a posteriori* probability (APP) decoding. Based on the coding constraint,

the k-th decoder generates the *a posteriori* LLRs $L_{dec}[c_k(n)]$ of the $\{c_k(n), \forall n\}$ by

$$L_{dec}[c_k(n)] = \log\left(\frac{Pr(c_k(n) = +1|L_m[c_k(n)])}{Pr(c_k(n) = -1|L_m[c_k(n)])}\right), \quad \forall k, n \tag{2.41}$$

The MAP algorithm explained in the preceding section can be used in the decoding process. An interesting argument in this algorithm is that it generates not only information about the information bits but also generates extrinsic information about the coded bits, which is an important criterion for structures with feedback. However, the optimal algorithm in real systems is too complex for estimating the information on a bit-by-bit basis. Some solutions have been proposed to reduce the complexity of the MAP algorithm. The Log-MAP algorithm in [72] gives almost exactly the same performance as the MAP algorithm. Therefore, it is a very attractive algorithm to use as the component decoders. The outputs of the decoder are fed to the k-th spreader to generate the chip level extrinsic information. After appropriate interleaving, the extrinsic information is computed as

$$L_{dec}[x_k(I_k(j))] = s(l)L_{dec}[c_k(n)] - L_m[x_k(D_k(j))], \tag{2.42}$$

where $j = (n-1)L + l$, $l = 1, ..., L$ and $n = 1, ..., N_d$. The feedback extrinsic information $L_{dec}[x_k(n)]$ will be used to update $E[x_k(n)]$ and $Var[x_k(n)]$ for the next iteration.

2.4.4 Differences to other Multiple Access Architectures

Although the CDMA approach may also have three components, namely an encoder, an interleaver and a spreader, reversing the ordering of interleaving and spreading in IDMA leads to chip-interleaving instead of bit-interleaving in CDMA. All the bandwidth expansion is exploited before the interleaver therefore a larger interleaver is guaranteed. The spreaders and correlators can be removed and the different users can be distinguished by their unique user specific chip-interleavers instead of spreading sequences. Since a conventional signature is not necessary for the system to operate, the correlator based CDMA structure is not suitable in IDMA. However, the repetition code may be used jointly with the encoder to simplify the overall encoder. These changes in structure show that the IDMA approach has several interesting advantages over CDMA.

Table 2.2: Comparison between IDMA and other multiple schemes

	FDMA	TDMA	CDMA	IDMA
Multiple user separation	frequency	time	spreading sequence	interleaver
Inter-cell intereference	sensitive	sensitive	mitigated	mitigated
Interference cancellation	not necessary	not necessary	MUD	MUD
ISI cancellation method	cyclic prefix	equalization	Rake receiver	turbo chip detection
High single user rate solution	high order modulation	high order modulation	multicode CDMA	variable coding rate

In CDMA, high data rates can be obtained by using multicode CDMA or reducing spreading factor, which results in decreased processing gain against interference. While in IDMA a high data rate can be achieved by using encoding with high coding rates. Due to the chip level processing that increases the achievable time diversity in time-selective channels, the interference for one chip is independent from that for another chip. Hence, the filtering process after soft interference cancellation is simply the summation of the LLR values for all the chips, enabling a low computational cost but yet powerful detector for the system. The computational complexity per user is independent of the number of active users and this good property remains in multipath channels because it only relates to channel taps. In addition, to maintain orthogonality, techniques such as TDMA and FDMA require frame synchronization. In contrast, no advanced synchronization requirements are necessary in IDMA. A comparison between IDMA and other multiple access architectures is outlined in Table 4.7 [73].

2.5 Summary

This chapter provided an overview of the UACs and the basics of SSS. The details of multipath propagation model and channel physics were discussed in Section 2.2. Characteristics such as path loss, ambient noise and multipath fading were also considered, when the channel is bandlimited. Background noise is often characterized as non Gaussian and severe fading occurs due to both time spreading and Doppler spreading of the transmitted signal. Furthermore, the systems are inherently wideband in the sense that the bandwidth is not negligible with respect to the carrier frequency. No standardized models exist for UACs, therefore, experimental measurements are often used to assess the channel statistical properties of particular sites.

Our attention was also focused in Section 2.3 on CDMA systems. A brief overview of a CDMA transmitter structure was given with emphasis on the matrix form of the signal model. The known spreading sequences were also introduced along with a representation of spreading waveforms. Some insightful explanation have been made in Section 2.3.2, by reviewing the receiver structures for CDMA with emphasis on the description of optimum, MMSE and single user architectures.

The transmission model of IDMA systems, where the chip-level interleavers are the only means for user separation, are presented in Section 2.4. Since multiple interleavers are key system components, it is important to choose good interleavers which are weakly correlated between different users. The correlation upper bound of interleavers and some common interleavers are also discussed. The functionality of the various system components is given and the IDMA scheme allows very low cost chip detection. The optimum approach and Gaussian approach of the detector are also explained in Section 2.4.3.

CHAPTER 3

CE Based Turbo Architectures

3.1 Introduction

IN turbo systems, channel information is required to reconstruct the interference signals as well as the LLR computations for every decoding iteration. Therefore, the accuracy of the CE is crucial to the effectiveness of the T-MUD algorithms that degrade significantly if the CE is not reliable. The estimation is typically performed using adaptive filters that introduce more degrees of freedom than necessary. In these adaptive techniques, training sequences are usually embedded in transmitted signals to acquire the CSI and facilitate synchronization and CE. In the presence of limited training sequences, iterative techniques can provide the required flexibility to improve the channel estimates and the complexity of this estimation needs to be low in an iterative process.

This chapter presents adaptive CE algorithms with joint phase tracking for IDMA and CDMA systems using two different training methods, time multiplexing pilot and continuous pilot or pilot-aided data. Based on the enhanced soft iterative information, the transversal filters and carrier tracking are performed jointly to ensure reliable communication, especially on long delay spread channels. The proposed algorithm with continuous pilots is similar to the semi-blind CE method in [23], but has much less computational complexity. However, this approach and the T-MUD algorithms of IDMA systems have yet to be fully studied, especially for real channel conditions. The chapter is organized as follows. In Section 3.2, the CDMA and IDMA system models are presented and used for the remainder of this thesis, while their corresponding receivers with the proposed CE are outlined in Section 3.3 to Section 3.5, respectively. Performance evaluation using simulation results is demonstrated for different channel conditions in Section 3.6. Finally, Section 3.7 concludes the chapter.

3.2 Transmission System Models

The complex baseband model for a synchronous IDMA system with K simultaneous users is presented in Fig. 3.1 (a). The information bits, $d_k(n)\epsilon\{0,1\}$, of user k are encoded by a rate R convolutional encoder of constraint length N_c. The output of the encoder is further processed by a rate R_r scrambling repetition code, which is necessary for the operation of PIC detectors and utilized to give the system MAI protection. The coded bits are additionally permuted by a user-specific interleaver,

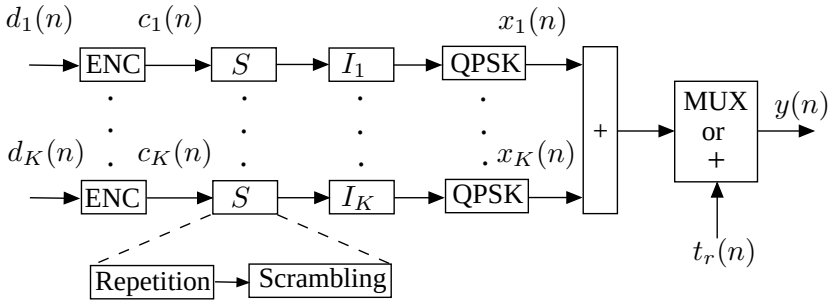

(a)

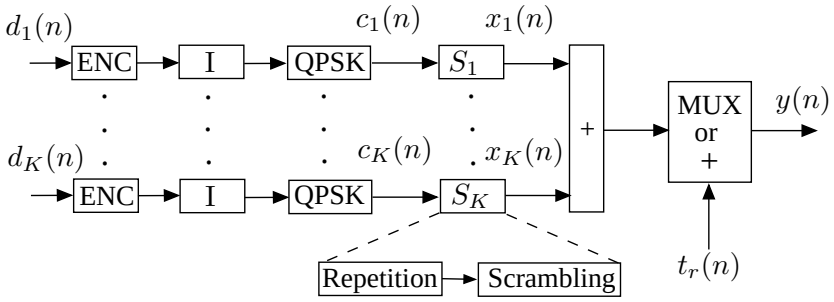

(b)

Figure 3.1: Downlink transmitters of IDMA (a) and CDMA (b) with multiplexing pilots or continuous pilots.

$I_k[.]$, so that adjacent chips are uncorrelated. This is required in order to facilitate a chip-level based detection strategy. The total number of chips becomes $N = N_d L$, where N_d represents the number of coded bits and L represents the spreading factor. The resulting signal for the kth user after memoryless quadrature phase-shift keying (QPSK) mapping can be written as

$$x_k(t) = A_k \sum_m \left[b^{I_k}(m) + j b^{Q_k}(m) \right] p(t - mT_s), \tag{3.1}$$

where A_k is the transmitted signal amplitude of the kth user. Additionally, $b^{I_k}(m)$ and $b^{Q_k}(m)$ are the mth coded chip bits for the kth user for the in-phase and quadrature-phase data streams, respectively

$$b(m) = I_k[c_k(n)s(l)],\ m = l + nL,\ l = 0, ..., L-1,\ \forall n, \tag{3.2}$$

where $c_k(n)$ represents the nth encoded user's bit and $s(l)$ is the spreading sequence. Conventionally, the same spreading sequence and encoder are used for all users; however, users are distinguished by utilizing distinct interleaver patterns.

For the CDMA-based system shown in Fig. 3.1 (b), the coded bits are interleaved by a bit-level interleaver and modulated using QPSK. These symbols are then upsampled by L and scrambled using a user-specific pseudorandom scrambling sequence S_k. It is worth highlighting that identical interleavers and encoders are utilized for all users. The resulting transmitted signal for the kth user can be expressed as [3, 74]

$$x_k(t) = A_k \sum_{m} \sum_{l=0}^{L-1} s_k(l) \left[c^{I_k}(m) + j c^{Q_k}(m) \right] p(t - lT_c - mT_s), \tag{3.3}$$

where $c^{I_k}(m)$ and $c^{Q_k}(m)$ are the mth coded bits of the in-phase and quadrature phase data streams for the kth user, respectively, whereas $s_k(l)$ represents the lth chip of the user's spreading sequence.

3.2.1 Training Schemes

The transmitted symbols are organized in packets built with a probe signal to synchronize the receiver, which is a training sequence to help the equalizer in the convergence process. The training symbols are generated randomly with a uniform distribution and are defined as $t_r = [t_r(1), ..., t_r(N_s)]$ with energy level $t_r \epsilon \{t_r, -t_r\}$. An important property of a training sequence is the length of its period. In general, a longer period leads to a better estimation. There exist two main training methods; time multiplexing pilot and continuous pilot. Unlike conventional methods where pilots are time-multiplexed with data symbols, the training sequence in pilot-aided data is continuously spread over the whole transmission frame. Each transmitted chip is added with one training chip and the bandwidth, as opposed to data-multiplexed pilot, is not affected. The overhead loss in data-multiplexed pilot can be measured by N_s/N ratio, where a small ratio implies a reduce overhead. The values N_s that are less than the channel memory length may cause interference among consecutive blocks.

The composite users' signal $x(n)$ is added to a continuous modulated signal $t_r(n)$ and the transmitted signal $y(t)$ can be written as

$$y(t) = t_r(t) + \sum_{k=1}^{K} x_k(t). \tag{3.4}$$

In contrast, $t_r(n)$ in Fig. 3.1 is multiplexed with the MAI signal for the time multiplexing pilot based systems and the transmitted signal $y(t)$ can be expressed as

$$y(t) = [t_r(t), \sum_{k=1}^{K} x_k(t)], \tag{3.5}$$

where the multiplexing is employed such that $t_r(n)$ is transmitted before the data sequence. However, other schemes, such as placing the data sequence in the middle of the data, are also possible. The training sequence and the energy level are known at the receiver, therefore it is possible to track and compensate for the fading channel effects. However, continuous pilots incur energy loss instead of an increase in bandwidth and can be used as a measurement tool, similar to the training channel in CDMA systems. Moreover, this approach is simplified for IDMA as the separation is achieved based on different chip interleavers instead of crosscorrelation between the spreading sequence and the training sequence as in conventional CDMA systems.

3.2.2 Multipath Fading Channels

The same bandwidth efficiency for both IDMA and CDMA is considered using the same convolutional encoder (i.e., $R_r = 1/L$). The transmitted signal $y(t)$ is then passed through a transmit filter exhibiting a raised cosine frequency response with a roll off factor of β, and then transmitted over the UAC channel. The majority of work in underwater communications is based on a general time-varying model. The TDL channel model with Rician statistics [74] is adopted for multipath propagation, and the baseband received signal can be expressed as [31]

$$r(t) = \sum_{p=0}^{P-1} h_p(t) y(t - \tau_p) e^{j\phi_p(t)} + w(t), \tag{3.6}$$

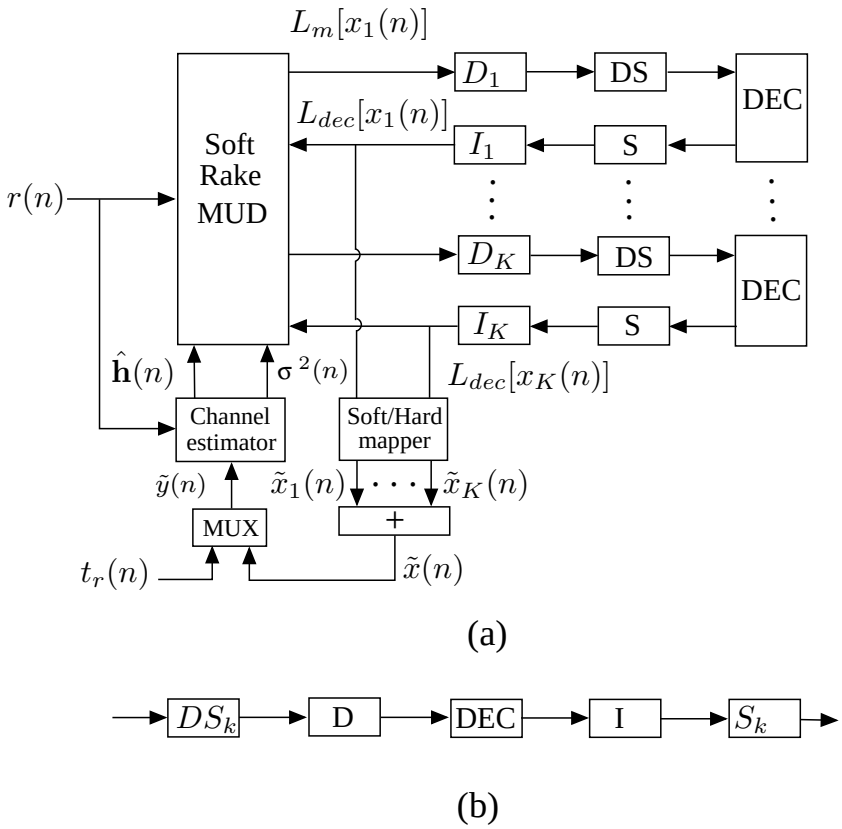

Figure 3.2: The IDMA receiver in (a) can be interpreted as CDMA by exchanging the order of I and S as in (b).

where $h_p(t)$ are the channel fading coefficients of the physical propagation path p at time t, and the corresponding path delay is τ_p. The total number of paths is P and the phase $\phi_p(t)$ represents the joint effects of phase distortion due to motion and carrier offsets.

3.3 Soft Rake IDMA Receiver Structure

The suboptimal receiver structure after the acquisition stage is presented in Fig. 3.2 (a). The structure consists of a MUD, K single user DECs and CE. The receiver, instead of treating the interfering users as background noise, exploits the signal structure to perform joint detection for all users' data by using the knowledge of interfering users. The detector takes soft information $r(n)$ and, after some processing, delivers refined *a posteriori* LLRs $L_m[x_k(n)]$, which are based on *a priori* known information and

the information gained by the equalization process. The outputs after deinterleaving and despreading are sent to the DECs. The kth user decoder output $L_d[x_k(n)]$ after spreading and user-specific interleaving is subtracted from $L_m[x_k(n)]$ to form the extrinsic information of the kth user as follows

$$L_{dec}[x_k(n)] = L_m[x_k(n)] - L_d[x_k(n)]. \tag{3.7}$$

This soft information is passed to the detector for the next turbo pass. Then, by the turbo-principle, the soft information is greatly enhanced and the process stops after a predetermined number of iterations or specific convergence criteria.

3.3.1 Soft-Rake Multiuser Detector

The detector operation follows the detection approach in [75] to compute the LLRs for the coherent receiver. Soft Rake and IC concepts are combined to handle the ISI and MAI effects jointly. The detector utilizes multipath and allows each arriving multipath signal to be individually detected and sums (P+1) LLRs per chip to provide strong and more accurate signals. However, the remaining interference $\eta_{k,p}(n)$ with respect to user k is modelled as a Gaussian random variable using the central limit theorem.

$$\tilde{r}(n+p) = h^*_{k,p} r(n+p) = |h^*_{k,p}(n)|^2 x_k(n) + \tilde{\eta}_{k,p}(n), \tag{3.8}$$

where $(.)^*$ denotes the conjugate operation, and

$$\tilde{\eta}_{k,p}(n) = h_{k,p}(n)\eta_{k,p}(n). \tag{3.9}$$

Therefore, the output distribution of the detector can be well approximated by a Gaussian distribution and this approximation is used by MUD to generate the LLRs of $x_k(n)$. In (3.8), the phase shift due to $h_{k,p}$ is removed, thus, the real part $\tilde{r}^I(n+p)$ is not a function of the imaginary part of $x^Q_k(n)$. The details of the log likelihood ratio combining (LLRC) detection algorithm in multipath complex time varying channels are listed as

- Interference mean and variance estimation

$$E[r(n)] = \sum_{k,p} h_{k,p}(n) E[x_k(n-p)], \ \forall n \tag{3.10}$$

$$Cov[r(n)] = \sum_{k,p} H_{k,p}(n) Cov[x_k(n-p)] H_{k,p}^T(n) + \sigma^2 I_2, \ \forall n \tag{3.11}$$

where $E[r(n)]$ and $Cov[r(n)]$ are the estimated mean and variance of the received signal. $E[\tilde{\eta}_{k,p}(n)]$ and $Var[\tilde{\eta}_{k,p}(n)]$ of the distortion term $\eta_{k,p}$ is calculated as

$$E[\tilde{\eta}_{k,p}(n)] = h_{k,p}^*(n) E[r(n+p)] - |h_{k,l}(n)|^2 E[x_k(n)], \ \forall k, n \tag{3.12}$$

$$\begin{aligned} Var[\tilde{\eta}_{k,p}(n)] = H_{k,p}^T(n) [Cov[r(n+p)] \\ - H_{k,p}(n) Cov[x_k(n)] H_{k,p}^T(n))] H_{k,p}(n), \ \forall k, n \end{aligned} \tag{3.13}$$

- LLR generation and combining

$$L_m[x_k^I(n)]_p = 2|h_{k,p}(n)|^2 \frac{\tilde{r}^I(n+p) - E[\tilde{\eta}_{k,p}^I(n)]}{Var[\tilde{\eta}_{k,p}^I(n)]}, \ \forall k, n \tag{3.14}$$

The distortion components from different paths in the received signal are assumed to be uncorrelated, thus, the LLRs based on individual chips, one for each path, can be summed in a Rake manner as

$$L_m[x_k^I(n)] = \sum_{p=0}^{P-1} L_m[x_k^I(n)]_p, \ \forall k, n \tag{3.15}$$

where I_2 is a 2×2 identity matrix, $(.)^T$ denotes the transpose operation, and

$$H_{k,p}(n) = \begin{bmatrix} h_{k,p}^I(n) & -h_{k,p}^Q(n) \\ h_{k,p}^Q(n) & h_{k,p}^I(n) \end{bmatrix}. \tag{3.16}$$

The *a priori* mean $E[x_k(n)]$ and variance $Cov[x_k(n)]$ of the transmitted signal are also required, which is calculated based on the extrinsic LLRs of the decoders.

$$E[x_k(n)] = \tanh\left(\frac{L_{dec}[x_k^I(n)]}{2}\right) + j \tanh\left(\frac{L_{dec}[x_k^Q(n)]}{2}\right), \tag{3.17}$$

$$Cov[x_k(n)] = \begin{bmatrix} 1 - E[x_k^I(n)]^2 & 0 \\ 0 & 1 - E[x_k^Q(n)]^2 \end{bmatrix}, \tag{3.18}$$

Table 3.1: PIC and SIC detection methods

Parallel IC	Serial IC
$\forall k, n : E[x_k(n)] = 0$	$\forall k, n : E[x_k(n)] = 0$
	For k=1,...,K
$\forall k, p, n$: compute $E[\tilde{\eta}_{k,p}(n)]$	$\forall p, n$: compute $E[\tilde{\eta}_{k,p}(n)]$
$\forall k, p, n$: compute $Var[\tilde{\eta}_{k,p}(n)]$	$\forall p, n$: compute $Var[\tilde{\eta}_{k,p}(n)]$
$\forall k, p, n$: compute $L_m[x_k^I(n)]_p, L_m[x_k^Q(n)]_p$	$\forall p, n$: compute $L_m[x_k^I(n)]_p, L_m[x_k^Q(n)]_p$

where the off-diagonal entries of $Cov[x_k(n)]$ are considered zeros, as the real and imaginary parts x_k^I and x_k^Q of $x_k(n)$ are assumed uncorrelated. The same procedure can be adopted to calculate $L_m[x_k^Q(n)]$. The channel coefficient estimates are not assumed to be perfect as in [8], in fact the estimated variance and channel are included into the detector algorithm, and these estimates in practice reduce the ability of the detector to remove the correlation introduced by the channel.

3.3.1.1 PIC and SIC detectors

The multiuser detectors are classified into two main types, successive interference cancellation (SIC) and parallel interference cancellation (PIC). The SIC type takes a serial approach to remove the MAI signals. In each stage, a regenerated interference replica cancels out one user from the received signal so that the remaining users see less interference in the next stage. Also the first user sees all of the interference from the remaining users. Therefore, this approach can be conducted in descending order of the received signal power of each user. The removal of the strongest signal gives the most advantage to the remaining users and the weakest users will see a great reduction in their MAI.

In contrast, the PIC detector estimates and simultaneously removes all the MAI produced by the other users accessing the channel. The initial estimates are used to generate a delayed estimate of the received signal for each user and sum all but the interested user's estimate to form the MAI estimate for each user. In this way, the MAI for each of user is generated in parallel and subtracted simultaneously from the received signal in a single stage. The process can be repeated for multiple stages and each stage takes the decision estimates of the previous stage [76].

The detection details for both methods in the first stage are outlined in Table. 3.1. These detectors provide significant improvement over conventional detectors. For every cancellation stage, a bit of delay is required. The SIC is accompanied by a long processing delay in the order of the number of active users and the computation stages required to complete the job. Hence, a balance must be made between the number of users that are cancelled and the delay that can be tolerated. The delay required to complete the operation in the PIC is at most a few bit periods and due to the inherent advantage of this short processing delay, PIC is more practical than SIC [77].

3.3.1.2 Oscillation problem in IC detectors

The IC detectors improve the system performance continuously with increasing number of stages. Due to error propagation, sometimes these detectors achieve a worse performance in the current stage than in the previous one. This problem is known as *oscillatory behaviour*, which may result in a failure of convergence [78]. In such detectors, the feedback decisions of (3.17) and (3.18) in the previous stage are used to estimate the channel coefficients and regenerate the MAI signal that is removed from the multiuser signal in the current stage.

However, the errors in the decisions result in an incorrect interference reconstruction and these false values of interference are subtracted from the received signal. Therefore, these errors are propagated to the corresponding bits of other users and the MAI signal can potentially be increased instead of removed. To reduce the effects of this phenomenon, some measures can be implemented as follows:

- The quality of data estimates can be improved before they are used to reconstruct the interference. In this way, error correction codes, such as convolutional code, are included in each iteration.

- Soft estimations rather than hard, can be fed to the CE and IC detectors. Thus, the generated interference is subtracted from the reliable data and limits the influence of the unreliable data.

- The partial IC that uses a weight factor can be utilized to scale the estimated MAI from the previous hard decisions before subtracting them from the multiuser signal. This scaling can also reduce the sensitivity to errors in the regenerated MAI signal.

3.3.2 MMSE Channel Estimation

As shown in Fig. 3.2 (a), the CE in coherent IDMA receivers is performed before despreading at chip level, where the SNR is very low, and it provides channel coefficients $\hat{\mathbf{h}}(n)$ to be used in the detector. The finite impulse response (FIR) filter in Fig. 3.3, is used in the estimation process and the output can be written as

$$\hat{r}(n) = \sum_{m=0}^{M-1} \hat{h}_m(n)\tilde{y}(n-m), \tag{3.19}$$

and in vector form as

$$\hat{r}(n) = \tilde{\mathbf{y}}^T(n)\hat{\mathbf{h}}(n), \tag{3.20}$$

where $\hat{h}(n) = [\hat{h}_0(n)...\hat{h}_{M-1}(n)]^T$ represent the filter coefficients and M is the order of the FIR filter. Thus, $\hat{r}(n)$ is simply the convolution between the *a priori* information $\tilde{\mathbf{y}}(n) = [\tilde{y}(n), ..., \tilde{y}(n+M-1)]^T$ and the filter $\hat{\mathbf{h}}(n)$. Based on the MMSE criteria, the cost function J_{min} corresponding to the optimal filter weights can be expressed as [79]

$$\begin{aligned} J_{min}(n) &= E\{|e(n)|^2\} = E\{|r(n) - \hat{r}(n)|^2\} = E\{|r(n) - \tilde{\mathbf{y}}(n)\hat{\mathbf{h}}(n)|^2\} \\ &= E[r^2(n)] - 2\hat{\mathbf{h}}^T(n)E[r(n)\tilde{\mathbf{y}}(n)] + \hat{\mathbf{h}}^T(n)E[\tilde{\mathbf{y}}(n)\tilde{\mathbf{y}}^T(n)]\hat{\mathbf{h}}(n). \end{aligned} \tag{3.21}$$

In training based algorithms, a short sequence of $\tilde{\mathbf{y}}(n)$ must be known in order to determine the optimal tap weight values of the filter. Assuming that the $\tilde{y}(n)$ and the received sequence $r(n)$ are stationary zero mean random processes, (3.21) can be written as

$$J_{min}(n) = \sigma_r^2 - 2\hat{\mathbf{h}}^T(n)\mathbf{c}_{r\tilde{y}}(n) + \hat{\mathbf{h}}^T(n)\mathbf{C}_{\tilde{y}\tilde{y}}(n)\hat{\mathbf{h}}(n), \tag{3.22}$$

where σ_r^2 represents the variance of $r(n)$. The autocorrelation matrix $\mathbf{C}_{\tilde{y}\tilde{y}}$ and the

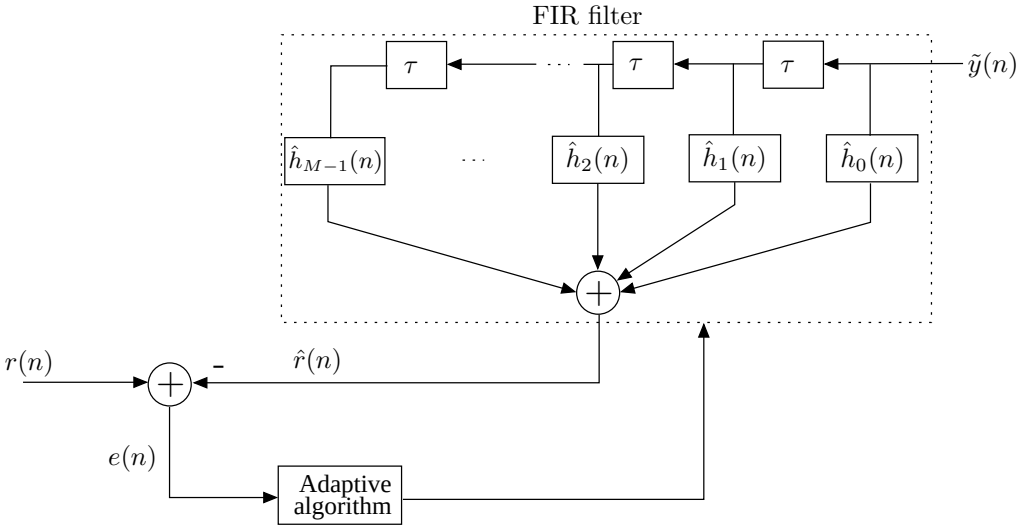

Figure 3.3: CE technique using FIR filter.

crosscorrelation vector $\mathbf{c}_{r\tilde{y}}$ are given by

$$\mathbf{C}_{\tilde{y}\tilde{y}}(n) = E[\tilde{\mathbf{y}}(n)\tilde{\mathbf{y}}^T(n)], \tag{3.23}$$

$$\mathbf{c}_{r\tilde{y}}(n) = E[r(n)\tilde{\mathbf{y}}^T(n)], \tag{3.24}$$

The cost function in (3.21) is a quadratic function of $\hat{\mathbf{h}}(n)$ and can be minimized by setting its gradient with respect to $\hat{\mathbf{h}}(n)$ to zero. That is

$$\nabla|_{\hat{\mathbf{h}}(n)} J_{min}(n) = -2\mathbf{c}_{r\tilde{y}}(n) + 2\mathbf{C}_{\tilde{y}\tilde{y}}(n)\hat{\mathbf{h}}(n) = 0, \tag{3.25}$$

therefore, the optimum filter coefficients are given by

$$\hat{\mathbf{h}}_{opt}(n) = \mathbf{C}^{-1}_{\tilde{y}\tilde{y}}(n)\mathbf{c}_{r\tilde{y}}(n). \tag{3.26}$$

The (3.26) is also referred to as the matrix form of the Wiener-Hopf equation. However, the estimation of Wiener filter coefficients requires inversion of the autocorrelation matrix $\mathbf{C}_{\tilde{y}\tilde{y}}(n)$, which can be impractical if M is large. Moreover, the channel coefficients might change over time and it is almost impossible to make an estimate that would be valid for the next symbol. Therefore, adaptive structures are often required to accomplish this task.

3.3.2.1 Adaptive LMS/NLMS channel estimation

Based on the MMSE criterion, the optimum channel coefficients were derived in the previous section. The MSE in (3.21) will be also used here but in a slightly different way. By substituting all expected values with their corresponding instantaneous values, the MSE can be expressed as

$$|e(n)|^2 = |r(n)|^2 - 2r(n)\hat{\mathbf{h}}(n)\tilde{\mathbf{y}}(n) + \hat{\mathbf{h}}^T(n)\tilde{\mathbf{y}}(n)\tilde{\mathbf{y}}^T(n)\tilde{\mathbf{h}}(n), \tag{3.27}$$

and the instantaneous gradient $\nabla|_{\hat{\mathbf{h}}}\{|e(n)|^2\}$ can be found by taking the derivative of (3.21) as

$$\begin{aligned} \nabla|_{\hat{\mathbf{h}}(n)}\{|e(n)|^2\} &= \nabla|_{\hat{\mathbf{h}}(n)}\{|r(n) - \tilde{\mathbf{y}}(n)\hat{\mathbf{h}}(n)|^2\} \\ &= -2\tilde{\mathbf{y}}(n)\{r(n) - \hat{\mathbf{h}}^T(n)\tilde{\mathbf{y}}(n)\} \\ &= -2\tilde{\mathbf{y}}(n)e^*(n), \end{aligned} \tag{3.28}$$

where $\tilde{y}(n) = [t_r(n), \sum_{k=1}^{K} \tilde{x}_k(n)]$ is the feedback *a priori* information about $x_k(n)$. The gradient in (3.28) represents the unbiased gradient estimate and can be used later to simplify the solution. However, the optimum set is approached by moving the non-optimal set in the opposite direction of $\nabla|_{\hat{\mathbf{h}}(n)}\{|e(n)|^2\}$. Thus, the MSE in its quadratic form can be written as

$$J(n) = J_{min}(n) + (\hat{\mathbf{h}} - \hat{\mathbf{h}}_{opt})^T \mathbf{C}_{\tilde{y}\tilde{y}}(n)(\hat{\mathbf{h}} - \hat{\mathbf{h}}_{opt}), \tag{3.29}$$

By taking the gradient of (3.29) with respect to the filter weights and moving in the negative direction of the gradient vector, a very simple recursion using a stochastic gradient algorithm can be found as

$$\begin{aligned} \hat{\mathbf{h}}(n+1) &= \hat{\mathbf{h}}(n) - \frac{\mu}{2}\nabla|_{\hat{\mathbf{h}}(n)}J(n), \\ &= \hat{\mathbf{h}}(n) - \frac{\mu}{2}\nabla|_{\hat{\mathbf{h}}(n)}\{|e(n)|^2\}, \end{aligned} \tag{3.30}$$

where the adaptation constant μ controls the algorithm convergence to the optimum filter weights, and the negative sign guarantees the movement in the opposite direction of the gradient.

By using (3.28) and after further algebraic manipulation, (3.30) can be represented as [80]

$$\hat{\mathbf{h}}(n+1) = \hat{\mathbf{h}}(n) + \mu\tilde{\mathbf{y}}(n)e^*(n). \tag{3.31}$$

The iterative algorithm in (3.31) is used by the well known least mean square (LMS) algorithm to find the filter tap weights. In addition, due to the estimation error $e(n)$, optimality can not be guaranteed. However, (3.31) is a function of the tap-input signal power of the vector $\tilde{\mathbf{y}}(n)$, which is unknown and varies with time. Consequently, this makes it very sensitive to select the adaptation parameter μ that guarantees the algorithm's stability. In order to overcome this difficulty the normalized LMS is employed. The Normalised least mean squares (NLMS) algorithm is a special realization of the LMS algorithm that solves this problem by normalising the step size parameter which results in a stable and fast converging algorithm. The coefficient update of the NLMS algorithm is [81]

$$\hat{\mathbf{h}}(n+1) = \hat{\mathbf{h}}(n) + \frac{\mu}{\epsilon + \|\tilde{\mathbf{y}}(n)\|^2}\tilde{\mathbf{y}}(n)e^*(n), \tag{3.32}$$

where $0 < \mu < 2$ represents the step size, ϵ is a small positive constant, and

$$\|\tilde{\mathbf{y}}(n)\|^2 = [\sum_{m=0}^{M-1} |\tilde{\mathbf{y}}(n,m)|^2], \tag{3.33}$$

is the Euclidean norm of the tap-input vector $\tilde{\mathbf{y}}(n)$ at time n. In rapidly time varying channels, it is practically impossible to remove the Doppler effects without an estimator. Therefore, $\hat{\mathbf{h}}(n)$ is computed as

$$\hat{\mathbf{h}}(n+1) = \hat{\mathbf{h}}(n) + \frac{\mu}{\epsilon + \|\tilde{\mathbf{y}}(n)\|^2}e^*(n)\tilde{\mathbf{y}}(n)e^{-j\hat{\phi}(n)}, \tag{3.34}$$

where the phase correction parameter $\hat{\phi}(n)$ is optimized using an explicit estimator, such as a phase-locked loop (PLL) explained in next section. An estimate of $\hat{\sigma}_w^2$ can be given using the time average of the squared error.

$$\sigma_{\hat{w}}^2 = \sigma_e^2 = E[e(n)e^*(n)]. \tag{3.35}$$

The problem with (3.34) is that not all of $\tilde{y}(n)$ is known to the receiver. Therefore, the soft/hard estimates of $\tilde{x}_k(n)$ are incorporated into the CE together with $t_r(n)$. Moreover, if the channel is varying slowly, it may be satisfactory to estimate a channel, which is constant over a frame of data; otherwise the channel coefficients should be updated every chip interval.

3.3.2.2 Sparse characteristics and parameters selection

In general, the choice of M is proportional to the channel dimension and it becomes more computational as it covers the overall delay channel spread. Therefore, M should be chosen such that the most significant part of the delay spread is covered to maintain the stability of the algorithm and reduce the noise error contribution. A large M will project too much noise on the channel response estimates as well as increase the estimation error. In contrast, a small M will project too little signal energy onto the channel estimates.

However, the extended multipath in real channels, such as UACs, may have a sparse structure or gaps in time where there is no ISI in the CIR. In such cases, most of the taps do not contain multipath components but noise. By using a threshold at the outputs of each tap, it suffices to keep only the taps with significant amplitude. The energy is considered to be noise if the amplitude is below the threshold, and the output from that tap will be zero. The energy is considered to have a signal component if the output is above the threshold, and will be combined with the other taps. As a result, the tracking capability of the algorithm will improve due to the reduction of the number of taps to be tracked. Then, algorithms with the generated sparse vector can have reduced complexity and memory requirement. In addition, with a long filter length, the assumption on tracking becomes unrealistic if the channel variation is significant. Unfortunately, an acceptable choice is not always available especially when the channel has long delay spread and fluctuates rapidly [19].

The value of μ decides how far the update will take the FIR coefficients in the negative direction of the gradient. Therefore, choosing a small value will lead to a slow convergence, while a very large μ might alter the coefficients too much. Consequently, there must be a compromise between the MSE value of the update process and fast tracking capability.

3.3.2.3 Soft/Hard feedback decisions based CE

For the classical theory of CE [81], the transmitted symbols are either considered completely unknown or completely known to the receiver. In iterative CE, the mean and variance in (3.17) and (3.18), respectively, of each transmitted symbol rather than the symbol itself is known from the previous iteration. The extrinsic information $L_{dec}[x_k(n)]$ is subtracted from $L_m[x_k(n)]$ before being used as input to the soft/hard mapper and MUD detector. Let $\Gamma(.)$ be the input/output relation of the chip mapper, which can be formulated as

$$\tilde{x}_k(n) = \Gamma_{\tilde{x}_k(n)\epsilon\gamma} \{L_{dec}[x_k^I(n)], L_{dec}[x_k^Q(n)]\}, \tag{3.36}$$

where γ is the space of the one-to-one function defined according to the mapping scheme and function type. In Fig. 3.4, in the case of hard mapping the sign function (sgn) is used as a mapping function and its space defined as $\gamma\epsilon\{-1, 1\}$, whereas the tanh(.) function is used in soft mapping. Thus, the outputs $\tilde{x}_k^I(n)$, $\tilde{x}_k^Q(n)$ of the chip detector are used to generate the QPSK symbols as

$$\tilde{x}_k(n) = \text{sgn}\left\{\frac{L_{dec}^I[x_k(n)]}{2}\right\} + j\text{sgn}\left\{\frac{L_{dec}^Q[x_k(n)]}{2}\right\}, \tag{3.37}$$

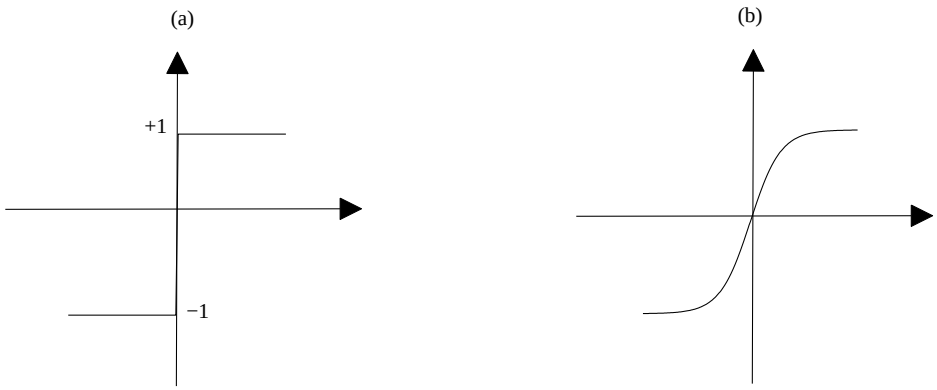

Figure 3.4: Tentative decision devices (a) Hard-limited (one bit quantizer) (b) Hyperbolic tangent (soft quantizer) .

for hard symbol estimation, and

$$\tilde{x}_k(n) = \tanh\left\{\frac{L^I_{dec}[x_k(n)]}{2}\right\} + j\tanh\left\{\frac{L^Q_{dec}[x_k(n)]}{2}\right\}, \tag{3.38}$$

for soft symbol estimation. Moreover, soft feedback is intuitively better than hard feedback as it improves tracking capability by reducing error propagation due to the relatively large detection amplitude errors of hard decisions for dynamic channels [11, 16].

3.3.3 Carrier Phase Tracking

In UACs, the symbol phase is often path dependent and rapidly varying with time. The residual phase fluctuations impair the estimation operation. A phase coherent system must estimate the carrier phase error in order to detect the transmitted symbols properly. In practice, a tracking mechanism is used to estimate the gradient in conjunction with a recursive equation of the form

$$\hat{\phi}(n+1) = \hat{\phi}(n) + a\varepsilon(n), \tag{3.39}$$

where $\varepsilon(n)$ represents the phase error measurement, and a is the positive adaptation constant selected to provide the desired loop gain and bandwidth. By restricting the observation interval to include only the current symbol a simplified expression for the phase error measurement can be given as

$$\varepsilon(n) = Im\{r^*(n)\hat{r}(n)\} = Im\{r^*(n)\tilde{y}(n)\hat{h}(n)\exp^{-j\hat{\phi}(n)}\}, \tag{3.40}$$

where $Im\{.\}$ refers to the imaginary part [82]. The phase synchronization technique is decision-directed, since it is assumed that over the observation interval the information sequence has been estimated correctly. During the training period $\tilde{y}(n)$ is precisely known, while in the decision directed mode it is derived from $\tilde{x}(n)$ by utilizing the feedback decisions.

3.3.4 Joint CE, PLL and Detection

The major difficulty in such receivers is the need to estimate the initial channel parameters as the estimation doesn't have the benefit of *a priori* information in the first iteration. Therefore, good initialization is necessary to minimize the error in (3.27). In the first iteration, where errors usually exist since no feed back decisions are available, a hypothetical transmit sequence $\tilde{x}_k(n)$ is considered, where the non-training symbols are made up of a sequence of symbols in [+1, -1]. Initializing to the zero vectors would require a larger number of iterations and higher computation cost. This estimate can then be used to start the equalization and detection in Section 3.3.1, and compute the LLRs after removing the training sequence part.

The detection process is used to reconstruct the channel symbols and mitigate the ISI and MAI jointly using a PIC approach. The LLRs after detection are passed through deinterleavers, despreader blocks and channel decoders. The decoders generate the LLRs of the coded bits $L_d[x_k(n)]$ for exchange after interleaving with iterative detection and CE. These feedback decisions in the form of extrinsic information are assumed to be correct. Therefore, the hypothetical sequence is replaced by $\tilde{y}(n)$ after the hard/soft feedback decision of (3.37) or (3.38), respectively, to refine the CE. Repeating the above procedure can improve the performance with enhanced channel tracking capability, and after a number of iterative operations, a hard decision is performed on the decoded data. During the process, the $\hat{\mathbf{h}}(n)$ update is guided by a common error signal $e(n)$, the initial estimates of the carrier phase can be obtained from the training sequence during training mode. Because the expected values of the priori information vary with time and iteration, the filter coefficients also change to track the channel variability. However, it is important to note that if there is no noise and if the channel response is of finite length, then it can be completely estimated using a training sequence equal to this length, and the estimation can be taken out of the turbo process.

3.4 Continuous Pilot-Based IDMA Architecture

In this section, the details of the IDMA receiver with continuous pilots in Fig. 3.5 are briefly presented with CE. The pilots are transmitted concurrently with the users' data and used to obtain an initial CE such that a turbo detection process can be

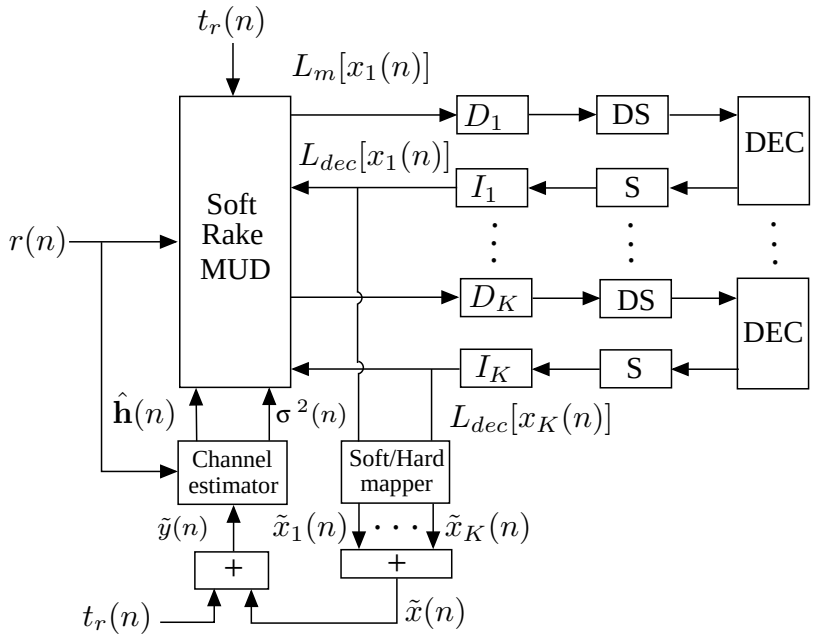

Figure 3.5: IDMA receiver with continuous pilots.

initiated. Moreover, the sequence could be also helpful for the acquisition stage and synchronization process.

3.4.1 Soft-Rake MUD

The LLRs values can be computed following an approach similar to the detection approach in Section 3.3.1. Since the continuous pilot sequence does not take part in the detection, the sequence is removed before detection and $E[\tilde{\eta}_{k,p}(n)]$ of the distortion term $\eta_{k,p}$ in (3.12) is calculated as

$$E[\tilde{\eta}_{k,p}(n)] = h^*_{k,p}(n)E[r(n+p)] - |h_{k,l}(n)|^2\{E[x_k(n)] - t_r(n)\}\,,\ \forall k,n \tag{3.41}$$

However, the parts of the receiver with channel decoding are also updated iteratively to break the correlation between users' data and enhance soft feedback chips that are subsequently used to improve CE and the detection process.

3.4.2 Channel Estimation

In training-based estimation, the receivers have *a priori* knowledge of the data being sent over the channel. This knowledge can be utilized to obtain an accurate estimate of the unknown channel and eliminate detection errors. The method is insensitive to noise, is hardware implementable and the sequence can be chosen to have certain desirable characteristics. However, the method with multiplexed pilots is wasteful in terms of bandwidth, and the unknown channel can only be estimated from the embedded sequence after receiving the whole frame. Moreover, the process might not be enough for fast varying channels since the channel coherence time might be shorter than the frame time. Therefore, semi-blind methods can be used with continuous pilots to improve the quality of training-based methods.

The continuous pilots are different from the conventional time multiplexed pilots, which consume part of the available system bandwidth and are used along with Wiener-Hopf filters to obtain reliable channel estimates. Such an estimate in UACs, where the SNR is very low and the channel is possibly fast fading channels, could only be achieved if a large number of pilot symbols were used. Moreover, a coarse estimate of the channel in the pilot assisted scheme may also be possible by using a small number of pilot symbols. However, the proposed approach in the sense of minimizing the MSE of the CE is different from the optimal approach in [23] as it allows us to take the fading characteristics properly into account. The computational complexity of this estimator in (3.26) is dominated by the inversion of a matrix with dimensions growing linearly with the number of chips. However, for the expression with time-varying channel coefficients, the LMS or NLMS algorithm is subsequently employed to estimate the tap values.

In this adaptive approach, the system begins with a coarse estimate of the channel and the initial estimates are obtained with help from the continuous pilots $t_r(n)$. The estimated channel derived from only pilots is unreliable and poor until the first channel has been used. The impulse response vector is used to start the joint MAI and ISI cancellation of (3.14), and compute $L_m[x_k(n)]$ for all users. At later iterations, $\tilde{y}(n) = t_r(n) + \sum_K^{k=1} \tilde{x}(n)$ is passed into the CE to update each path. Thus, channel information is refined with the combination of the pilot sequences and the updated soft estimates. The advantage of the training sequence is that the CE is actually trained at each time instant where the estimate is needed for detection.

3.5 Soft-Rake CDMA Receiver Architecture

Most existing multiuser detection CDMA algorithms (e.g., [9]) usually operate at symbol level, unlike the chip detection strategy in the IDMA system. The CDMA receiver is reformulated in a similar way to the IDMA receiver in Fig. 3.2 (a). Although the chip detection strategy is developed for IDMA systems, it can be directly applied to CDMA systems as well [83]. By doing so, CDMA is only a special case of IDMA and the differences between them are illuminated. However, CDMA separates multiple users using different spreading codes, which are random and differ from symbol to symbol. In addition, CDMA places the interleavers between the despreaders and decoders as in Fig. 3.2 (b), operating at the bit level, and are used to alleviate the fading effect.

3.6 Simulation Results and Discussions

In this section, simulation results of the IDMA and CDMA architectures explained in the preceding sections are presented under different simulation environments. The performance of these architectures is tested with various adaptive algorithms, training sequence approaches and channel conditions.

3.6.1 PIC versus SIC

The IDMA system employing K=4 users with equal power and N_b=512 randomly generated information bits are encoded by a repetition encoder with L=8. After scrambling and interleaving, the chips are modulated by a QPSK mapping, and then linearly superimposed and transmitted over the AWGN channel. Fig. 3.6 shows the BER results obtained using PIC and SIC of the uncoded IDMA system. The solid lines and dashed lines represent the BERs obtained using the PIC and SIC, respectively, after iterations 1, 2, 4 and 8. As the number of iterations and $\mathrm{E_b/N_0}$ increases the PIC converges to the SIC. Iteration gains can be obtained with SIC even at the second iteration, which is enough to achieve a BER greater than 10^{-4}. However, PIC can also reach this limit but after the fourth iteration. In other words, SIC needs less iterations than PIC to reach the same performance, therefore, the behaviour of SIC only differs from PIC with respect to the required number of iterations. However,

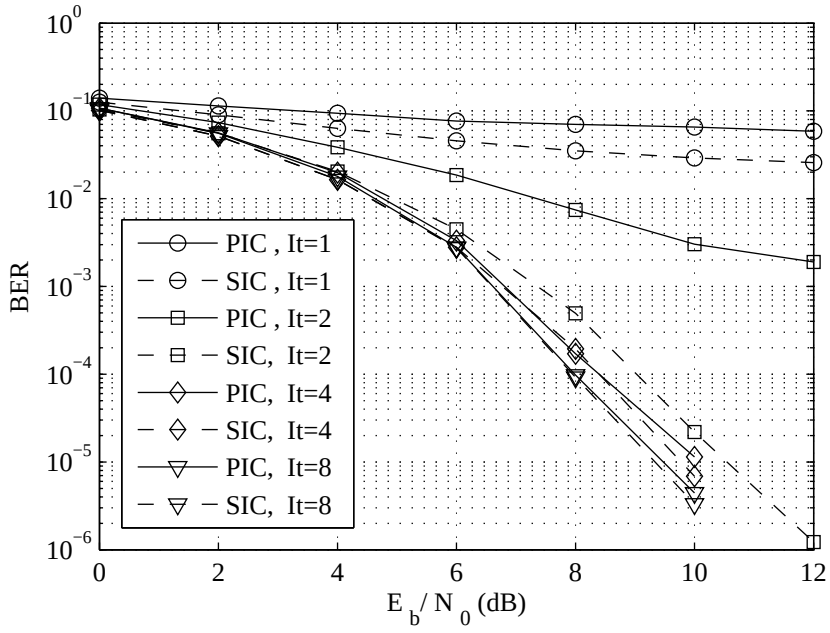

Figure 3.6: Performance of uncoded PIC/SIC IDMA with different number of iterations.

parallel processing is the reason for considering PIC in this thesis.

3.6.2 Performance Results over Time-invariant Channels

In this section, simulations have been performed to evaluate the performance of IDMA and CDMA systems over time-invariant channels. The performance of IDMA and CDMA systems over a 24-path fixed channel with exponentially decaying power profile is shown in Fig. 3.7 for coded systems. In these simulations, there are four and eight equal energy users, K= 4, 8, N_b=512, R=1/2 and L=8. Thus, the system throughput is $(K \times 1/N_s \times R)$ representing the overall bandwidth efficiency. It is assumed that the channel is known at the receiver and 8 iterations were selected for both systems. All the interleavers and spreading codes are independent and randomly generated.

It can be seen that IDMA and CDMA systems require a E_b/N_0 of more than 6 dB to achieve the BER of 10^{-4}. The IDMA system performs the best in all cases with different numbers of active users and the performance of long code CDMA is quite close to the performance of the short code CDMA. The performance with K =4 for high values of E_b/N_0 is similar to the performance when there is no ISI and it requires

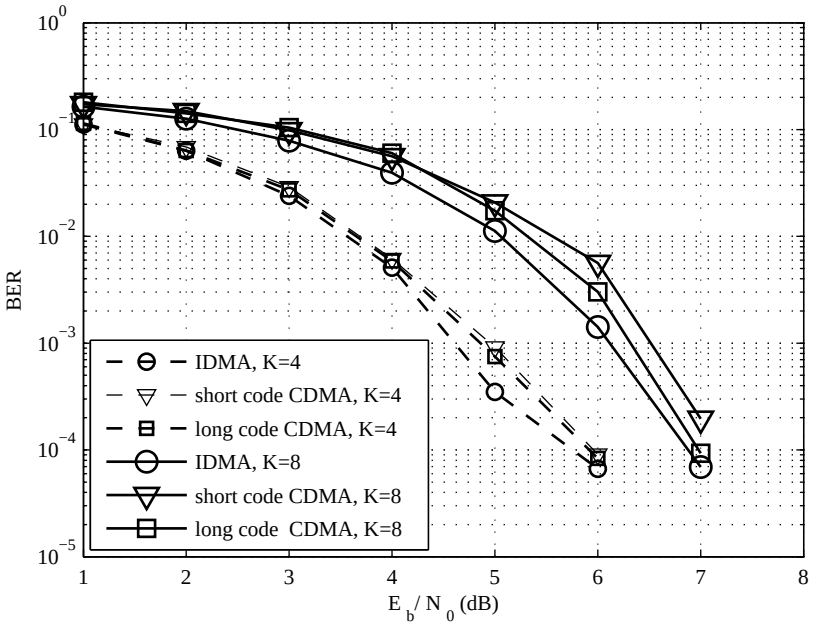

Figure 3.7: The BER results of CDMA and IDMA over fixed known channel.

only a 1 dB improvement to get the same BER of 10^{-5}. While in a highly user-loaded scenario with K =8, the performance can be further improved by performing more iterations or increasing the spreading gain. This improvement can be explained since IDMA uses chip level extrinsic information instead of bit level information in CDMA systems, which is more accurate and results from the spreading operation incorporated into the algorithm.

In reality, the channel coefficients are unknown at the receiver and the equalization process should be adaptive. Fig. 3.8 illustrates the performance of the IDMA and CDMA receivers using LMS and NLMS algorithms over a multipath channel with impulse response $h(n) = [0.04, -0.05, 0.07, 0.21, 0.72, 0.36, 0.21, 0.03, 0.07]$. This channel has minimum phase characteristics and is widely used in the literature, e.g. [60]. Besides the data symbols, a pseudo random QPSK training sequence of length 100 known to the receiver is multiplexed to form the transmitted signal. The same previous parameters are employed with four active users K=4. The adaptive constants μ for the LMS and NLMS algorithms with M=12 were chosen empirically to be 0.01 and 0.03 with ϵ =10^{-6}, respectively. Similar performance results that illustrate the comparison between IDMA and CDMA are also visible in Fig. 3.7. Moreover, the

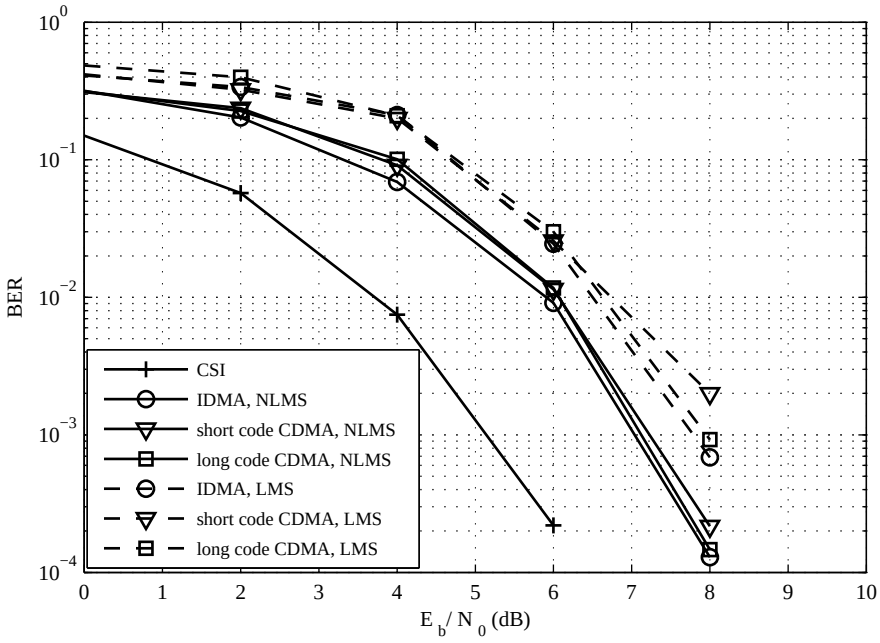

Figure 3.8: BER comparison of CDMA/IDMA over unknown fixed channel using different adaptive algorithms.

performance of the LMS algorithm is 3 dB away from the ideal case of the known channel denoted as CSI. The performance using the NLMS algorithm is much closes and is only 2 dB away from the CSI bound. These results can be justified as the LMS algorithm exhibits the slowest convergence compared to the NLMS algorithm, which shows rapid convergence properties. Therefore, the NLMS algorithm will be used in the remainder of the thesis, unless otherwise stated, to track the dynamic nature of the channel.

3.6.3 Performance Results over Time-varying Channels

In this section, the IDMA system is simulated over time varying channels with K=2, 4 equal power users, 1024 information bits and QPSK mapping. All active users employ the same convolutional code with rate $R = 1/2$, and the repetition length was L=8 chips per information bit. The interleavers and the pilot sequences are generated randomly and independently with length 100 and 1024 QPSK symbols for the multiplexed and continuous pilots approach, respectively. The results are obtained using 4 to 8 iterations and the receiver has no knowledge of the delays. The simulated

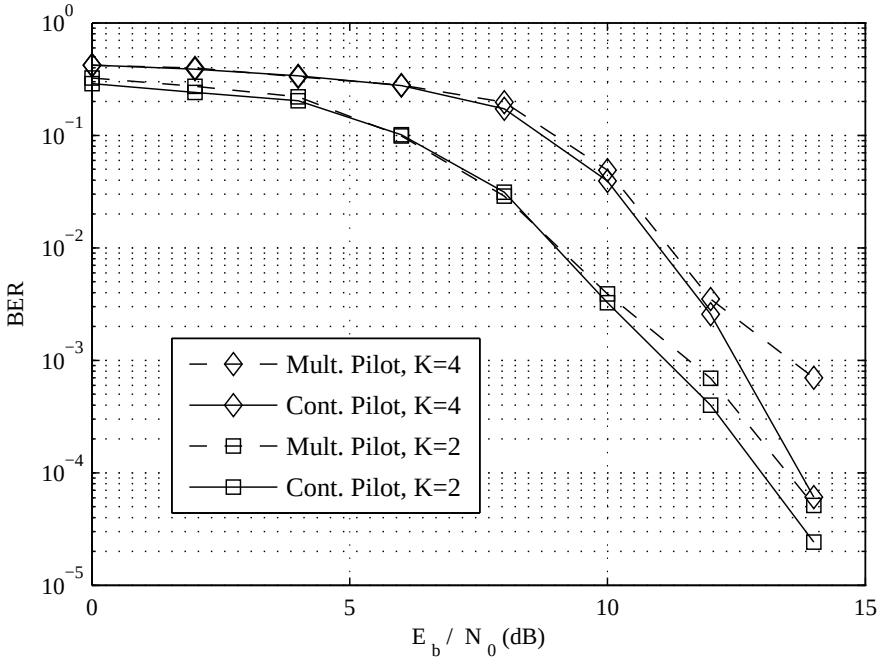

Figure 3.9: The performance of IDMA over time varying channel, T_c=10^{-4}, F_d=10 Hz and adaptive parameters: (a) Mult. pilot (M, μ)=(8, 0.01), (b) Cont. pilot (M, μ)=(8, 0.01).

channels are modelled by utilizing Rician characteristics with a direct path and four secondary paths resulting from bottom and surface reflections. The multipath spread was 6 ms and the maximum Doppler frequency varied from 10 to 100 Hz. The value of the Rice factor is chosen to be 2 for all simulations. The channel has a normalized Doppler frequency $F_d.T_c = 0.001$ with a system load 4/12.

Fig. 3.9 presents the BER results after 5 iterations with the continuous pilots embedding method. The results of the multiplexed pilot method are also included for comparison. It is seen that the pilot assisted method loses very little performance compared to the case of a continuous pilot method at high values of E_b/N_0. The two methods have the same performance at low E_b/N_0. However, the system with continuous pilots transmits each packet in a shorter time duration. Therefore, the proposed pilot is more bandwidth efficient than the multiplexed pilot schemes. All the adaptive parameters are indicated in Fig. 3.9.

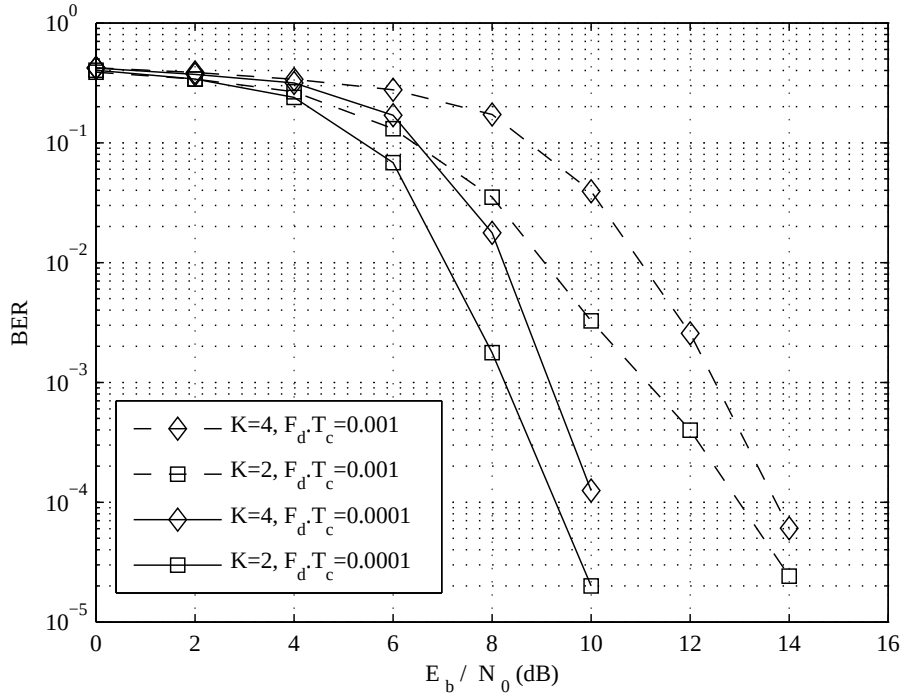

Figure 3.10: The performance of IDMA over different fading rate, the system parameters: (a) slow fading rate (T_c, F_d, M, μ)=(10^{-6}, 100 Hz, 8, 0.001), (b) fast fading rate (T_c, F_d, M, μ)=(10^{-4}, 10 Hz, 8, 0.01).

For both slow and fast fading channels, the results of continuous pilot based CE are shown in Fig. 3.10 with normalized Doppler frequency $F_d.T_c$= 0.0001 and $F_d.T_c$ = 0.001, respectively. The total performance degradation incurred by an adaptive NLMS CE depends on the actual fading rate and on the deviation of the adaptive constant. The performance of the scheme with a slow fading rate is better than the performance with a higher fade rate. The performance degradation is about 2 dB at a BER of 10^{-4}. However, the performance of the CE with continuous pilots is limited by the energy of the training chips. In addition, increasing the number of users will reduce the convergence speed of the NLMS algorithm compared to the scenario with no interference due to an increased input energy. The CIR estimates and the actual channel with $F_d.T_c = 0.001$ for paths 1, 2 are illustrated in Fig. 3.11 for the first 4000 chips with the corresponding MSE. The plot shows how the simulated channel varies with time and how the estimated taps coefficients are close to the simulated ones.

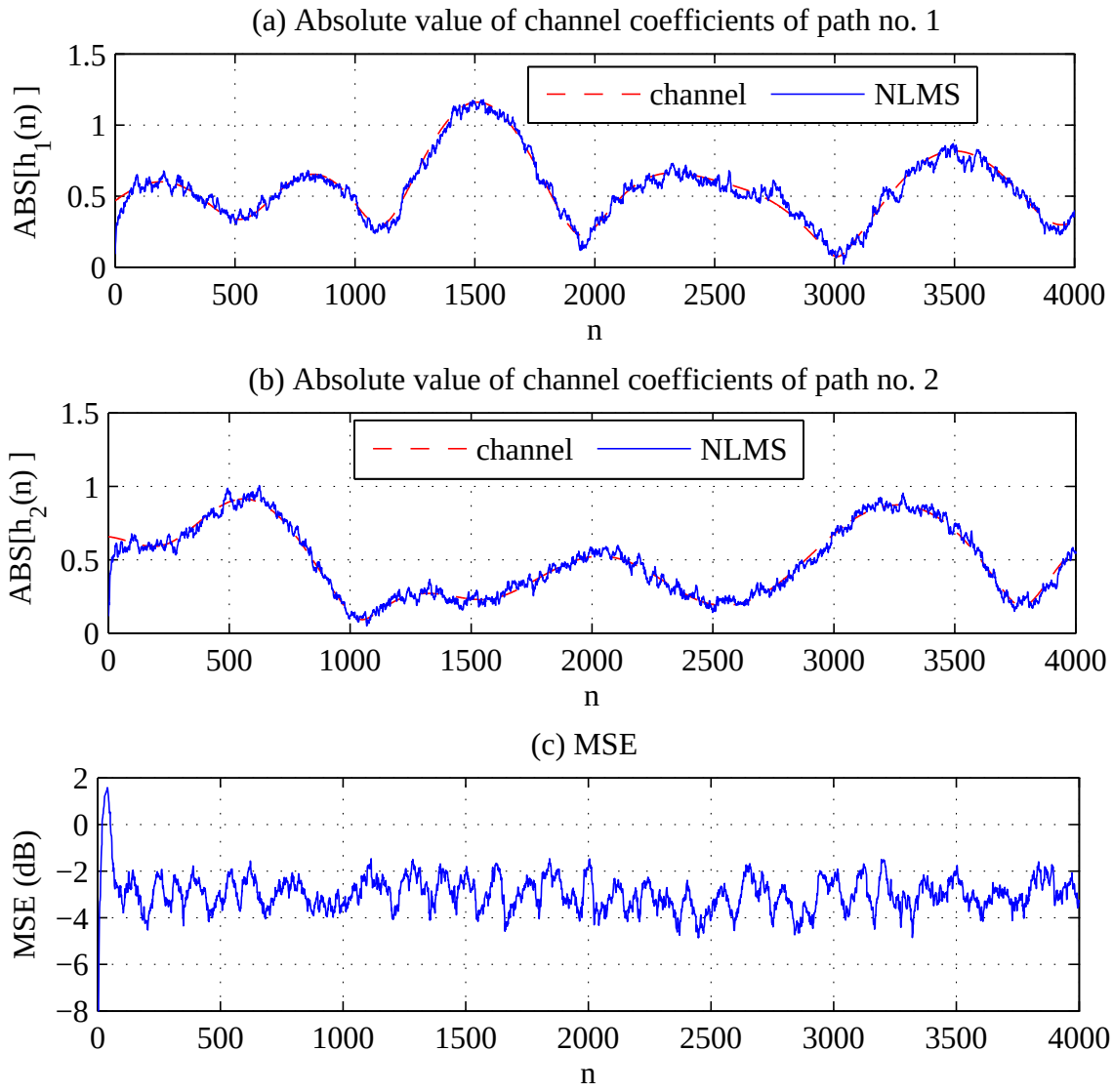

Figure 3.11: Channel tracking performance using continuous pilot of paths 1, 2 and MSE over a five-path fading channel at $F_d T_c = 0.001$.

3.7 Summary

In this chapter, two different T-MUDs both employing spread spectrum techniques, are examined for reliable communication over different channels. By interleaving chips differently for different users, the IDMA system outperforms CDMA slightly in terms of BER performance. Furthermore, a time-domain CE and phase correction

scheme that are suitable for integration in turbo IDMA and CDMA architectures are developed in Section 3.3.2 using two different pilot methods. The semi-blind CE schemes adapt the filter coefficient at chip rate and are capable of tracking rapid time variations of the channels. In Section 3.3.2.1, two different adaptive algorithms, LMS and NLMS, are used to estimate the channel parameters with low computational complexity. The adaptive estimation was significantly refined by using either multiplexed pilots or continuous pilots and soft feedback symbol estimates after channel decoding. Since pilot symbols are transmitted along with the data, tracking using continuous pilots in Section 3.4 was found to be more bandwidth efficient and the performance was shown to be a better technique than the conventional pilot-based approach. In addition, the SIC performance only differed from PIC with respect to the required number of iterations. Further investigation is required to enhance the reliability of the proposed algorithm particularly in highly dynamic mediums.

CHAPTER 4

Direct Adaptation Based Turbo Architectures

4.1 Introduction

THE realization of a robust receiver that constantly tracks the channel is difficult due to the dynamics of multipath arrivals, causing severe ISI. Unfortunately, for sound channels, which significantly vary over symbol duration, proper CE becomes very difficult at low probability of intercept. Chip-level DFE can have better immunity against the spectral channel characteristics, reduce the noise enhancement effect and also give the forward filter greater flexibility in handling ISI. In this chapter, the principles of direct adaptive techniques are extended to the context of downlink IDMA transmissions. Since IDMA is a variation of CDMA but with long random chip interleavers, IDMA detection methods are introduced to the CDMA systems to improve performance. These direct adaptive turbo receivers for IDMA and CDMA systems utilizing coherent detection, joint chip-level DFE and turbo IC detectors, are investigated under different channel conditions, where all the users' signals are distorted by the same multipath channel.

In addition, the convergence behaviour of the proposed detectors over unknown time variant channels is evaluated with the help of EXIT charts. However, the convergence property of T-MUDs is not only related to its architecture and channel conditions, but also related to the system parameters. Specifically, the mutual information exchanges between the MUD unit and channel decoders can further provide information on the interfering users' signals and the correct selection of such significant parameters. The impact of these parameters, e.g., the user number, the spreading factor, different code memory lengths and the block length, can be easily analyzed with EXIT charts to obtain a better understanding in the design of successful T-MUDs. An overview of the proposed IDMA/CDMA receivers is presented in Section 4.2 and Section 4.4, respectively, based on MMSE criterion and using two different training methods. Channel coding and spreading trade-off are explained in Section 4.5, and Section 4.6 introduces the EXIT chart principles. Our simulation results and EXIT chart analysis are presented in Section 4.7, followed by the summary in Section 4.8.

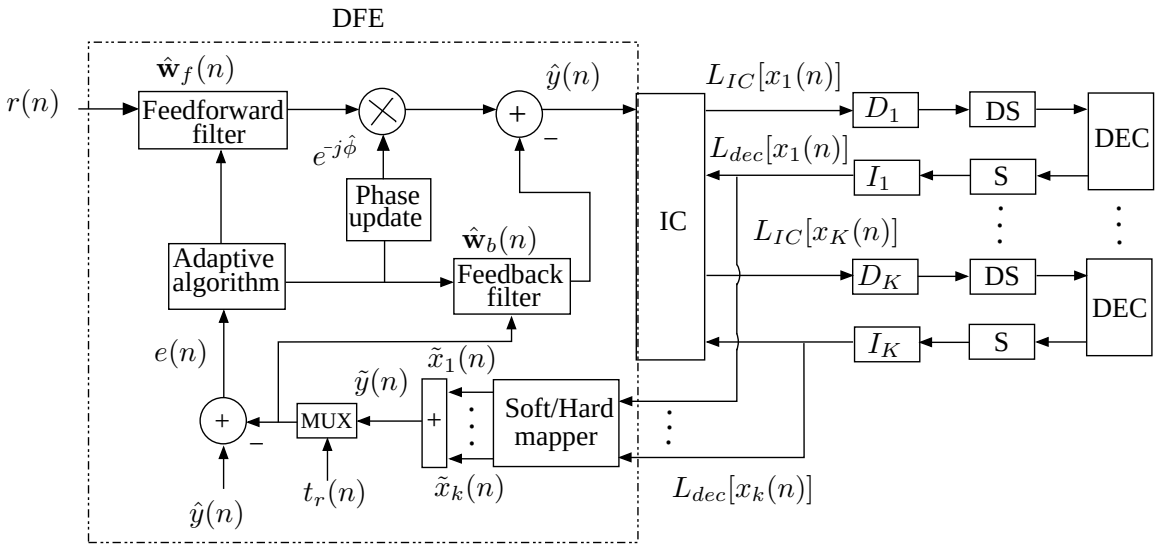

Figure 4.1: Adaptive DFE-IDMA receiver architecture

4.2 Chip-level DFE-IDMA Receiver Architecture

The receiver operations consist of an acquisition stage, an adaptive DFE joint phase tracking stage, a cancellation process stage and channel decoding. A block diagram of the receiver is presented in Fig. 4.1. In the original IDMA receiver, the soft Rake and interference cancellation (IC) concepts are combined, which allows each arriving multipath signal to be individually detected and summed to recover the K users' bits, respectively. The iterative receiver, instead of treating the interfering users as background noise, exploits the signal structure to perform joint detection for all users' data by using knowledge of the interfering users. The IC unit employs a low cost chip detection strategy which avoids matrix operations [9] or conventional MAP detection [65], and applies only IC in contrast to the MMSE filtering utilized in CDMA [9].

4.2.1 Optimal Chip-level DFE

A chip level DFE block diagram is depicted in Fig. 4.1. The optimization of the FIR filters is performed through minimization of the MSE, $e(n) = \tilde{y}(n) - \hat{y}(n)$, which is determined in the decision-directed mode as the difference between the output of the equalizer $\hat{y}(n)$ and the reconstructed MAI transmitted signal $\tilde{y}(n)$ of a feedback

decision device. The minimization problem of the cost function $J(n)$ can be stated as [29, 84]

$$J(n) = \min_{\hat{\mathbf{w}}_f(n), \hat{\mathbf{w}}_b(n)} E\{|e(n)|^2\}, \tag{4.1}$$

where the $\hat{\mathbf{w}}_f(n) = [w_0(n) \cdots w_{M_f}(n)]^T$ and $\hat{\mathbf{w}}_b(n) = [w_{-1}(n) \cdots w_{-M_b}(n)]^T$ are the complex-valued tap-weight vectors of the feedforward (FF) and feedback (FB) filters, with M_f and M_b taps, respectively. The symbol estimate output from a DFE structure can be given as

$$\hat{y}(n) = \hat{\mathbf{w}}_f^H(n)\mathbf{u}_f(n) + \hat{\mathbf{w}}_b^H(n)\mathbf{u}_b(n), \tag{4.2}$$

where the $\mathbf{u}_f(n) = [r(n+M_f) \cdots r(n)]^T$ and $\mathbf{u}_b(n) = [\tilde{y}(n-1) \cdots \tilde{y}(n-M_b)]^T$ are the contents of the FF and FB equalizers during the n-th transmitted symbol, respectively. By assuming that the noise variance σ^2 and channel coefficients h are known and constant, i.e. $h_p[n] = h$ for all p. The optimal MMSE-filter coefficients under the correct feedback decisions can be computed as [85]

$$\hat{\mathbf{w}}_{f,op}(n) = (\mathbf{H}_f \hat{\mathbf{V}} \mathbf{H}_f^H + \sigma^2 \mathbf{I})^{-1} \mathbf{h}_c, \tag{4.3}$$

where $\mathbf{H}_f$ is the channel convolution with the form

$$\mathbf{H}_f = \begin{bmatrix} h_0 & h_1 & \cdots & h_{P-1} & 0 & \cdots & 0 \\ 0 & h_0 & h_1 & \cdots & h_{P-1} & 0 & \vdots \\ \vdots & & & \ddots & & & 0 \\ 0 & \cdots & 0 & h_0 & h_1 & \cdots & h_{P-1} \end{bmatrix}, \tag{4.4}$$

the $\hat{\mathbf{V}}$ is a $(M_f + P) \times (M_f + P)$ diagonal matrix, where the first $(M_f + 1)$ diagonal elements are 1 and the remaining $(P - 1)$ diagonal elements are 0. The $\mathbf{h}_c$ is the $(M_f + 1)$-th column of $\mathbf{H}_f$, and $\mathbf{I}$ is the identity matrix with dimension $(M_f + 1)$. The corresponding filter coefficients of the FB are

$$\hat{\mathbf{w}}_{b,op}(n) = -\mathbf{H}_b^H \hat{\mathbf{w}}_{f,op}(n), \tag{4.5}$$

where $\mathbf{H}_b$ is the $(M_f + 1) \times M_b$ matrix

$$\mathbf{H}_b = \begin{bmatrix} \vdots & 0 & & & & & 0 \\ 0 & \vdots & \cdots & & & & \\ h_{P-1} & 0 & & & & & \vdots \\ \vdots & h_{P-1} & & & & & \\ h_2 & \vdots & \ddots & & & & \\ h_1 & h_2 & \cdots & h_{P-1} & 0 & \cdots & 0 \end{bmatrix}. \tag{4.6}$$

From the (4.5) and (4.6), the only first $P-1$ elements of $\mathbf{H}_b(n)$ are non zero, thus, the length M_b does not need to be larger than $P-1$. Repeated matrix inversions would be necessary if the channel was non stationary, so the approach would also be expensive computationally. However, the advantage of this technique can be well approximated by an adaptive FIR filters.

4.2.1.1 Adaptive chip-level DFE

In most practical applications, due to the time varying nature of the communication channels, the filters' coefficients should be estimated in a recursive manner in order to track changes of the phase and channel response. The recursive algorithm is obtained by performing the differentiation with respect to the parameters of interest and setting the gradients to be equal to zero. Therefore, the MSE minimization with respect to the filter tap weights and carrier phase in (4.1) can be simplified by employing an iterative procedure using a stochastic gradient algorithm. The LMS/NLMS algorithms are used to resolve the minimization problem as [81]

$$\hat{\mathbf{w}}_f(n+1) = \hat{\mathbf{w}}_f(n) + \frac{\mu_f}{\delta + \|\mathbf{u}_f(n)\|^2}\mathbf{u}_f^H(n)e(n)e^{-j\hat{\phi}(n)}, \tag{4.7a}$$

$$\hat{\mathbf{w}}_b(n+1) = \hat{\mathbf{w}}_b(n) + \mu_b\mathbf{u}_b^H(n)e(n), \tag{4.7b}$$

where $\hat{\phi}(n)$ is a phase correction parameter, $0 < \mu_f < 2$ and $0 < \mu_b < 2/||\mathbf{u}_b(n)||^2$ are the step-size adaptation constants, δ is a small positive constant employed to avoid numerical instabilities, $(.)^H$ is the Hermitian transpose operator, and $\|\mathbf{u}_f(n)\|^2$ is the Euclidean norm of the FF filter input vector.

An equalizer can compensate for phase variations introduced by the multipath channel, but this is not the case especially in underwater communications, where the residual carrier frequency offset causes equalization tap rotation and missadjustment may eventually cause the taps to diverge. Therefore, proper equalization operation requires a phase compensator [1]. The phase update is optimized jointly using a first order PLL [82]

$$\hat{\phi}(n+1) = \hat{\phi}(n) + a\varepsilon(n), \tag{4.8}$$

where a is a positive adaptation constant, and $\varepsilon(n)$ represents the phase error measurement, defined as

$$\varepsilon(n) = \mathrm{Im}\{\tilde{y}^*(n)\hat{y}(n)\}, \tag{4.9}$$

where $\mathrm{Im}\{.\}$ refers to the imaginary part and $(.)^*$ represents the complex conjugate operation. After phase correction, the output of the DFE is computed as

$$\hat{y}(n) = \hat{\mathbf{w}}_f^H(n)\mathbf{u}_f(n)e^{-j\hat{\phi}(n)} - \hat{\mathbf{w}}_b^H(n)\mathbf{u}_b(n). \tag{4.10}$$

In addition, the recursive nature may sometimes cause problems such as error propagation if the training sequence is not used and the approach without a training sequence is only possible once the eye is initially wide open. However, the desired signal $\tilde{y}(n)$ in the training mode is precisely known and the error signal is written as

$$e(n) = t_r(n) - \hat{y}(n), \tag{4.11}$$

where $t_r(n)$ is the training sequence, which is common for all users. It is worth mentioning that, although the error $e(n)$ contains the signals of all users including the desired one, the equalizer does not suppress them due to the common propagation channel in the forward direction.

4.2.1.2 Feedback ISI Canceller

The estimate of future data symbols, as well as past symbols, of the previous stage can be utilized to further improve the feedback ISI cancellation process as in [84, 86]. In such approach, the impulse responses h_f and h_b of the FF filter and the FB filter, respectively, must satisfy the condition

$$h_f = C_p^h, \quad -P \leq p \leq -1, \tag{4.12}$$

$$h_b = C_p^h, \quad 1 \leq p \leq P, \tag{4.13}$$

in which the autocorrelation channel function C_p^h defined by

$$C_p^h = hh_p = \sum_{i=-\infty}^{\infty} h_i h_{i-p}^*. \tag{4.14}$$

However, in the absence of significant pre-cursor arrivals in the CIR and assuming that the length, M_b, of the FB filter is equal to or greater than the channel dispersion P, post-cursor ISI due to the previous symbols, $\hat{I}(n)$, can be completely removed as

$$\hat{I}(n) = \hat{\mathbf{w}}_b^H(n)\mathbf{u}_b(n), \quad M_b \geq P. \tag{4.15}$$

Thus, the optimum choice of filter length greatly depends on the shape of the CIR. Under the assumption that all detected symbols are correct, then given perfect knowledge of the ISI structure, all the pre-cursive and post-cursive ISI could be cancelled exactly without any noise enhancement. In practical situations, the FF and FB filters have different lengths and large filter lengths may be required to achieve satisfactory implementation of the FF and FB filters. The exact selection of M_f and M_b is explained later in Section 5.6.1.1.

4.2.1.3 Error propagation problem

In general, the chip level DFE produces errors due to the fact that the DFE is a non-linear device and has been designed under the assumption that the delay hard feedback decisions are correct, which is not the case in practice. Therefore, error propagation can occur due to uncorrelated errors of the decision detector or decoders that result from the combinations of noise and residual ISI/MAI. Moreover, due to decision delays and modelling errors over the observation intervals, the fading rate results in prediction errors.

An erroneous decision tends to propagate and cause a burst of errors in future symbol decisions. This effect becomes a major impairment to the equalizer behaviour in UACs and the performance will degraded relative to the optimal DFE. In practice, iterative DFE and powerful coding techniques are needed to achieve low bit error rates under severe multipath conditions. The soft estimations explained in Section 4.2.3 rather than the hard, are required to avoid unreliable adaptation.

4.2.2 Chip-level IC Detector

Iterative detector is used to separate the equalized mixed signal $\hat{y}(n)$ coming from the DFE and decode the transmitted data from each of the users. The IC stage is developed from the IDMA concepts described in [8]. One of the key advantages of this concept is the inherent output of reliability information, which helps to reduce error propagation in the DFE efficiently. The DFE does not heavily depend on the assumptions regarding the statistical properties of the input signal and its performance in the absence of decision errors is comparable to that of a ML sequence estimator [1]. Assuming that the adaptive equalization is ideal, we may express the soft output $\hat{y}(n)$ as

$$\hat{y}(n) = x_k(n) + \eta_k(n), \tag{4.16}$$

where

$$\eta_k(n) = \sum_{k'=1,\ k' \neq k}^{K} x_{k'}(n) + w(n), \tag{4.17}$$

consists of MAI and the noise signal present in $\hat{y}(n)$ with respect to user k. If we assume $x_k(n)$ is an independent and identically distributed (i.i.d) random variable, the remaining interference $\eta_k(n)$ with respect to user k can be approximated by a Gaussian random variable. Due to the central limit theorem this approximation is sufficiently good especially for a large number of users. However, the Gaussian approximation of the distortion term may be inaccurate as the number of users becomes small. Nevertheless, the benefit of less interference generally offsets the problem due to inaccurate interference modelling [87]. Therefore, $\hat{y}(n)$ can be characterized by a conditional probability density function. The $L_{IC}[.]$ of the real part, $x_k^I(n)$, of $x_k(n)$ can be estimated as

$$\begin{aligned} L_{IC}[x_k^I(n)] &= \log\left(\frac{Pr[\hat{y}^I(n)|x_k^I(n)=+1]}{Pr[\hat{y}^I(n)|x_k^I(n)=-1]}\right) \\ &= \log\left(\frac{\exp\left[-\dfrac{\{\hat{y}^I(n)-E[\eta_k^I(n)]-1\}^2}{2Var[\eta_k^I(n)]}\right]}{\exp\left[-\dfrac{\{\hat{y}^I(n)-E[\eta_k^I(n)]+1\}^2}{2Var[\eta_k^I(n)]}\right]}\right) = \frac{2\{\hat{y}^I(n)-E[\eta_k^I(n)]\}}{Var[\eta_k^I(n)]}. \end{aligned}$$

Thus,

$$L_{IC}[x_k^I(n)] = \frac{2\{\hat{y}^I(n)-E[\hat{y}^I(n)]+E[x_k^I(n)]\}}{Var[\hat{y}^I(n)]-Var[x_k^I(n)]},\ \ \forall k,n, \tag{4.18}$$

with

$$E[\hat{y}(n)] = \sum_{k=1}^{K} E[x_k(n)], \quad \forall n, \tag{4.19}$$

and

$$Var[\hat{y}(n)] = \sum_{k=1}^{K} Var[x_k(n)] + \sigma_w^2, \quad \forall n, \tag{4.20}$$

where $E[.]$ and $Var[.]$ represent the mean and variance, respectively. The noise $w(n)$ is not available and is replaced by the error signal of (4.11). Therefore, an estimate of $\hat{\sigma}_w^2$ can be obtained by time averaging the squared error

$$\hat{\sigma}_w^2 = \sigma_e^2 = E[|e(n)|^2]. \tag{4.21}$$

Furthermore, the $L_{IC}[.]$ of the imaginary part, $x_k^Q(n)$, of $x_k(n)$ can be computed in a similar manner as the real part $x_k^I(n)$. The *a priori* means and variances of the transmitted signal $x_k(n)$ are also required, which are calculated as in [9] based on the chip feedback information $L_{dec}[x_k(n)]$, that is

$$\begin{aligned} E[x_k^I(n)] &= \frac{Pr[x_k^I(n) = +1] - Pr[x_k^I(n) = -1]}{Pr[x_k^I(n) = +1] + Pr[x_k^I(n) = -1]} \\ &= \frac{\exp\{x_k^I(n)\} - 1}{\exp\{x_k^I(n)\} + 1} = \tanh\{L_{dec}[x_k^I(n)]/2\}, \quad \forall k, n, \end{aligned} \tag{4.22}$$

and

$$Var[x_k^I(n)] = 1 - \{E[x_k^I(n)]\}^2, \quad \forall k, n, \tag{4.23}$$

according to [8], the term $\{\hat{y}^I(n) - E[\eta_k^I(n)]\}$ is the soft-interference cancellation step for chip n. In general, very large LLRs values may cause divergence of the iterative detection, while the decrease in $e(n)$ with time and very small LLRs cause the detection process to converge slowly and the impact of the decision feedback error vanishes iteratively. Therefore, to avoid instability caused by the positive feedback during an iterative operation, the *a priori* information of $x_k(n)$ should not be used itself. For this reason, during detection the *a priori* mean $E[x_k(n)]$ and $Var[x_k(n)]$ in (4.22) and (4.23), respectively, are used.

4.2.2.1 PIC based IC detector

The detection/decoding algorithm can be carried out by a PIC. For the detection process in (4.18)-(4.23), the de-correlating and decoding operations can be carried out simultaneously for all users to update the *a priori* information for the next iteration. Alternatively, the same set of equations may be utilized using a successive interference cancellation (SIC) scheme. In the case of the SIC algorithm, the operations are carried out on a user-by-user basis and the means and variances of interference are partially updated after the decoding of user k is completed. In an optimal manner and with Rake reception, the details of these schemes with and without channel coding are presented in [76] and [83], respectively. Moreover, the comparative performance in Chapter 3 demonstrated only a small difference between these schemes in terms of bit error rates when the scrambling code is used. However, if all signals from separate users are received with equal power levels, and due to the short processing delay present irrespective of the number of active users, the PIC is preferred in practice. In contrast, the SIC has long processing latency, which is proportional to the number of active users.

4.2.3 Soft Estimation Based Turbo Architectures

Equalization and detection requires spread and modulated chips to improve the ISI rejection iteratively. The extrinsic information $L_{dec}[x_k(n)]$ is subtracted from $L_{IC}[x_k(n)]$ before being used as input to the soft/hard mapper and IC detector. Thus, the outputs $\tilde{x}_k^I(n)$, $\tilde{x}_k^Q(n)$ of the chip detector can be used to form QPSK symbols as (3.37) and (3.38). If the regeneration and cancellation of interfering user signals use hard feedback decision functions, the interference may increase from the error propagation of incorrect chips. Therefore, the hard chip decisions are replaced by soft decisions of (3.37), because an error in the feedback decisions will propagate in subsequent iterations and the performance of the adaptive process regresses due to this error-propagation.

In addition, the soft approach decreases the probability of error propagation in the feedback decisions and gradually improves system performance in terms of BER and tracking ability. Due to the absence of error propagation, the soft device tends towards the hard limiter at very high SNRs and hard mapping is considered to be optimal in this case.

4.2.4 Joint Chip-level DFE and IC Detector Operation

Joint adaptive multiple access systems using error correcting codes are considered to be serially concatenated systems, in which the adaptive detectors take the role of the inner decoder, and the decoders take the role of the outer decoder. The iterative receivers effectively exploit the *a priori* information of coded symbols, to repeat the equalization and improve their convergence performance.

In the training mode, the signal $\tilde{y}(n)$ in (4.10) represents the known training symbols, $t_r(n)$, so that equalizer coefficients, $\hat{\mathbf{w}}_f(n)$ and $\hat{\mathbf{w}}_b(n)$, are initially derived from correct decisions in order to speed-up the convergence of the algorithm. However, in the decision-directed mode, there are no $L_{dec}[x_k(n)]$ values at the first iteration from the single-user detectors, therefore, the input of the FB filter is not available. In order to overcome this problem, the hard limited $\hat{y}(n)$ can be used for the initial input of the FB filter. At that time, the MSE is used as follows

$$e(n) = \mathrm{sgn}\{\hat{y}(n)\} - \hat{y}(n). \tag{4.24}$$

The equalized soft symbols $\hat{y}(n)$ during iterative interference cancellation, are given to the IC and the LLRs for each user are obtained using (4.18), where the initial prior information is zero. The extrinsic information is processed by the deinterleavers and the despreader blocks. The decoders generate the bit-level extrinsic LLRs, which are also processed by the interleavers and spreaders. In the next iteration, the new *a priori* information is given to the DFE and the IC, to improve the ISI and MAI cancellation. The newly obtained extrinsic information is mapped according to the decision function and the corresponding constellation points to form new decision symbols $\tilde{x}_k(n)$, which are summed to form $\tilde{y}(n) = \sum_{k=1}^{K} \tilde{x}_k(n)$ and fed to the FB filter. As a result, the estimation of the information of interference can be refined, and the reliability of these new symbols increases with the number of iterations, which in turn helps to reduce the error propagation in the DFE and completely remove residual ISI and MAI. Finally, the output of the decoders are hard limited to form the reconstructed data symbols $\hat{d}_k(n)$.

During the decision-directed mode, $\hat{\mathbf{w}}_f(n)$ and $\hat{\mathbf{w}}_b(n)$ are adapted using the common error signal, $e(n)$, given by (4.7); the initial estimates of the carrier phase can be obtained from the training sequence during training mode, and the phase estimation error is estimated using (4.9). However, since the expected values of the *a priori*

information vary with time and iteration, the filter coefficients also change to track the channel variability.

4.2.5 Partial knowledge detectors

It is an important issue to design the user end without needing to know the other users' parameters. In RF wireless communication, a time reversal (TR) technique is used by [88] with Time-division duplexing (TDD) to develop a simplified downlink transmission. The technique is similar to the pre-Rake operation used in CDMA for alleviating ISI. By exploiting the weak correlations of fading channels for different mobiles, it is helpful to alleviate the interferences. TDD mode is employed to share common channel information and simplify user mobile design; however, perfect channel knowledge is required at the receiver, which is not realistic in practice.

The MMSE multiuser detectors can be adapted blindly without the knowledge of interfering spreading codes. Adaptive forms of these detectors are among the most likely candidates for practical application of MUD. However, as the mobile receiver usually only has knowledge of its own interleaver pattern or spreading code, equalization techniques relying on IC or decision feedback cannot subtract a sufficient amount of interference to yield an acceptable performance, especially with increased number of active users. The performance gain in terms of BER is quite significant and the best performance is achieved by a detector employing knowledge of all interleaver patterns. Therefore, in order to avoid performance degradation, near-far resistant or MUD can be used [66]. In the uplink direction, a common MUD is shared by all users and a bank of DFEs is the possible choice for these receivers, where the channel at the base station is different for every user. Therefore, in order to cancel the interference, knowledge of all user parameters, such as timing and power levels, is required so that users can be separated by means of the different interleavers and different training code. An individual MUD is required for each user in the downlink. At each iteration, a chip level receiver minimizes the MSE according to the available information, which makes the receiver robust in some cases to the presence of unknown codes.

In Section 5.6.2, the partial knowledge of the interfering users is successfully exploited and used to design partially blind detectors. The performance loss in a blind detector is also evaluated quantitatively as compared to MUDs with full knowledge.

4.2.6 Complexity Issues and Channel Decoding

The adaptive receiver differs from conventional IDMA [8], in that the impairments caused by ISI due to multipath propagation effects are processed via an adaptive DFE, and the soft signal $\hat{y}(n)$, as well as, signals originating from different users' decoders are utilized by the IC to remove MAI. The computational cost of the proposed receiver includes reconstructing the channel symbols using the DFE filters, cancelling the interference and channel decoding. The related complexity of the proposed receiver per user is linear in the number of taps $O(P)$, regardless of user number K. In contrast, the complexities of the iterative receivers employing MMSE filtering and optimum detection are $O(K^2)$ and $O(2^K)$, respectively [7–9]. The computational complexity comparison with standard IDMA is detailed in Section 5.7.1. In addition, the required signal processing in underwater communication is often complex due to the physical channel characteristics, which are expected to be of considerable length. Therefore, efficient adaptive algorithms with low complexity are required to achieve the reduction in complexity and improve tracking properties by adjusting receiver parameters. The best choice of adaptive algorithm may change on a packet-by-packet basis and low cost algorithms are less able to decode highly distorted data than other complex algorithms. In this work, LMS and NLMS offer reasonable performance at a tremendous computational saving over RLS. Moreover, in many UACs, the reverberation time may cover tens of symbols, thus making the complexity of the adaptive receiver so large that real time detection becomes impractical.

The decoders calculate the extrinsic LLRs for each bit by exploiting the code structure as well as $L_{IC}[x_k(n)]$. The convolutional decoding process is based on the widely known BCJR algorithm [89]. The BCJR algorithm provides excellent decoding results, but with higher complexity because of K independent decoders. Therefore, reducing the complexity using a switching strategy such as the one proposed in [90] can balance the complexity and performance of such receivers.

4.3 Continuous Pilot Based DFE-IDMA Receiver

Practical adaptive implementations of the chip receivers that can track fast fading multipath channels are not straightforward since no continuous training chip sequence is available. The availability of the continuous pilot signal in Fig. 4.2 enables the

continuous updating of the equalizer parameters to track the channel changes in fast fading mediums. The differences compared to DFE-IDMA with multiplexing pilots are briefly discussed below.

4.3.1 Adaptive DFE Equalization

The forward filter processes the received samples, and ISI at the combiner output is suppressed by the output of a feedback filter fed by the soft estimated multiuser symbols. The filter coefficients are derived from the pilot sequence at the first iteration. Thus, the input of the FB filter can be written as

$$\tilde{y}(n) = t_r(n) + \sum_{k=1}^{K} \tilde{x}_k(n) = t_r(n), \tag{4.25}$$

and this sequence is removed from the equalized received signal $\hat{y}(n)$ before any further processing to form $z(n)$ as

$$z(n) = \hat{y}(n) - t_r(n). \tag{4.26}$$

Moreover, the adaptive algorithm with one stage continuously update the tap weight vectors based on the error signal between the equalized symbols and reconstructed MAI signal at each instant n.

4.3.2 Chip-level IC Detector

The $L_{IC}[.]$ of the real part $x_k^I(n)$, of $x_k(n)$ can be estimated as

$$L_{IC}[x_k^I(n)] = \frac{2\{z^I(n) - E[z^I(n)] + E[x_k^I(n)]\}}{Var[z^I(n)] - Var[x_k^I(n)]}, \forall k, n, \tag{4.27}$$

where $E[z(n)]$ and $Var[z(n)]$ are defined as (4.22) and (4.23), respectively. When the estimated user chips are very reliable and close to the transmitted data, the multiuser chips are equal to their transmitted values. The proposed approach is applicable in the uplink direction like multi-layer IDMA [23], where the channel at the base station is different for every user. Therefore, in order to cancel multi-layer interference, knowledge of all layers is advantageous and the layers can be separated by means of different interleavers and common code. However, extra operations need to be introduced to handle the continuous training sequence contribution in comparing

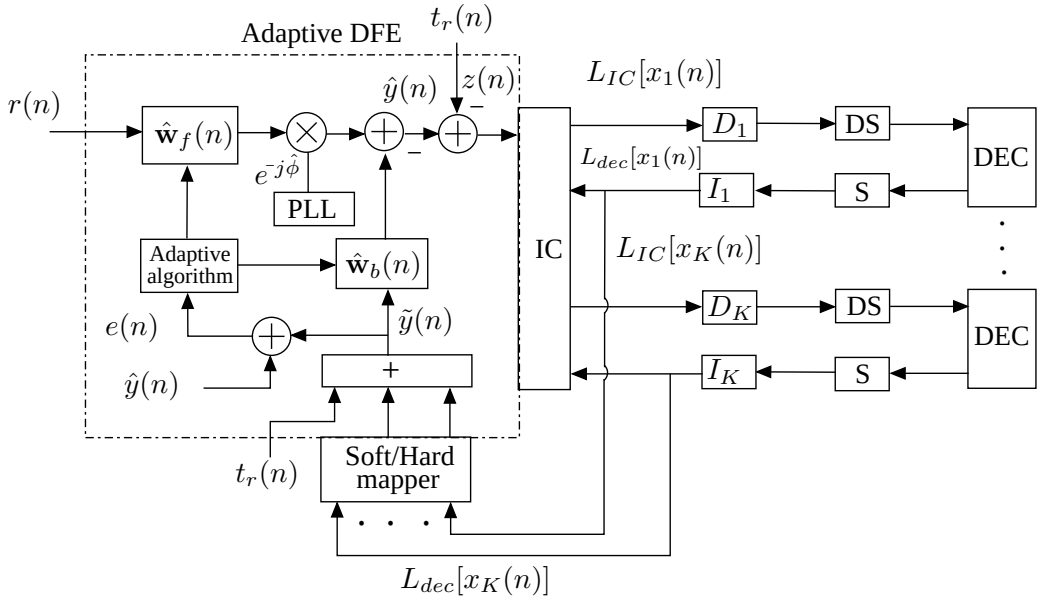

Figure 4.2: Adaptive DFE-IDMA receiver architecture with continuous pilots.

with the conventional concept.

4.4 Adaptive DFE-CDMA Receiver

In the last few years, downlink CDMA receivers have been the subject of an intensive research effort. The use of hypothesis feedback in [3, 32] can be very effective in mitigating ISI in a single user scenario, but for CDMA downlink, the hypothesis for all users should be included and that it is extremely complex. Chip level equalization has been proposed in [91, 92] using non-iterative two-stage equalizer structures that consists of linear equalization and DFE as a second stage. The same receiver structure in [93] with MMSE criterion and decoding units is compared to the conventional MMSE channel equalization. Moreover, DFE based CDMA with short spreading codes is proposed in [29] and with long scrambling codes in [94], whereas linear receivers are investigated in [91]. Most of these receivers have been used for known channels and operate at the symbol level.

The proposed adaptive DFE-CDMA receiver is formulated in a similar way to the DFE-IDMA receiver in Fig. 4.1 and Fig. 4.2, by exchanging the order of I and S as in Fig. 3.2 (b). CDMA separates multiple users using different scrambling codes, which are random and differ from symbol to symbol. The proposed sub-

optimal DFE-CDMA receiver relies on the chip detection approach and avoids matrix operations [9], which are needed to handle the correlation among the user specific sequences. Therefore, the complexity reduction is greatly reduced when compared with other sub-optimal and optimal detection approaches.

4.5 Channel Coding and Spreading Tradeoff

In general, wide-band transmission is more robust against noise or fading problems and the spreading gain is directly proportional to the system bandwidth. However, due to the limited availability of bandwidth in underwater channels increasing the spreading gain to achieve better performance is not efficient. Therefore, in order to maintain a high data rate, spreading sequences of a short length are more desirable. Moreover, as this is a multiuser scenario, each signature sequence must have both good auto-correlation and cross-correlation properties.

The trade-off between channel coding and spreading is another important parameter to maximize capacity. The optimal multiple access channel capacity is achievable only when the entire bandwidth expansion is devoted to coding. This suggests combining the coding and spreading operations using low-rate codes to maximize coding gain. The receivers in combination with very low rate will benefit from the additional coding gain and the added redundancy protects the bits from the errors resulting from the channel. However, the bandwidth expansion is undesirable since the systems imposed by spreading codes decrease the obtainable system capacity, and the choice of spreading codes represents a poor case of coding. Additionally, more uniform performance among the users is available using most of the bandwidth expansion for more sophisticated coding schemes [6, 95]. System design based on coding, thus, provides an efficient use of the limited bandwidth in a multiuser underwater acoustic system [96]. However, one may argue that the potential is greater for systems using only channel coding for bandwidth expansion.

On the other hand, unlike IDMA, the separation of users in CDMA systems without the spreading operation is not feasible. In fact, lower complexity codes such as repetition codes or convolutional codes have been preferred in almost all publications on turbo multiuser detection. However, the optimal bandwidth allocation and coded spread spectrum are the subject of on-going research for shallow water networks.

4.6 Analysis of T-MUD Architectures

The concept of EXIT charts was introduced in [33] as a semi-analytical technique. The substantial technique advantages are to examine the convergence properties and trace the evolution of different receivers' parameters through multiple iterations. The analysis relies on computing the mutual information of the two major components, MUD and decoding blocks, which are denoted by I_m^i, I_m^o and I_d^i, I_d^o, respectively. The inputs of the detector are the received channel impaired signal, $r(n)$, and *a priori* information in the form of LLRs, $L_{dec}[x_k(n)]$. The output is the extrinsic information, $L_m[x_k(n)]$. The decoder has a single input, $L_m[x_k(n)]$, which is the *a priori* information, and outputs extrinsic information, $L_{dec}[x_k(n)]$.

Since the output of the detector is the input of the decoding components, both non-linear transfer functions, $I_m^o = T_m[I_d^i, E_b/N_0, \hat{h}(n)]$ and $I_d^o = T_d[I_d^i]$ are drawn in the same chart with coordinate axes $(I_m^i, I_m^o), (I_d^i, I_d^o)$, where the indexes i and o refer to the input and output respectively. These functions are mapping from input extrinsic information to output extrinsic information, and measure the improvements of the LLR transformations as each block takes LLRs as input and output. However, the input LLRs to the modules are not known, and they are modelled as independent Gaussian variables. During iterations the mutual information points for both blocks forms a detection trajectory and are evaluated independently in a separate process. This process reaches a saturation point, when no innovation can be gained from the modules and the two characteristics intersect in this case. Then, histograms can be used to numerically represent the output probability density function (PDF) and the analysis of these histograms after each iteration provides enough information to predict the convergence behaviour of the iterative system.

4.6.1 Mutual Information Measure

The performance of the receiver components can be evaluated using several measures. The most effective measure is the mutual information, which can be defined between two random variables as [97]

$$I(X; L_m) = \frac{1}{2} \sum_{x_k \in \pm 1} \int_{-\infty}^{\infty} p(l|x_k) \log_2 \left(\frac{2p(l|x_k)}{p(l|x_k = -1) + p(l|x_k = +1)} \right) dl. \qquad (4.28)$$

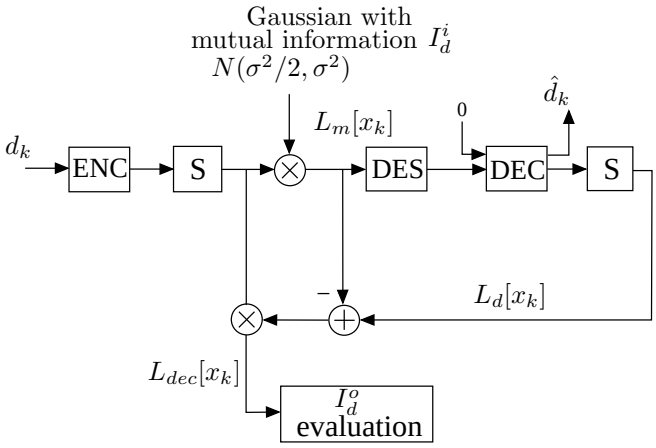

Figure 4.3: Simulation setup for generating transfer function of the joint spreader and decoder.

The symmetry property, $p(l|x_k = +1) = p(-l|x_k = -1)$, holds for any linear code decoded by APP, and the consistency property, $p(l|x_k = +1) = p(-l|x_k = +1)exp(l)$, is satisfied when the output LLRs are accurately computed. If these properties are combined with (4.28), a simple approach to evaluate the mutual information can be obtained as

$$I(X; L_m) = 1 - \int_{-\infty}^{\infty} p(l|x_k = +1) \log_2(1 - e^{-l}) dl, \tag{4.29}$$

which can be closely approximated by the time averages and obtain

$$I(X; L_m) \simeq 1 - \frac{1}{N} \sum_{n=1}^{N} \log_2(1 + \exp^{-L_m[x_k]}), \tag{4.30}$$

where N is the total number of LLRs, $L_m[x_k]$ [98].

4.6.2 EXIT Charts for Decoding Unit

The transfer function of the decoding unit, $I_d^o = T_d[I_d^i]$, maps the input extrinsic information I_d^i of L_m, into output extrinsic information I_d^o of L_{dec}. This transfer function of the joint decoder and spreader is generated using the setup shown in Fig. 4.3. Independent data is encoded using a convolutional encoder and then spread using a simple scrambling repetition code. The input LLRs, $L_m[x_k]$, to the system are modelled as independent Gaussian variables with probability density function $p(l|x_k)$ and variance $\sigma^2/2$. The variance is chosen to match a given input mutual information

value I_d^i such as

$$\sigma = J^{-1}(I_d^i), \tag{4.31}$$

where J is monotonically increasing function and thus invertible. With this transformation, $I_d^i = 0$ represents no reliability information, while $I_d^i = 1$ represents exact knowledge of associated bits. Fig. 4.4 illustrates the variation of mutual information with the variance. After the decoder, the soft extrinsic output symbols are fed to the sink where the mutual information is computed as

$$I_d^o \simeq 1 - \frac{1}{N}\sum_{n=1}^{N} \log_2(1 + \exp^{-L_{dec}(x_k)}), \tag{4.32}$$

The specific value of I_d^o in the range $[0, 1]$ characterizes the quality of the output LLRs of a receiver component. Despite the fact that the LLRs are assumed to be Gaussian distributed, the analysis can also be successfully adopted in multiuser CDMA receivers over multipath channels, where the output of the detector can not be accurately approximated with Gaussian variables [97].

4.6.3 EXIT Charts for MUDs

For the CE based MUD receiver, the system setup used for obtaining the extrinsic information transfer function, $I_m^o = T_m[I_d^i, SNR, \hat{h}(n)]$, is shown in Fig. 4.5. The function maps the input extrinsic information, I_d^i of L_d, into output extrinsic information, I_m^o of L_m, for given channel conditions. The MUD function changes at each iteration, and depends on the variance, channel realizations and other users' priori information. In the setup, the users' data and pilots are generated randomly, summed after QPSK mapping and sent through the channel. In addition, for each of the users' coded symbols, the LLRs are generated and mapped to soft symbols before being sent to the channel estimation as *a priori* information. The *a priori* information of the CE inputs may be generated independently from the code being used or the decoders. However, the CE and detector are not considered as a single unit as in most previous work and the analysis would involve simultaneous activations of the CE and detector. In contrast, the extrinsic information in the DFE-IDMA receiver is exchanged only between the direct adaptive DFE-IC detector and the decoding blocks. Fig. 4.6 describes the system used to generate the EXIT chart of the direct form DFE-IC detector.

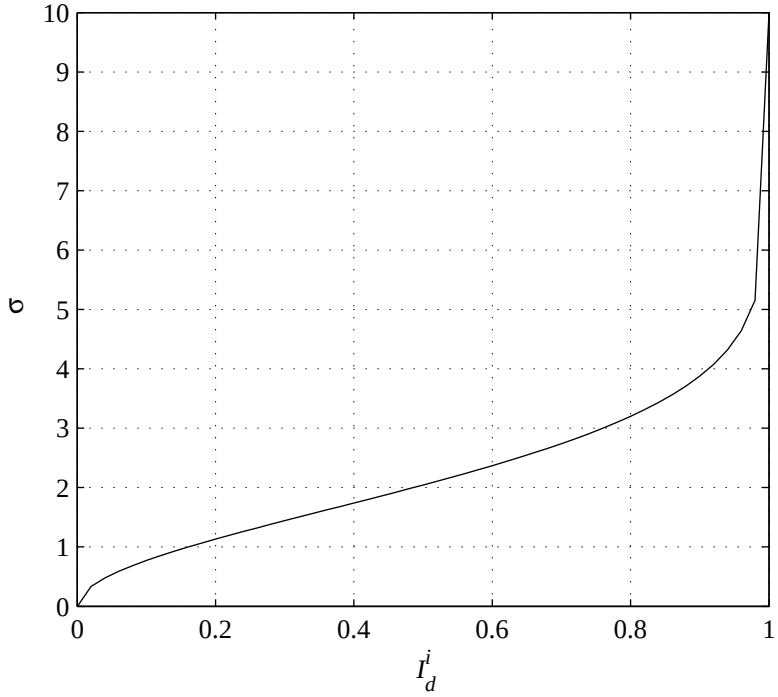

Figure 4.4: The mapping between variance σ and input mutual information I_d^i.

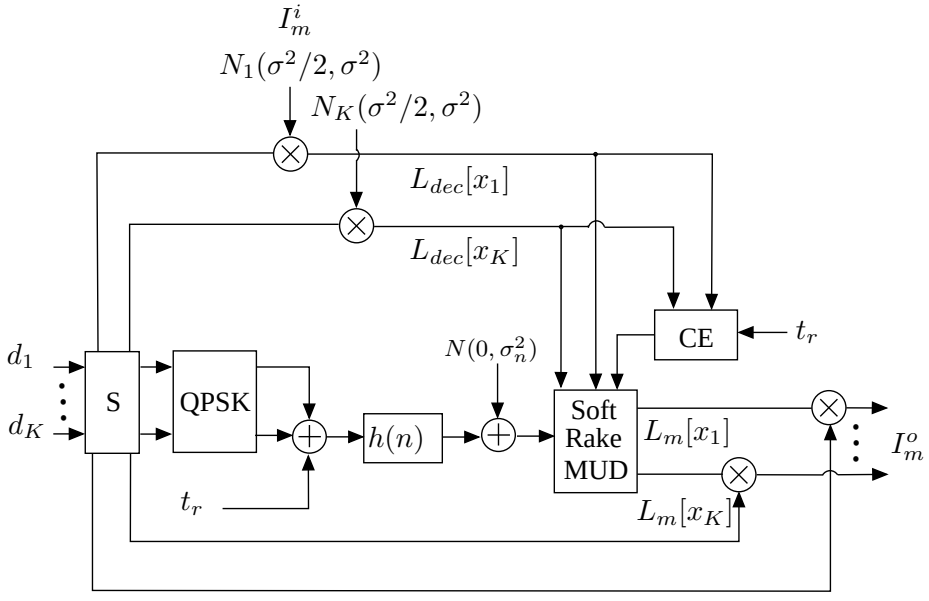

Figure 4.5: Simulation setup for soft Rake multiuser detector with CE.

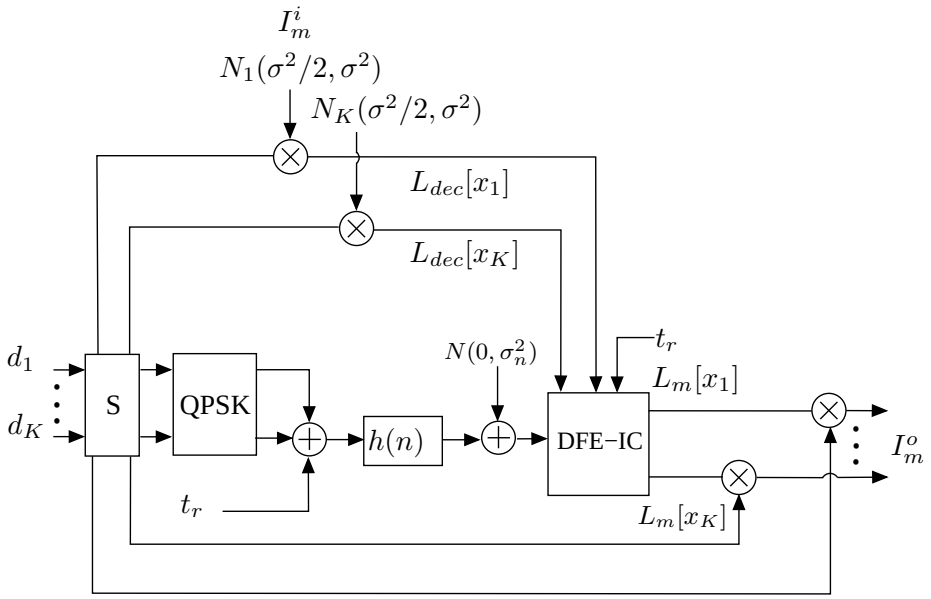

Figure 4.6: Simulation setup for direct form DFE-IC multiuser detector.

4.7 Simulation Results and Discussion

The different receivers of IDMA and CDMA systems are investigated under different parameters and then compared under various scenarios in terms of bit error rates. The simulation results are performed for the forward link of a DFE based IDMA/CDMA system with 2 and 4 active equal power users using QPSK modulation. The information of 512 bits is encoded with a R=1/2 convolutional code with polynomials g=[23, $35]_8$ and spread by a length 8 scrambling repetition code. Both the continuous and time multiplexing pilots are generated randomly and the length of the multiplexing pilot sequence was a 100 chips complex sequence. The results are obtained by 4 to 8 iterations and the Doppler shift compensation is assumed correctly, which simplifies the received signal. All simulation results are carried out on the simulated channels, which are modelled by utilizing Rician characteristics and long multipath spread. The value of the Rice factor is chosen to be 2 for all the simulations and the system parameters are given in the figures. The multipath spread was 3 ms and the maximum Doppler frequency was between 10 and 100 Hz. Identical system configurations are kept for a fair comparison.

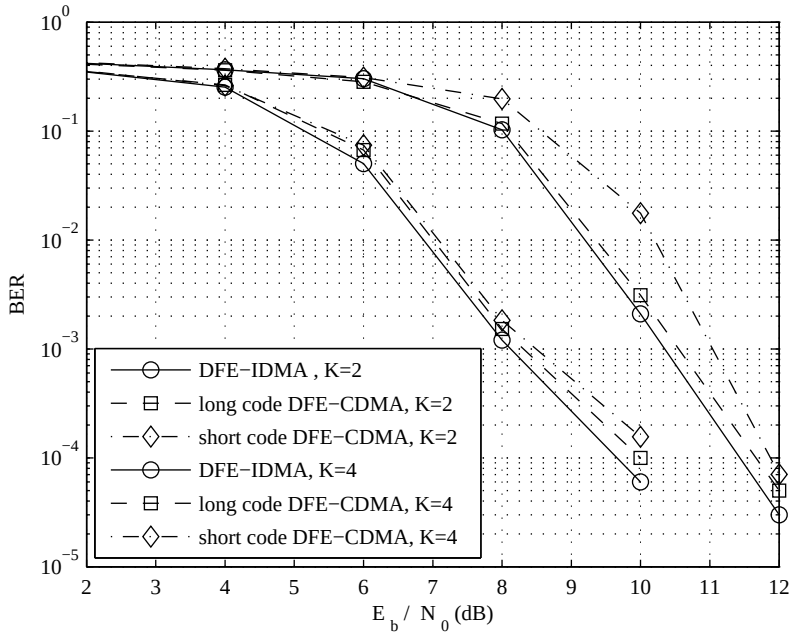

Figure 4.7: Performance comparison of DFE-IDMA, long code DFE-CDMA and short code DFE-CDMA with F_dT_c=0.001, system parameters: (M_f, M_b, μ_f, μ_b) = (6, 6, 0.001, 0.001).

4.7.1 Performance of DFE-IC Based Receivers

The performance of DFE-IDMA is depicted in Fig. 4.7 with other CDMA forms, long code DFE-CDMA and short code DFE-CDMA. The users' spreading sequences in the investigated CDMA systems are randomly generated and they remain the same for all symbols in short code DFE-CDMA, whereas they vary for different symbols in long-code CDMA. The plot shows that the proposed approach can also detect as well CDMA signals and DFE-IDMA performs best in all cases with different number of users due to long period of chip interleavers, which is more effective in highly correlated systems with severe ISI and MAI than the bit level interleavers in CDMA systems. By employing the adaptive DFE-IC technique and despite of its simplicity, both DFE-CDMA forms in Section 4.4, can achieve performance close to that by DFE-IDMA. In the high values of $\mathrm{E_b/N_0}$ and with a relatively small number of iterations, the BERs of all systems with $K = 4$ converge to the $K = 2$ performance. Moreover, the adaptive equalization can provide better performance by suppressing MAI, which is the major distortion factor.

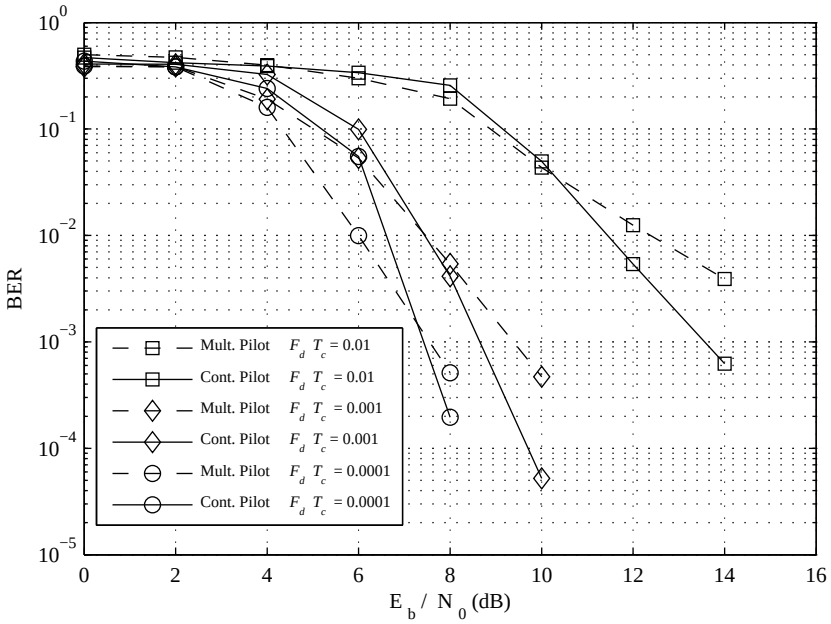

Figure 4.8: DFE-IDMA performance with different Doppler spreads and $K = 2$, system parameters: (a) Mult. pilot (M_f, M_b, μ_f, μ_b)= (8, 8, 0.01-0.001, 0.001-0.0001), (b) Cont. pilot (M_f, M_b, μ_f, μ_b)= (8, 8, 0.01-0.005, 0.01-0.005).

4.7.2 Performance using Different Pilots Schemes

Fig. 4.8 shows the BER versus the SNR of the proposed receiver using a five multi-path time-variant channel with different normalized Doppler spreads. The maximum Doppler frequency is normalized to the chip rate. It is evident that the performance of continuous pilot based equalization remains reasonable over a large range of normalized Doppler spreads. In contrast, the performance of the conventional approach deteriorates for a normalized fade rate F_dT_c=0.01, where the adaptive algorithm with the absence of continuous pilots has difficulty tracking the variation of the channel.

Fig. 4.9 also highlights the performance gains of the continuous pilot based DFE-IDMA receiver, where the continuous pilot approach needs less iterations than the multiplexing training approach to achieve reasonable performance. The performance gain between the third and eight iterations of both turbo multi-user receivers is about 1 dB for a BER of 10^{-3} with normalized fade rate F_dT_c=0.001. The impact of feed back decisions is illustrated in Fig. 4.10. The performance loss of 0.5 dB at BER level of 10^{-3} results from using hard decisions rather than soft decisions. This minor

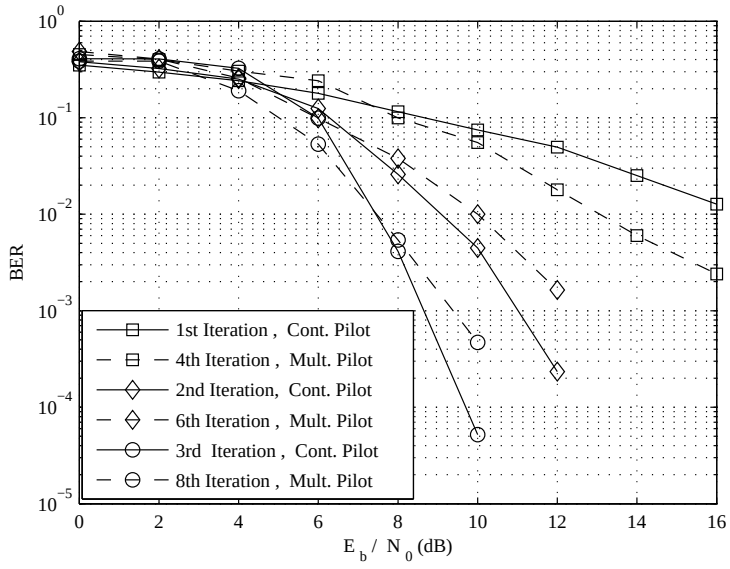

Figure 4.9: DFE-IDMA performance with different iterations, F_dT_c=0.001 and $K = 2$, system parameters : (a) Mult. pilot (M_f, M_b, μ_f, μ_b)= (8, 8, 0.01, 0.001), (b) Cont. pilot (M_f, M_b, μ_f, μ_b)= (8, 8, 0.001, 0.0001).

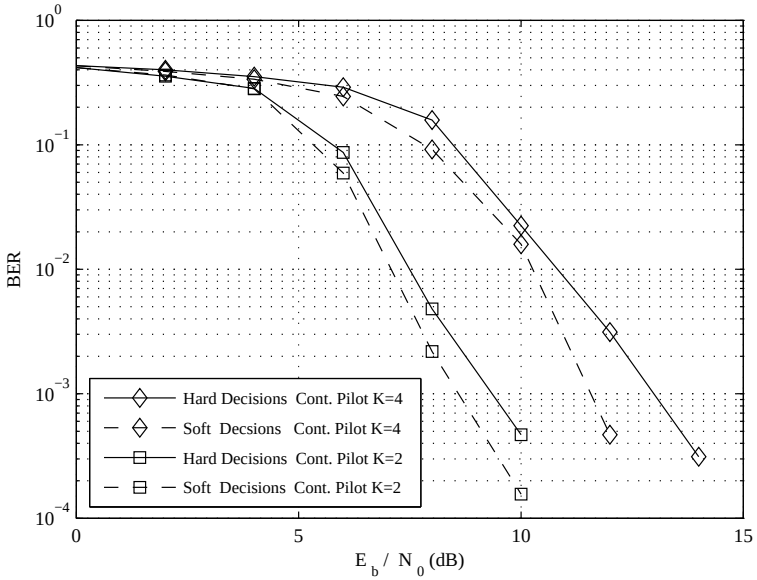

Figure 4.10: Hard and soft feedback decisions comparison of DFE-IDMA with cont. pilot and F_dT_c=0.001, system parameters:(M_f, M_b, μ_f, μ_b)= (12, 12, 0.005, 0.005).

improvement with soft decisions has the advantage of effectively updating the chip-level DFE to track time-variant channels. In general, a key source of performance improvement in the iterative multiuser receiver is the reliability of the extrinsic information and the equality of feedback chips that improve using channel coding and increasing the number of iterations, which in turn reduces DFE error-propagation and ISI efficiently.

4.7.2.1 Effects of power energy overhead

The pilot energy level has to be large enough to have an accurate measurement and small enough not to decrease the energy efficiency. Moreover, the system energy efficiency can be calculated as in [75] by defining an energy overhead ς, which can be written as

$$\varsigma = \frac{\text{pilot energy}}{\text{pilot energy} + \text{chip energy}} = \frac{t_r^2}{t_r^2 + A_k^2}, \tag{4.33}$$

where A_k is the transmitted signal amplitude of the kth user. The system performance with different ς values is shown in Fig. 4.11, where the optimal energy overhead was 0.4. The BER improves with increasing ς, and the performance gain was negligible for values greater than the optimum value. Therefore, the energy overhead value should be chosen as a balance between system performance and power loss due to the pilot signal. The normalized Doppler frequency was $F_d.T_c = 0.0001$ and $K = 2$.

4.7.2.2 Effects of interleaver length

In general, the interleavers in IDMA systems are used for users' separation, therefore, it is necessary that it is long enough to break the correlations between users' data that is shuffled between the turbo receiver stages. Additionally, they are used to break up burst errors and convert them to random errors, which may result from correlated fading channels. Fig. 4.12 shows the effects of interleaver length on the direct form receiver performance. The increase in data length helps to improve the performance by reducing error-propagation in the feedback decisions and the error floor introduced by channel decoding.

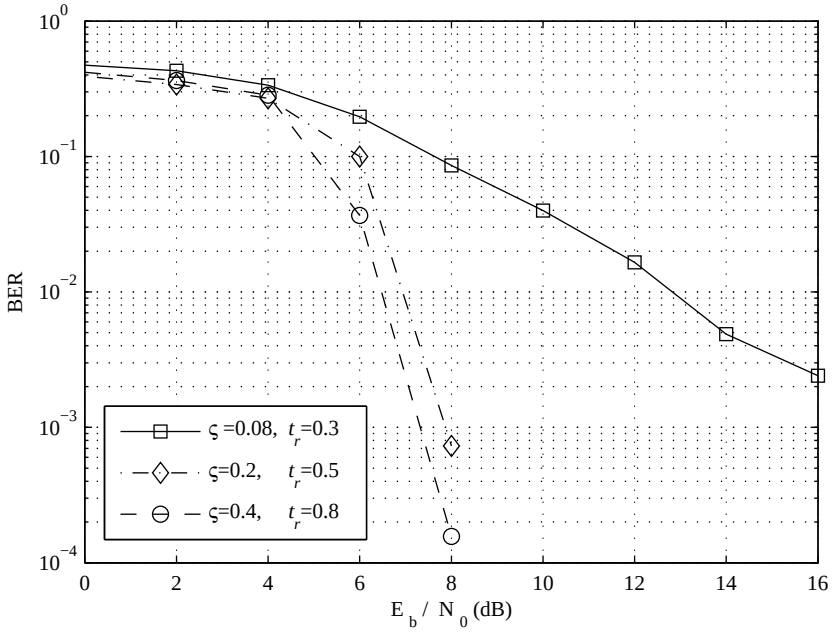

Figure 4.11: DFE-IDMA performance with different energy overhead, $F_d.T_c$=0.0001 and $K = 2$.

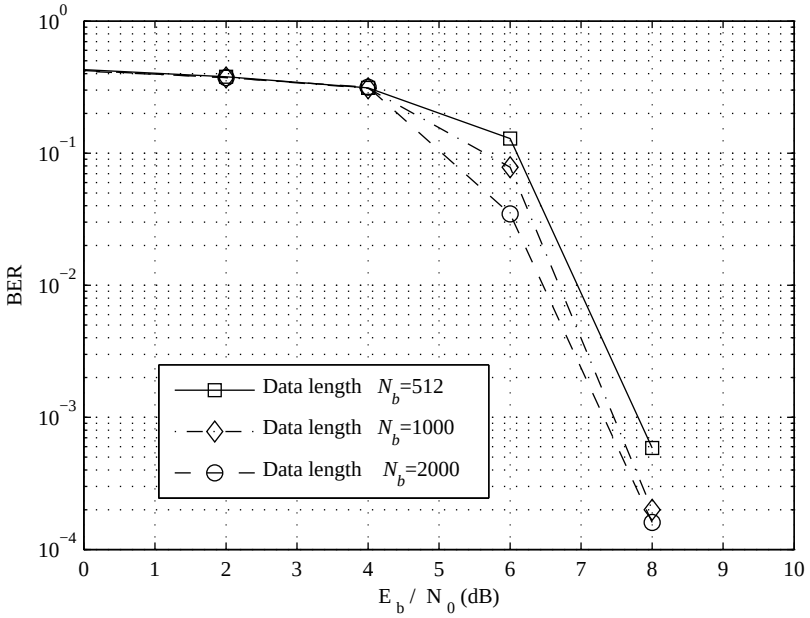

Figure 4.12: DFE-IDMA performance with different data length, $F_d.T_c$=0.0001 and $K = 2$.

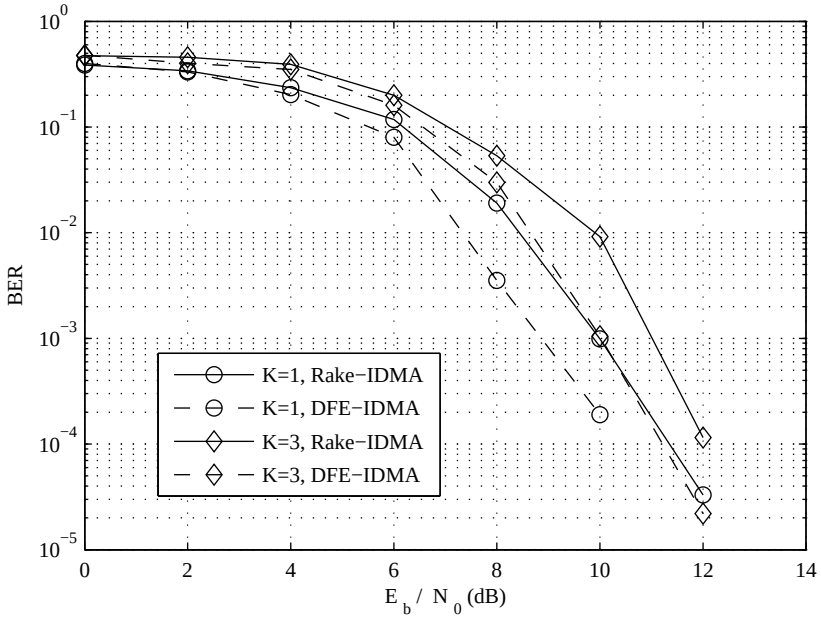

Figure 4.13: Performance results of Rake-IDMA and DFE-IDMA receivers, F_dT_c=0.001, system parameters: (a) CE based Rake-IDMA detector (M, μ)= (8, 0.001), (b) DFE-IC detector (M_f, M_b, μ_f, μ_b)= (12, 12, 0.001, 0.001).

4.7.3 Comparison of Rake/DFE Based IDMA Receivers

The systems are simulated with K=3 equal power users, 1024 information bits and the results are obtained after 5 iterations. The multipath spread and the maximum Doppler frequency were 6 ms and 10 Hz, respectively. The performance improvements obtained using DFE-IDMA in comparison with Rake-IDMA are demonstrated in Fig. 4.13. The direct form receiver outperforms the standard receiver by approximately 1 dB at a BER of 10^{-3}. The performance gap shows that the Rake-MUD exhibited errors due to residual interference that prevents the CE from functioning normally, whereas the errors with DFE-ICA are reduced within the same E_b/N_0 range. The presented results also show that the proposed algorithms in conjunction with continuous pilots are able to track fast fading channels and approach the single-user bound after a BER level of 10^{-4}, where a few iterations can bring the BER down to an acceptable level. Therefore, the performance of the equalization process is significantly improved but the background noise is quite dominant at low values of E_b/N_0 and diversity techniques are required to improve the performance.

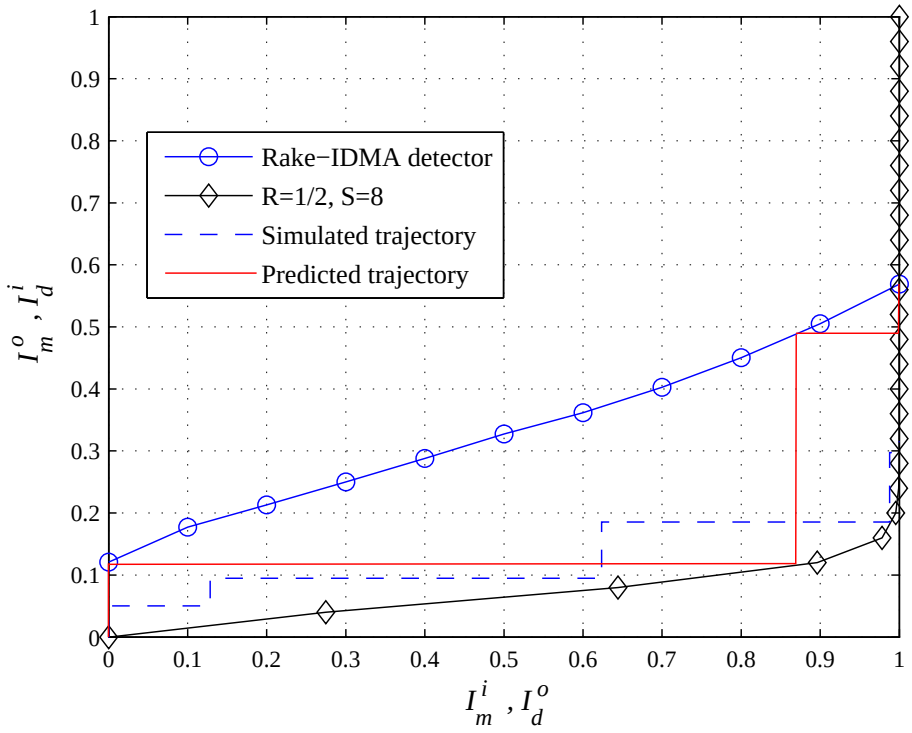

Figure 4.14: EXIT chart and simulated traces of the Rake-MUD with CE on a multipath fading channel at E_b/N_0=10 dB, system parameters: (M, μ)= (8, 0.001).

4.7.4 Results of EXIT Charts

The detection process starts from $I_m^i = 0$, where the feedback *a priori* information is absent. Then, the output LLRs described by $I_m^o = I_d^i$ are fed to the the joint despreader and decoding components, yielding the LLRs described by $I_d^o = I_m^i$, which are then fed back to the detector and so on. The prediction of the iterative processing behaviour is presented by the staircase (solid lines) between the multiuser detector and decoding curves. The vertical and horizontal axes represent the input and output information of the receiver components and a larger number of iterations is required when the tunnel between transfer curves narrows. Since there is no direct input from the channel, the decoding process depends only on the quality of the input information as in Fig. 4.3. In contrast, the detection process depends on the channel, E_b/N_0 and other system parameters accessing the channel.

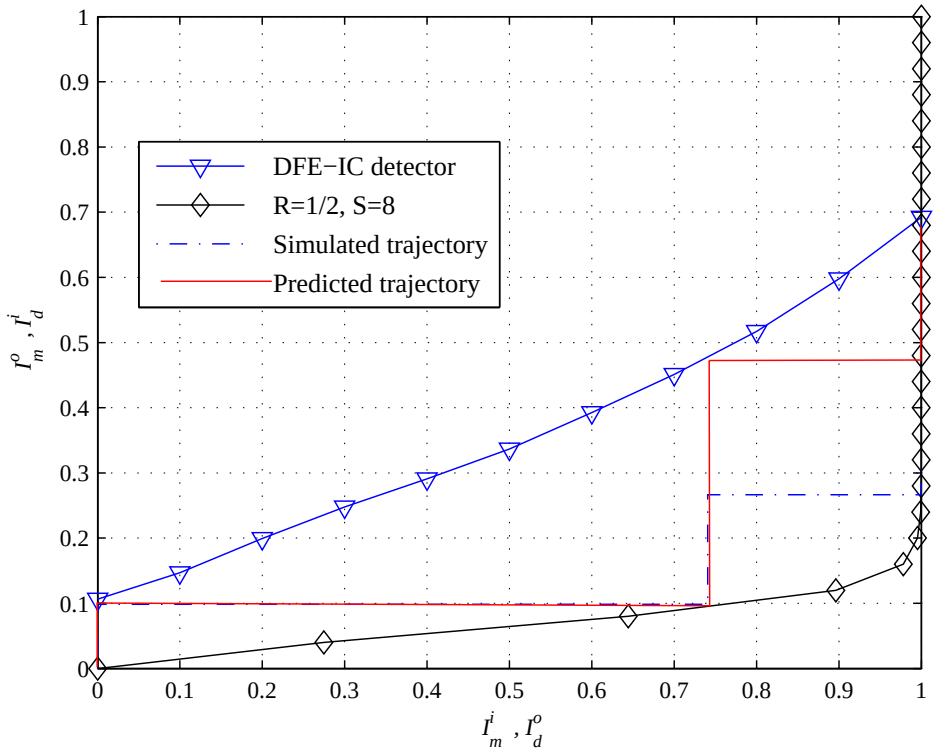

Figure 4.15: EXIT chart and simulated traces of the DFE-IC detector on a multipath fading channel at E_b/N_0=10 dB, system parameters: (M_f, M_b, μ_f, μ_b)= (10, 10, 0.001, 0.001).

Figs. 4.14 and 4.15 illustrate the EXIT curves of the decoding components and detectors with $K = 3$ users at E_b/N_0=10 dB. These curves correspond to the systems' performance in Fig. 4.13. The performance converges to a final point at the intersection of the DFE-IC, Rake-IDMA and the decoding curves. The mutual information improves by following the guide of the tunnel between the curves. The trajectories show that the structures can converge in five iterations under the finite block length. Due to more reliable interference cancellation, the DFE-IC detector in Fig. 4.15 produces better mutual information than the other detector in Fig. 4.14. Therefore, the widest tunnel is observed when the DFE-IC detector is used. This means that convergence to the single user bound is possible after a different number of iterations for each detector at high E_b/N_0. However, the receivers' performance will deteriorate when the I_d^0 or E_b/N_0 is low due to unreliable feedback information.

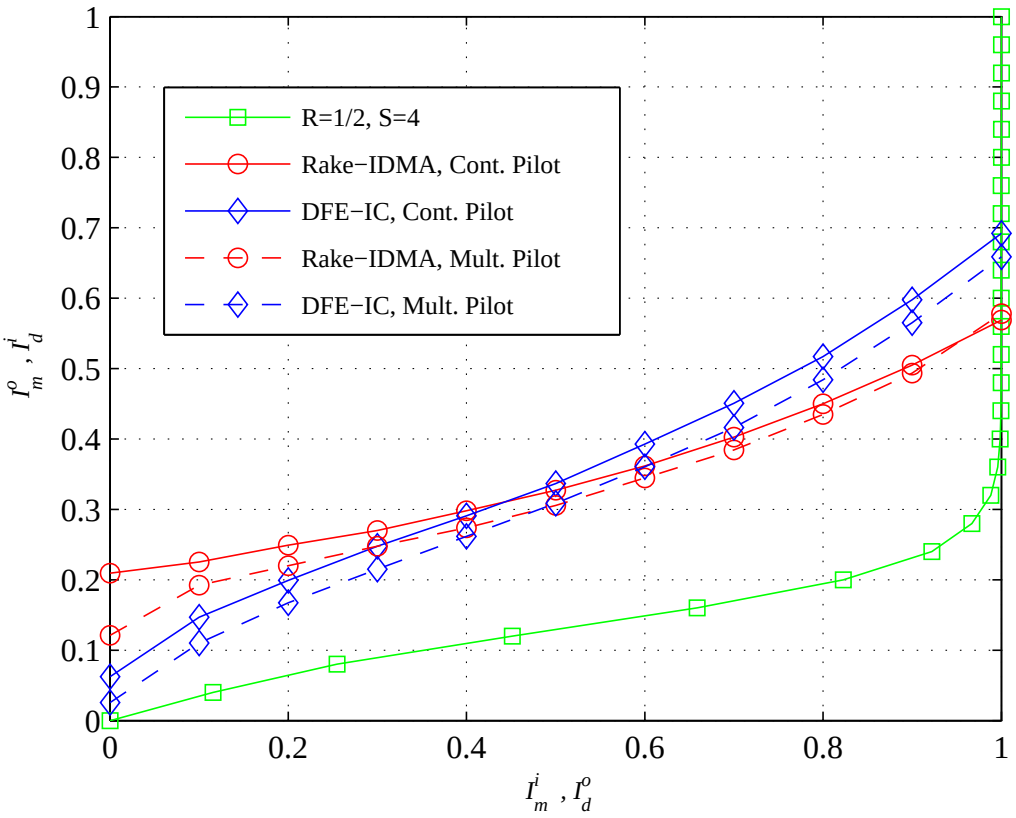

Figure 4.16: EXIT chart of the IDMA detectors with different training methods.

Additionally, these figures also show the detection trajectories (the dotted line) of the iterative process obtained by the simulation. The predicted trajectories follow roughly the same paths of the simulated trajectory in most iterations while in others deviate due to the limited interleaver size. However, the predicted trajectory and performance from the EXIT chart can be viewed as a practical bound on the achievable performance.

The EXIT charts of IDMA detectors are depicted in Fig. 4.16 with different patterns of training symbols. All the parameters are kept constant as in Figs. 3.9 and 4.9. When the I_m^i is increased, the output information I_m^o will also increase causing the curves to move upward at high I_m^i. At E_b/N_0=10 dB and with K=2, the detectors with the continuous training method shows a minor improvement in I_m^o compared to those with multiplexing pilots. With the increase of I_m^i, the *a priori* soft decisions

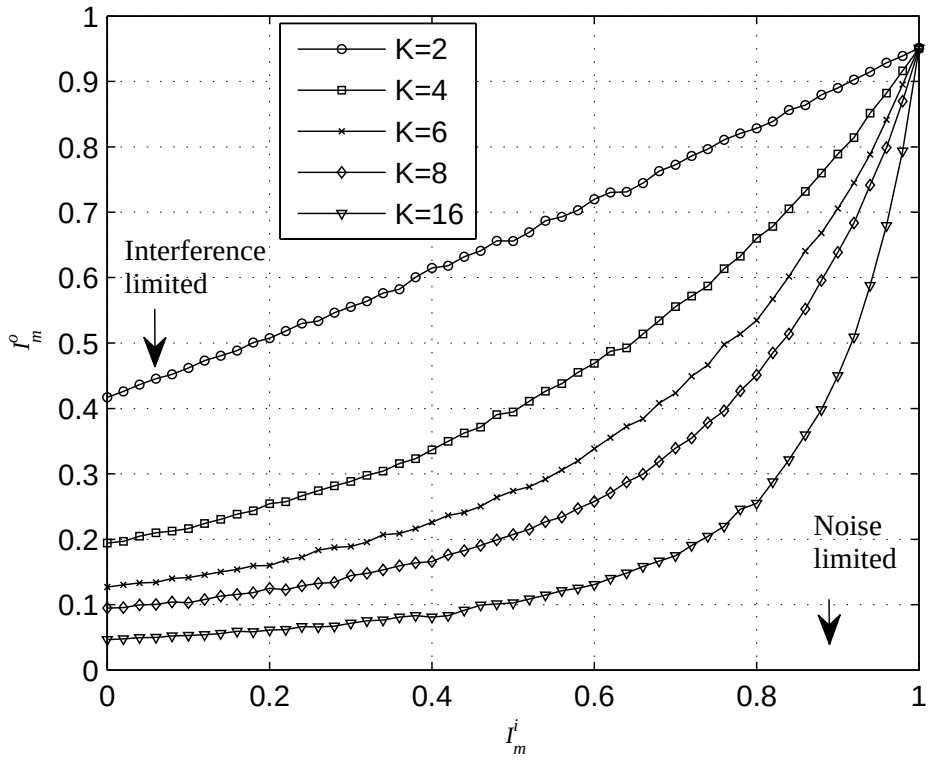

Figure 4.17: EXIT chart of Rake-IDMA over AWGN channel at SNR=4 dB.

become more and more reliable, and this will narrow down the gap between the two algorithms. Thus, the major differences between the two training methods are therefore the number of iterations needed to converge at each E_b/N_0 value. In addition, the mutual extrinsic information I_m^i of the DFE-IC detector, has a peak at approximately $I_m^o = 0.7$, while it decreases to the 0.59 for the Rake detector. Thus, the tunnel of the DFE-IC algorithms are wider than others of the Rake detector algorithms, therefore, it can converge with fewer iterations and reduce the overall complexity of detectors.

The mutual information I_m^o depends strongly on the E_b/N_0, and the higher E_b/N_0 is the larger mutual information at the detector's output. However, these curves are influenced not only by the input E_b/N_0 and the channel, but also by other parameters, such as the spreading codes, and the number of active users accessing the channel. In Fig. 4.17, the effect of the MAI on the convergence of the Rake detector is investigated and shows that the higher number of active users, I_m^o is low. A greater I_m^o means a better estimation of the transmitted chips and thus better performance. When the

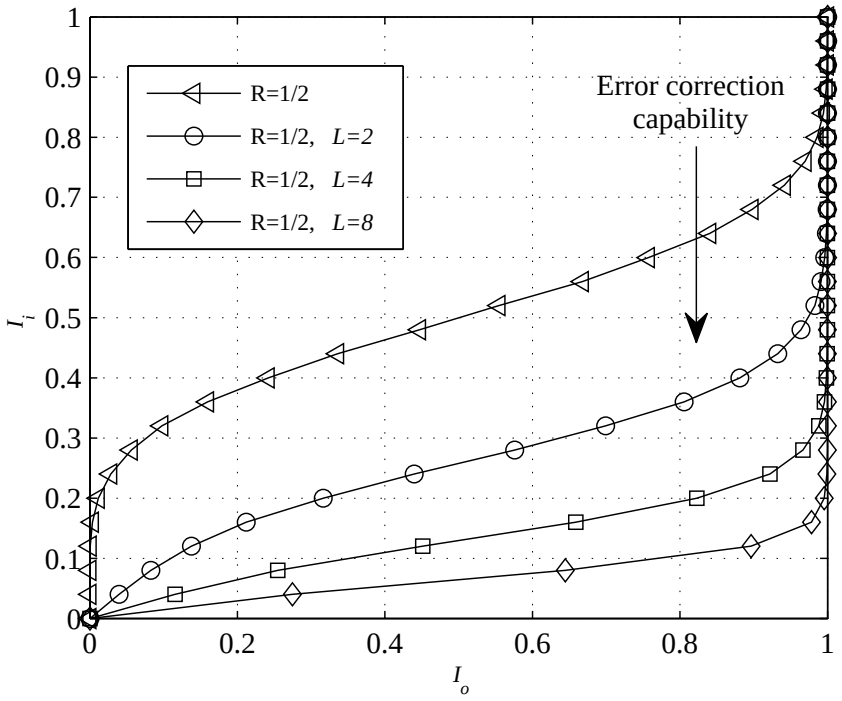

Figure 4.18: EXIT chart of joint spreading and decoding blocks.

effects of MAI have been eliminated, these curves tend to the right region of Fig. 4.17, which represents the noise-limited region.

When the number of active users K is large, the low codes rates are necessary. The corresponding EXIT chart of the decoding blocks is shown in Fig. 4.18 for the different code rates. It is seen the advantage of low rate, where even the simple spreading codes can improve the capability of the correction and mitigation of MAI/ISI. However, the systems with the small spreading factors become limited by the MAI/ISI and further iterations are required. In contrast, the long spreading factors reduce the effective data rate in already band-limited channels.

4.8 Summary

In this chapter, the architecture of a DFE-IC is proposed in Section 4.2 for synchronous IDMA and CDMA systems operating over frequency selective channels. Chip level equalization and detection are the major features of these architectures.

Both the optimum and MMSE approach of the chip level DFE are explained in Section 4.2.1, while the derivation of the soft IC cancellation technique is given in Section 4.2.2. The proposed receivers integrate the functions of the DFE, phase tracking and IC techniques into one structure, which requires partial or full knowledge of interfering users. In Section 4.4, the iterative DFE based CDMA receiver has been formulated based on the derivation of the adaptive DFE-IDMA receiver.

The details of simulation setups used to generate EXIT charts are presented in Section 4.6 for the T-MUD architectures in multipath fading channels. The convergence behaviour of such architectures is analysed and used for comparing the detectors' behaviour and it is quite close to the real simulated trajectory. The EXIT chart analysis is also used to investigate the effect of the different training approaches, and to compare between different detection algorithms. However, it was shown that the proposed DFE-IC not only reduces the error propagation problem but also reduces the bit error floors introduced by the Rake based receivers. The presented results also show that the proposed continuous training approach in Section 4.3 outperforms the conventional approach over a wide range of normalized Doppler spreads. The EXIT charts results show that the tunnel of the DFE-IC algorithms are wider than others of the Rake detector algorithms, therefore, it can converge with fewer iterations. The transfer functions are also highly dependent on different system parameters and channel conditions. The effects of choosing different receiver parameters have been also studied.

CHAPTER 5

Off-line Implementation and Experimental Results

5.1 Introduction

In this chapter, the performance and analysis of data obtained via sea trial experiments are presented in order to assess the reliability of the suggested architectures in the real environment. Initially, comprehensive descriptions of the signal design, in conjunction with the setup of the experiments are outlined. The investigated scenarios are used to demonstrate the capability of different schemes to deal with the dynamic nature of the UACs and simultaneously cope with the MAI in the network, where the number of active users is maximally four. Significant performance gains can be achieved by accurately identifying and selecting adaptive parameters, which help to minimise the metric measurement in these schemes, and reach steady-state convergence. The effects of these important parameters and the performance with partial knowledge of the interleavers' patterns have been also investigated.

In addition, to show that the proposed structures are actually manageable on current hardware, we will also present details about some obvious system constraints that affect the design of many real-time processing systems, and the hardware structures such as digital signal processor (DSP) typically used in such systems.

5.2 The Description of the Experiments

5.2.1 Experiment Setup and System Parameters

In order to evaluate the performance of the proposed receiver schemes, experimental signals were recorded and processed off-line. The recorded signals were acquired during sea trials carried out by Newcastle University in the summer of 2009 in the North Sea, a few miles off the UK coast. The experimental setup configuration is illustrated in Fig. 5.1, and the system parameters are summarized in Table 5.1. The transmission power was fixed at 180 dB re μPa at a carrier frequency of 12 kHz band-limited to 4 kHz. The shallow water channels in this area typically exhibit long and rapidly varying multipath due to the hard surface of the sea bottom. The depth of the water column typically varies between 25 and 30 m. The experiment investigated three different ranges between the transmitter and the receiver, i.e. 200, 500 and 1000 m. Moreover, the transmitter and the receiver were positioned at 10 and 5 m from the sea surface, respectively.

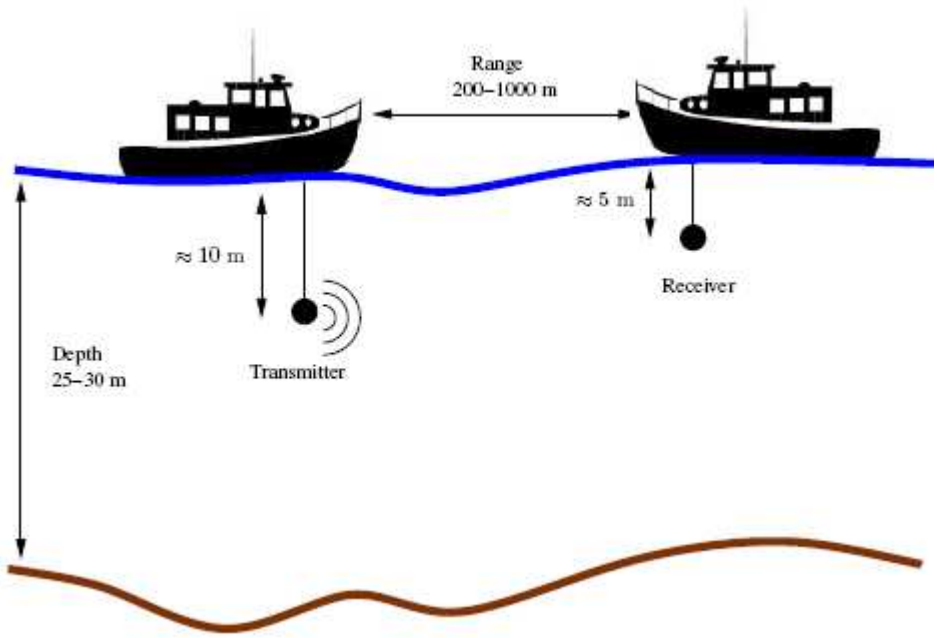

Figure 5.1: Experimental configuration for sea trial.

Table 5.1: Main System Parameters

Carrier frequency f_c	12 kHz
Sampling frequency f_s	48 kHz
Depth	25-30 m
Operating ranges	200, 500, 1000 m
Modulation scheme	QPSK
Cosine roll-off factor β	0.98
Generator polynomial g	$[23, 35]_8$
Packet duration	2.33 s
Total packets number	270
Training symbols N_s	511

5.2.2 Transmission Signal Models

The signal models of IDMA and CDMA systems presented in Section 3.2 are used in the experiments. Information bits of length 1024 are encoded by a rate R=1/2 non-systematic convolutional (NSC) code, with polynomials $[23, 35]_8$ expressed in octal form, resulting in 2056 coded bits. For IDMA, the coded bits are further encoded by

Table 5.2: Signatures of short code CDMA

User number	Spreading sequences
1	+1, -1, +1, +1, +1, +1, +1, +1
2	+1, +1, +1, +1, -1, -1, -1, -1
3	-1, +1, +1, -1, +1, -1, +1, +1
4	+1, -1, -1, -1, -1, +1, -1, -1

the rate R_r=1/8 repetition code, which gives 16448 coded bits. The repetition code adopts the same spreading sequence, i.e. $\{+1, -1, +1, -1, +1, -1, +1, -1\}$, for all users as in [37]. All interleavers are randomly generated using a uniform distribution. Furthermore, a longer interleaver size is required in IDMA in order to break the correlation between the LLRs that are shuffled between the detector and the decoders. Therefore, the size of the interleavers is accordingly determined to be 2056 and 16448 bits, for CDMA and IDMA, respectively.

In addition, the users' spreading sequences in the investigated CDMA systems are also randomly generated. In short code CDMA packets, the signatures assigned to users during simulation are listed in Table 5.2, and they are periodic or remain the same for all symbols. In long code CDMA, they are aperiodic or essentially pseudorandom and vary for the different 1028 transmitted symbols [76].

5.2.3 Transmitted Packet Structure

For each system during the experiments, the transmission was organized in packets of equal duration, that is, 270 data packets of 2.33 s were transmitted every ninth second. The transmitted frame employed a sub-frame of each scheme separated by gap periods of 100 ms introduced to avoid inter-packet interference. Each signalling frame comprised a 511 BPSK modulated training sequence required for equalizer training in case of multiplexing pilot based system, encapsulated with QPSK symbols, and 1024 QPSK symbols in case of continuous pilots, two 50 ms linear frequency modulated chirp signals (LFM) at the start and end of each frame, and 12.5 ms gap periods. These were interspersed throughout the block, as shown in Fig. 5.2. The initial and maximum frequencies of the 8 kHz bandwidth chirp signal were set to 8 kHz and 16 kHz, respectively.

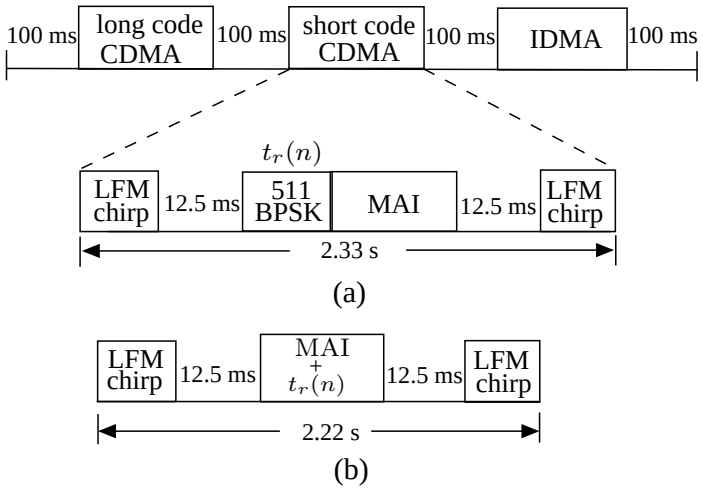

Figure 5.2: Transmitted data packet (a) with multiplexing pilots and (b) with continuous pilots.

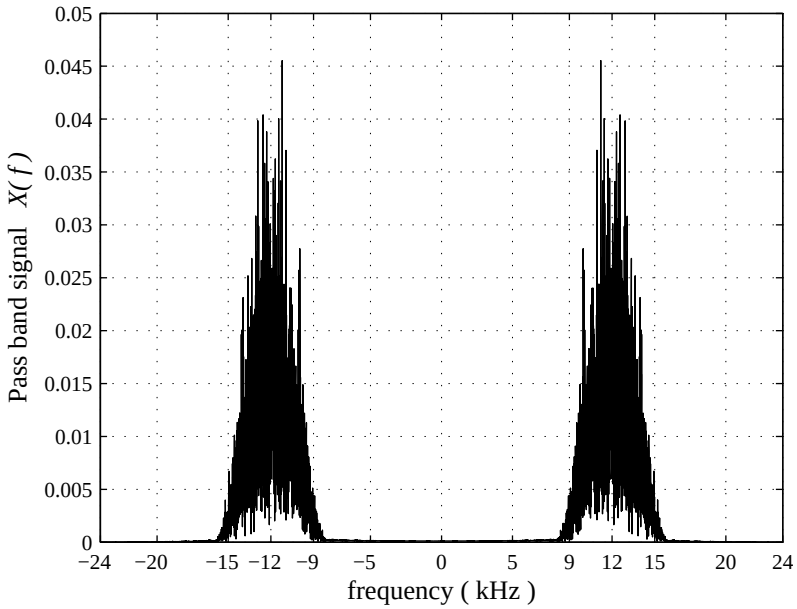

Figure 5.3: Transmitted signal in passband.

Before frequency translation, the signal is transformed into a baseband waveform using pulse shaping filter. A root-raised cosine pulse with roll-off factor $\beta = 0.98$ was used for pulse shaping, resulting in the overall bandwidth of the 4 kHz. Thus, the signal after the pulse shaping is limited within the bandwidth of the real channel,

which is limited by the transmission loss that increases with frequency and range. The upsampling factor was set to 12 to provide an ease and accuracy in processing at the receiver. Since the physical media accept only the real values, only the real part of the signal is transmitted. Fig. 5.3 shows the transmitted signal in passband. Bandwidth expansions, which are an order of magnitude greater than this, have been considered in [3]. However, due to the limited availability of bandwidth in the UACs, the use of long spread factors will result in inefficient low data rate transmission, thus, it is generally avoided. The bandwidth expansion factor is set in the experiments to $L/R = 16$ chips. The corresponding effective data rate amounts to 1024 information bits divided by a block duration of 2.33 s, which equals 439.5 bps per user, producing an aggregate bit rate of 879 and 1758 bps for the systems with K=2 and K=4 users, respectively. These data rates can be characterized as moderate transmission rates.

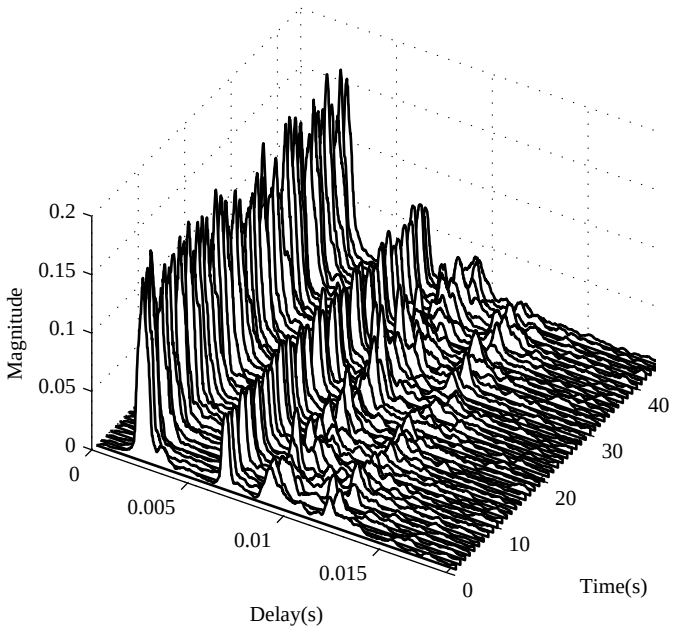

Figure 5.4: Normalized channel impulse responses profile of 200 m channel range.

5.3 Experimental Channel Characteristics

Figs. 5.4 to 5.6 show the detected profile of the CIRs observed by the input sensor for different short range multipath channels, all taken from ocean experiments. These CIRs were determined by the complex passband correlation process with the up-chirp (8-16 kHz) signal of 50 ms at the beginning of each packet. Clearly, all the channels responses have a relatively stable principal arrival with significant time varying ISI on the order of tens chips and the energy of these arrivals varies with the location. These principal components appear to have around 1 ms lag and are followed by micro-paths or echoes of decaying energy, which may be due to scattering by small inhomogeneities in the environment and other incomplete scatterers. The structure for these micro-paths influences the shape of the arrival for that ray tube and results in temporal spreading of the main paths. Thus, the arrivals structure will change on a time scale with the structure of the micro-paths. However, there are infinitely many micro-paths but those that have lost much of the energy as a result of multiple reflections can be neglected and leave only significant paths. Therefore, these channels have very few non zero arrivals and hence, they are known as sparse channels. In addition, the number of these significant paths, their delays and strengths is affected by the channel geometry and its scattering functions.

For comparison of the three responses, the snapshots of the CIRs in Fig. 5.7 show that the channels exhibit maximum delay-spread times of up to 11, 8 and 6 ms, for 200, 500 and 1000 m channel ranges, respectively. The delay spread of the CIRs appears to be inversely proportional to the distance between the transmitter and the receiver. Furthermore, four or five significant arrivals are present followed by long reverberations of lower energy.

To illustrate the channel variation within data packets, matched filtering was also performed using one period of the LFM chirp signal over the entire received acquisition preamble. The results for 2 minutes of the 1000 m channel range is shown in Fig. 5.8. The plot shows the time channel variation besides showing the multipath arrivals of a particular channel. Clearly, the strength of the channel components within these packets varies with time and these fluctuations may be caused by the environmental fluctuations.

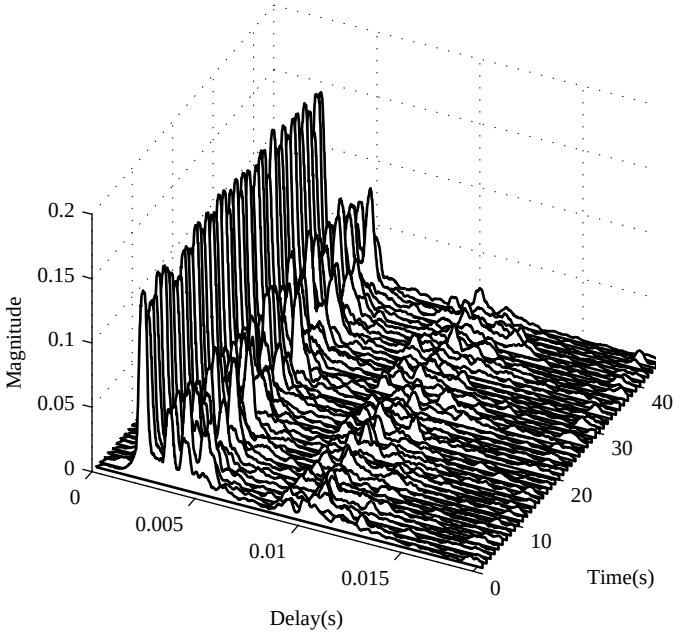

Figure 5.5: Normalized channel impulse responses profile of 500 m channel range.

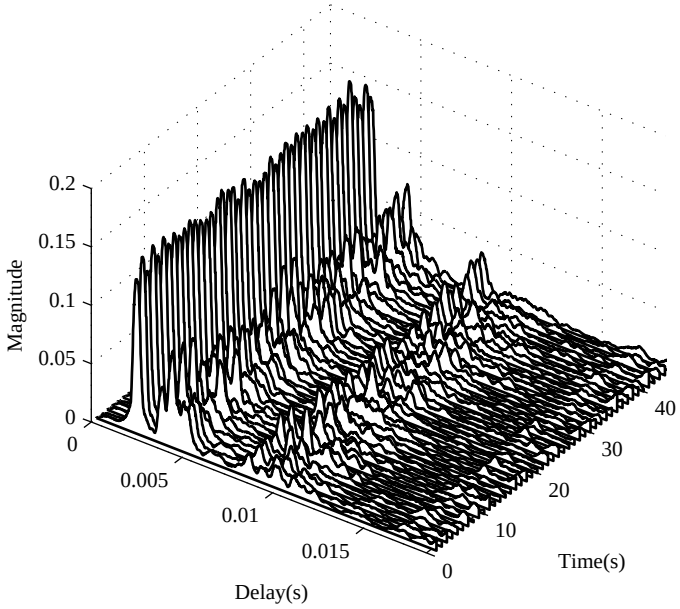

Figure 5.6: Normalized channel impulse responses profile of 1000 m channel range.

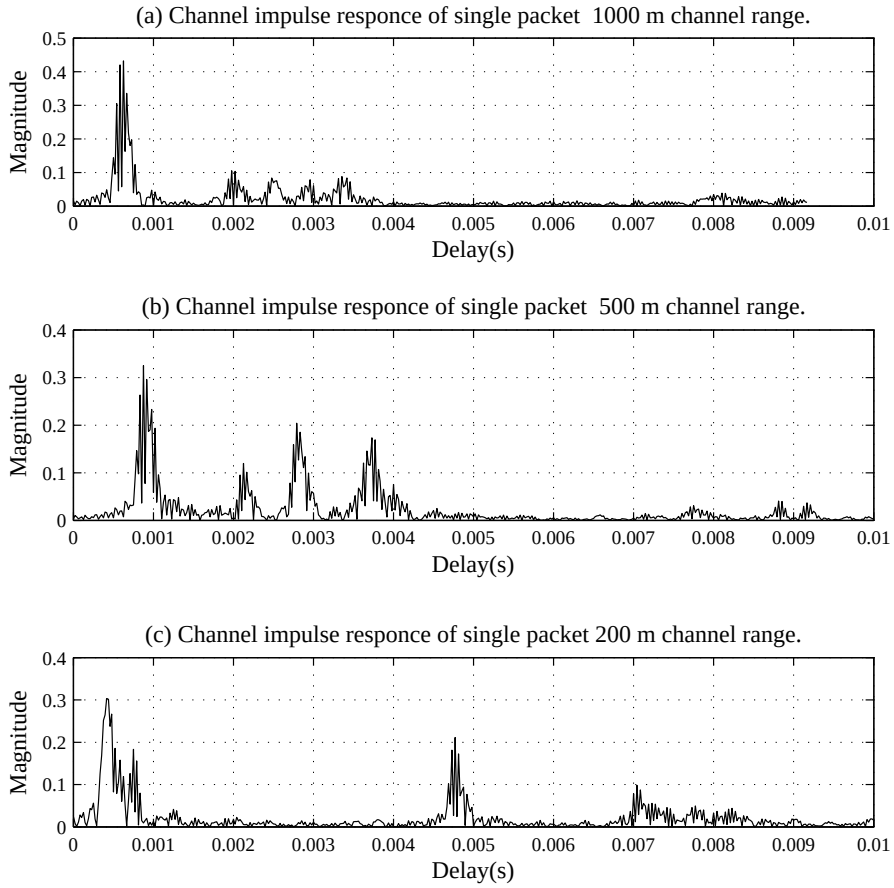

Figure 5.7: Normalized channel impulse responses, obtained from the frequency sweep probe at the beginning of each multiuser signal.

5.4 Signal Acquisition Stage

The front-end of the off-line receiver is illustrated in Fig. 5.9. The bandpass received signal, $z(t)$, is first passed through a bandpass filter (BPF) with carrier frequency f_c, to remove unwanted low-frequency disturbances such as ship engine noise. Subsequently, the signal is frame synchronized by matched filtering with the 50 ms chirp signal to identify the start of each packet. Fig. 5.8 shows the peaks at the output of the matched filter that used to determine the start of the frame and contains time-averaged CIR estimates. After the signal is shifted to the complex baseband by employing in-phase and quadrature-phase oscillator mixers and lowpass filters (LPF), the acquired signal is sampled using a one sample per chip interval and used as in-

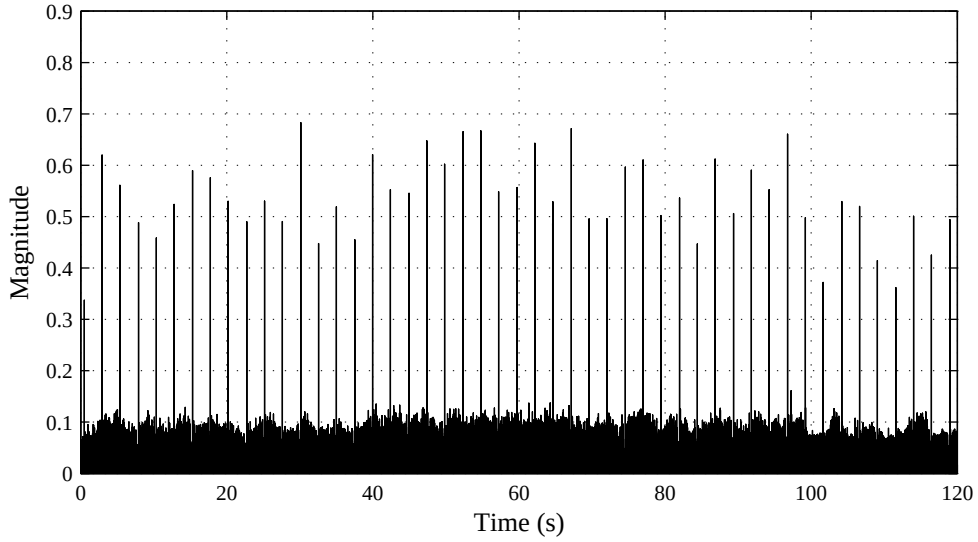

Figure 5.8: Normalized energy levels at the output of the matched filter for 2 minutes of 1000 m channel range.

Figure 5.9: Front-end of the receiver.

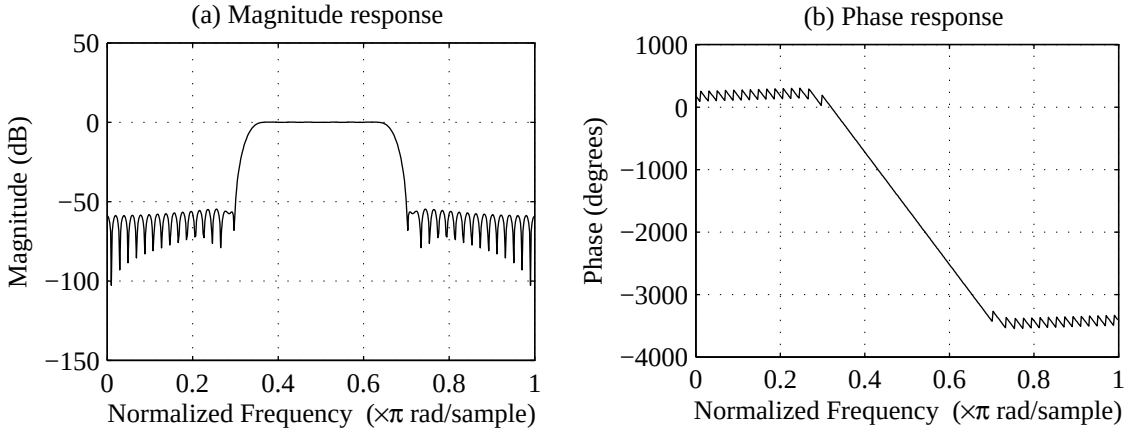

Figure 5.10: Magnitude and Phase response of the BPF filter.

put to the adaptive iterative receiver. Fig. 5.10 illustrate the frequency response characteristics of the BPF filter.

The BPF filter is designed with a center frequency equal to the f_c and a bandwidth matching the bandwidth of the transmitted MAI signal. It is worth mentioning that if the bandwidth of the BPF is chosen too narrow, the signal will be distorted and if it is too large, more noise will pass on to the subsequent stages. However, the filter was designed based on equiripple linear FIR filter design and the f_s was set to 48 kHz. Fig. 5.11 shows the effect of the BPF on the reception of a multiuser packets over 200 m channel range.

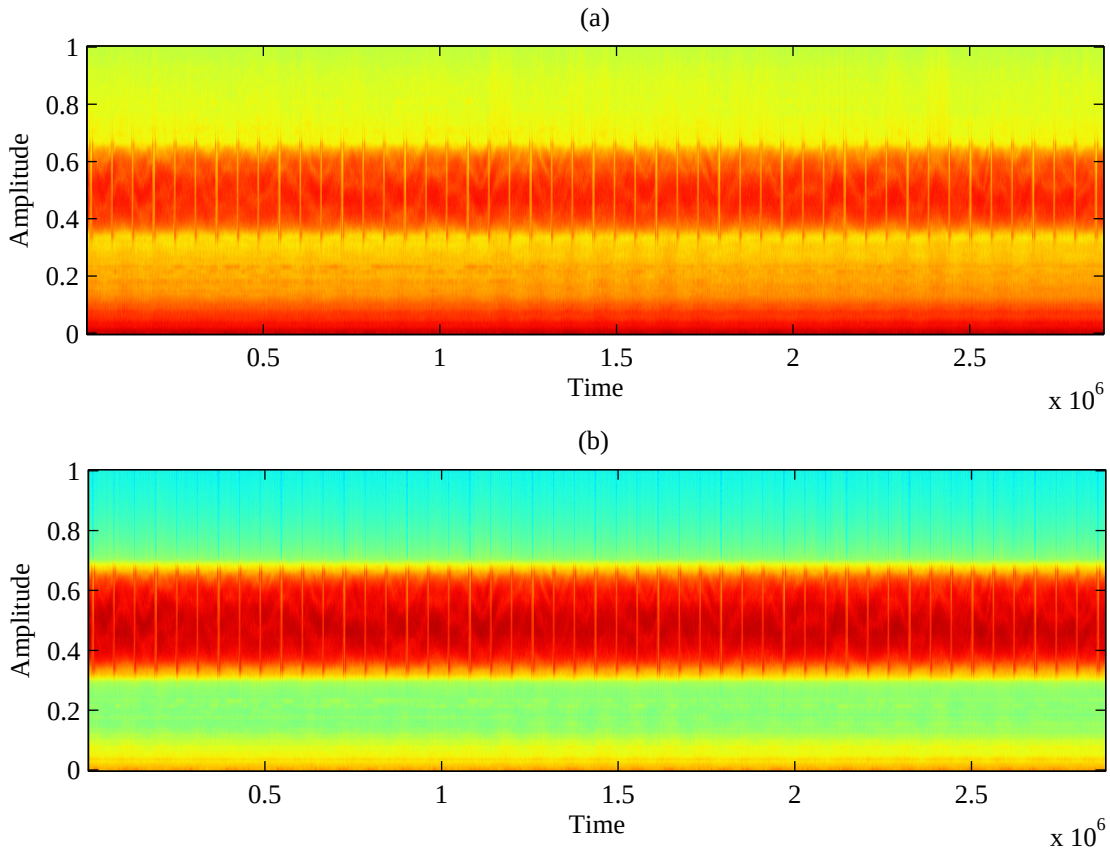

Figure 5.11: Effect of the BPF on the reception of multiuser packets over 200 m channel range, where the plot (a) represents the spectrogram of the unfiltered signal and the lower plot (b) represents the filtered signal.

Table 5.3: Performance results of CE based turbo schemes with multiplexing pilot

	K=2								
	IDMA			long code CDMA			short code CDMA		
Ch. Range(m)	200 m	500 m	1000 m	200 m	500 m	1000 m	200 m	500 m	1000 m
Av. BER	0	0	0	19/30690	4/30690	0	36/30690	0	0
Av. SNIR	7.2	11.5	13.3	7.1	11.3	13.6	6.9	11.2	13.1
	K=4								
Av. BER	1174/61440	980/61440	46/61440	3124/61440	2066/61440	1992/61440	1954/61440	1886/61440	1794/61440
Av. SINR	4.9	6.8	7.9	4.7	6.7	7.6	4.7	6.7	7.6

5.5 CE Based Turbo Architectures

5.5.1 Performance Results with Multiplexing Pilots

The performance and reliability of the proposed iterative receivers are evaluated using the channel models described in Section 5.3. Each system is experimented with 2 and 4 simultaneous users over three different channels ranges. The output SINR represents an approximation of the steady state signal at the output of the detector. Experimentally, SINR can be calculated as [60]

$$\begin{aligned} \text{SINR (dB)} &\cong 10\log_{10}\left(\frac{E[\tilde{y}(n)\tilde{y}^*(n)]}{\frac{1}{N}\sum_{n=1}^{N}|e(n)|^2}\right) \cong 10\log_{10}\left(\frac{E\{|\tilde{y}(n)|^2\}}{J}\right), \\ &\cong 10\log_{10}\left(\frac{1-J}{J}\right), \end{aligned} \tag{5.1}$$

where J is the expectation of the MSE employed in the update process of the adaptive algorithms, and N is the number of transmitted symbols within a packet excluding the symbols corresponding to the training sequence. The algorithm is switched to the decision directed mode after 511 symbols in case of multiplexing pilot method. In Table 5.3, the total numbers of bit errors averaged over 15 packets for IDMA, long code CDMA and short code CDMA are given, along with the achieved average output SINR in dB.

For a two-user scenario (K=2), error-free transmission is achieved with IDMA over three different channels. The errors in short code CDMA are 36 bits with the 200 m channel and free of errors with the other channels, whereas long code CDMA errors are 19 bits and 4 bits with 200 and 500 m respectively. The MSE of the algorithm at the last iteration is drawn in Fig. 5.12, along with the receiver parameters of packet

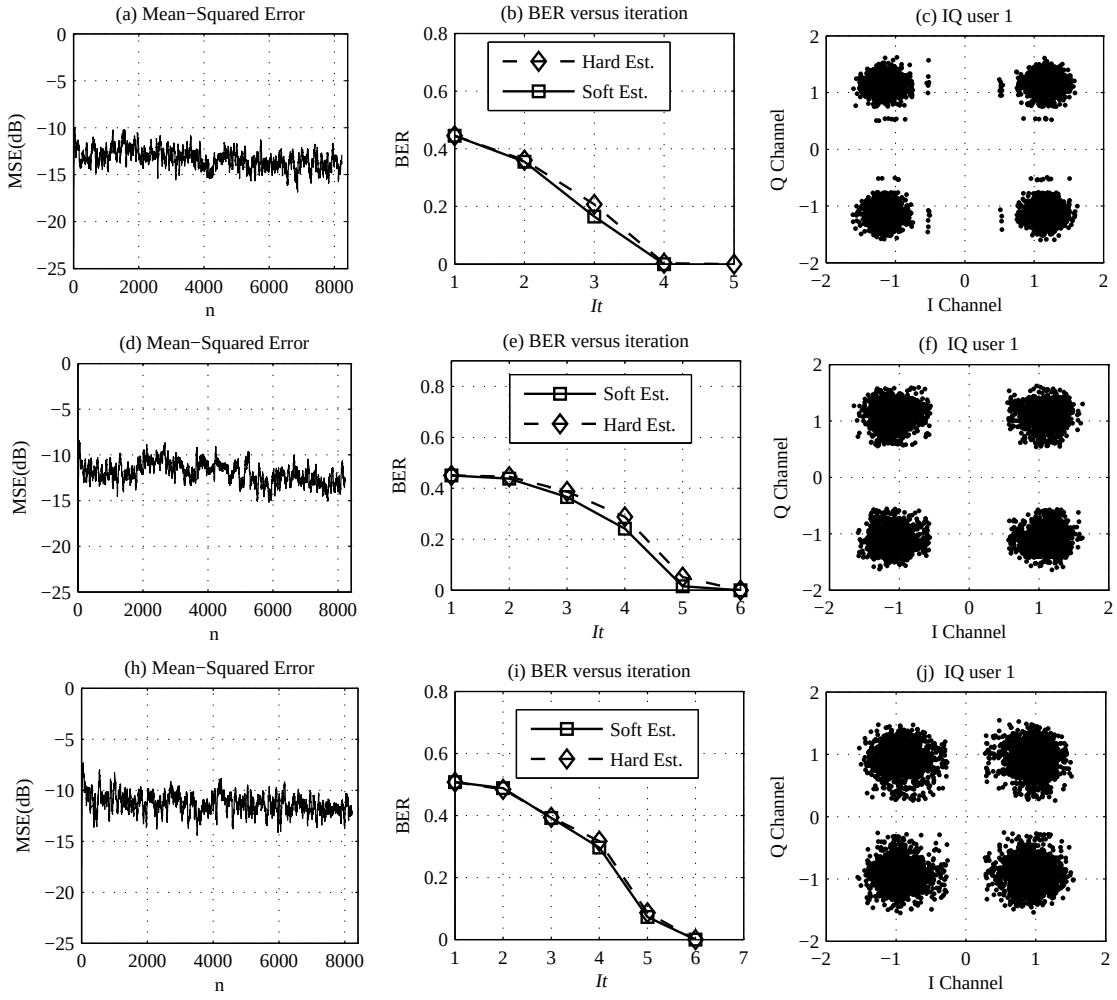

Figure 5.12: Performance results of IDMA (a - c), long code CDMA (d - f) and short code CDMA (h - j) with K=2, where SINR= 7.8, 7.2, 7.1 dB, respectively, and M=16, μ=0.1, a=0.001.

no.1. The bit error versus iteration number of soft and hard CE is also depicted in the figure. In most packets, the soft CE has less decision feedback errors and rapid convergence speed compared with hard decision CE. These figures also illustrate the number of errors with each pass, where the bit errors reduce dramatically. The residual errors in MSE may be attributed to the errors caused by inaccurate decision feedback symbol, which used in the channel tracking causes noise in the channel estimate and has higher occurrences at low SINR. However, the reason underlying this improvement is due to the redundancy introduced by the spreading and channel

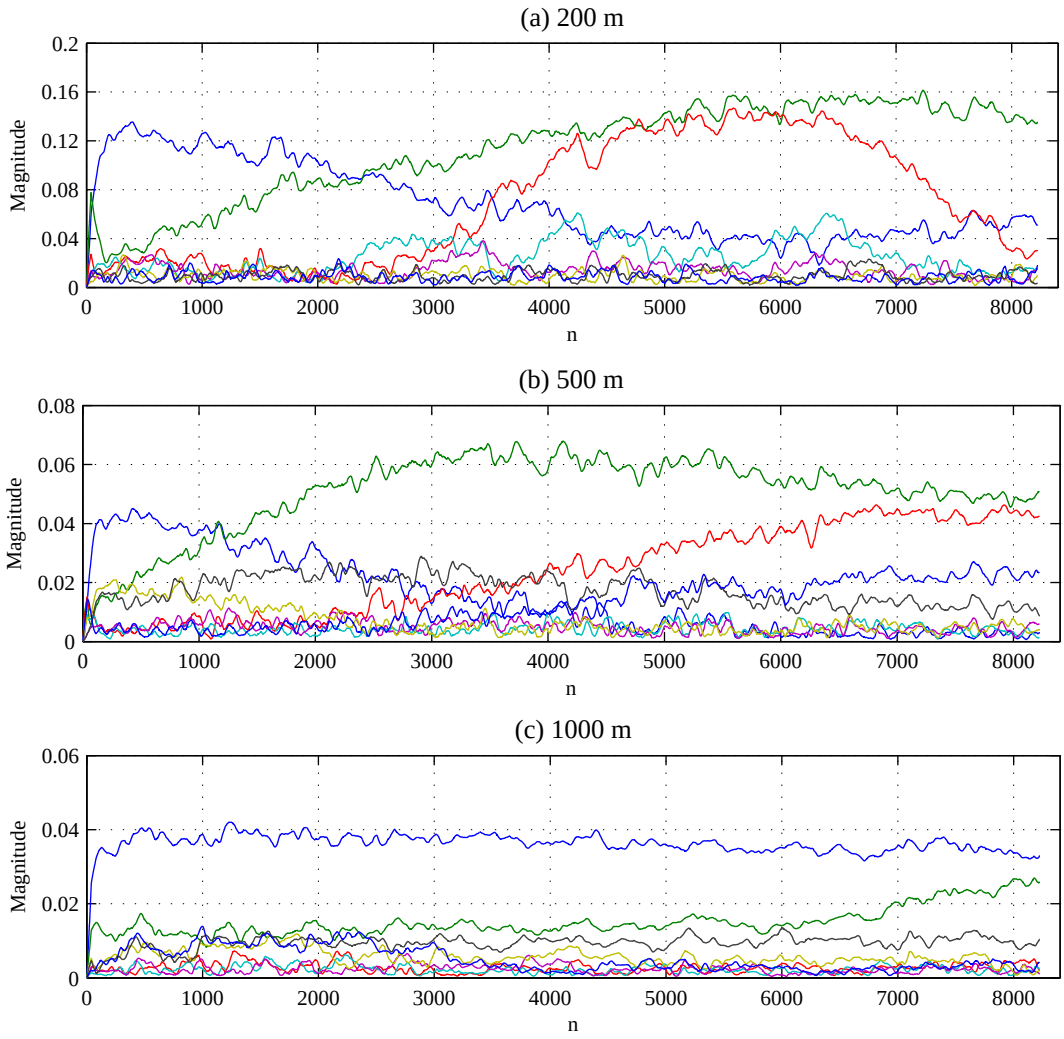

Figure 5.13: Channel estimator output over (a) 200, (b) 500 and (c) 1000 m channel range.

coding. The reliable chip decisions help to improve weak chip decisions iteratively until the feedback eventually consists almost entirely of correct chips. Fig. 5.13 shows the output of channel tracking for packet no.1 of IDMA system over 200, 500 and 1000 m channel ranges.

For the $K = 4$ active users scenario, the achieved output SINRs differs significantly. As the number of active users' increases, there are more incorrectly decided symbols and the accuracy of CE will be negatively affected by error propagation, where an error in one decision might lead to errors in subsequent decisions. The bit

Table 5.4: Performance results of CE based turbo schemes with continuous pilot

	K=3								
	IDMA			long code CDMA			short code CDMA		
Ch. Range(m)	200 m	500 m	1000 m	200 m	500 m	1000 m	200 m	500 m	1000 m
Av. BER	808/46080	75/46080	0/46080	1681/46080	84/46080	359/46080	859/46080	151/46080	307/46080
Av. SNIR	7.4	9.8	10.9	6.3	9.8	9.3	6.6	9.3	9.2

errors over each packet are plotted in Fig. 5.14 over the channel ranges 200, 500 and 1000 m. The penalty in performance with the 200 m channel range in almost all the combinations is significant when comparing with the 500 and 1000 m ranges. The underlying reason for this performance deterioration is due to the channel coefficients to be estimated increasing, and the correlation among channel coefficients decreasing due to fading rate. This causes noise in the channel estimate and inaccurate decision feedback symbols which has a higher occurrence at low SINR. Therefore, the channel estimates degrade and the receiver will be not able to reconstruct the MAI and ISI properly. However, a reasonable performance in IDMA over 1000 m is still achieved, which speaks for the robustness of the iterative receivers. Additionally, the results of the BER and SINR reveal that the IDMA performance is as good as, or slightly outperforms, the long code CDMA and short code CDMA in most configurations. This is due to the fact that in IDMA based systems, the chip level interleavers are more effective in dispersing the bits throughout the packet than their bit-level equivalents in CDMA.

5.5.2 Performance Results with Continuous Pilots

In these experiments, the NLMS algorithm is continuously updated at the chip rate using continuous pilots. In Table 5.4, the receivers with K=3 also produced errors over 15 transmitted packets except for 1000 m trial with IDMA. The performance of the receivers is also affected by CE errors. In the case of high variation of the transmission channel as in the 200 m channel range, the performance of various receivers is deteriorated since the equalization is not perfect in a time-varying fading environment. However, the degradation in performance due to CE is not severe and the receivers still demonstrate expectable performance for some of these trials. Further, the Rake-IDMA receiver shows better performance than both forms of Rake-CDMA in most packets. See Appendix A for detailed results of BER and SINR values for all transmitted packets.

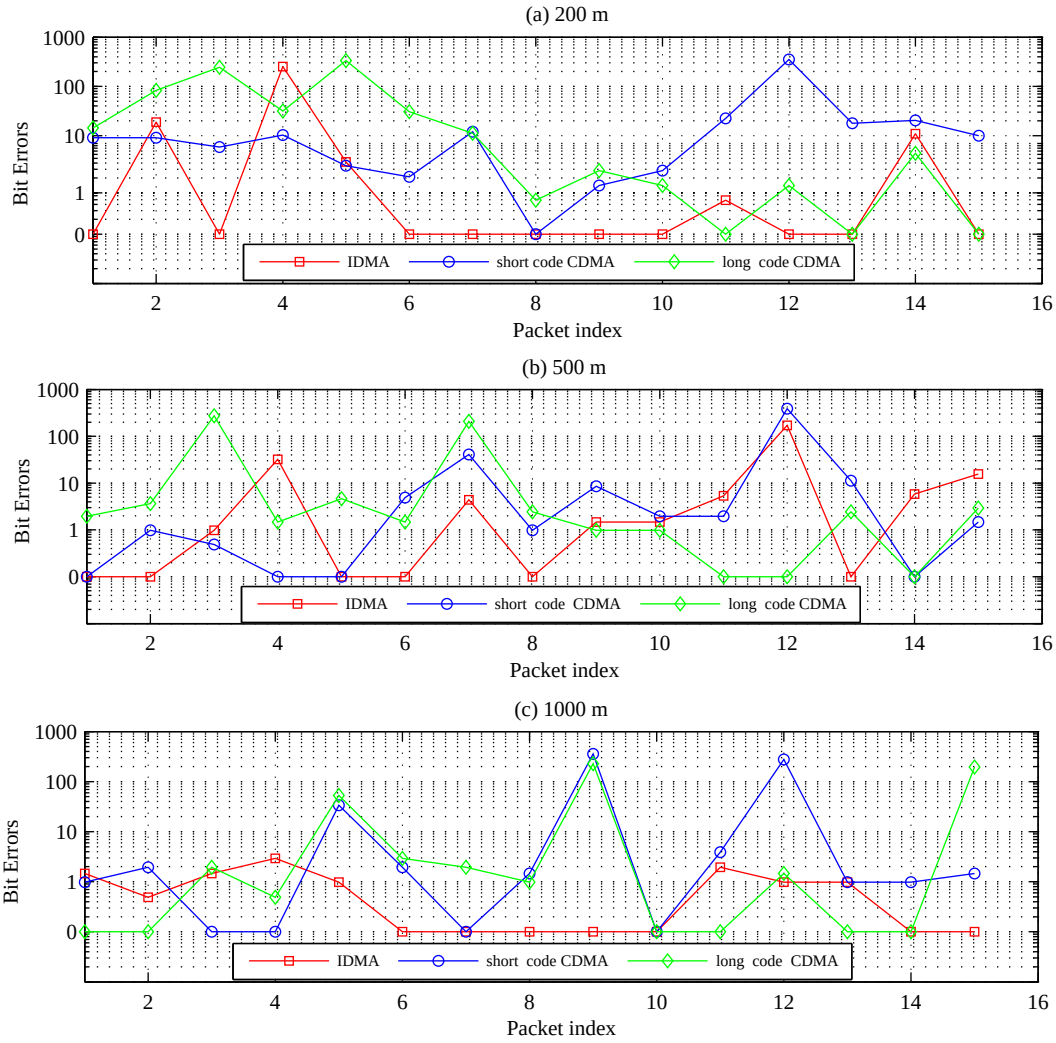

Figure 5.14: Bit errors of IDMA, short CDMA and long CDMA over each packet with $K = 4$ over (a) 200, (b) 500 and (c) 1000 m channel range.

5.6 Direct Adaptation Based Turbo Architectures

5.6.1 Performance Results with Multiplexing Pilots

The performance of the proposed direct adaptive receivers is also evaluated using the transmitted signals through the multipath channels described in Section 5.3. For a two-user scenario (K=2), Table 5.5 lists the average BER of soft and hard estimation for DFE-IDMA, long code DFE-CDMA and short code DFE-CDMA over a 314.55

Table 5.5: Results of DFE-IC based turbo schemes with multiplexing pilot, K=2

	K=2								
	DFE-IDMA			long code DFE-CDMA			short code DFE-CDMA		
Ch. range (m)	200	500	1000	200	500	1000	200	500	1000
Av. BER - hard	0	0	0	0	0	0	1/30690	0	0
Av. SINR - hard	11.7	12.9	13.4	10.9	11.6	12.1	11.1	11.8	11.9
Av. BER - soft	0	0	0	0	0	0	1/30690	0	0
Av. SINR - soft	11.9	12.9	13.5	11.5	11.9	12.8	11.6	11.9	12.6

s (5.2425 minutes) long transmission, which corresponds to 135 transmitted packets. In the table, the total number of bit errors averaged over 15 packets is given, along with the average achieved output SINRs in dB.

In both estimation types, error-free transmission is achieved in DFE-IDMA and long code DFE-CDMA, whereas an error of 1 bit was observed for short code DFE-CDMA in the case of the 200 m channel. In most trials, there were small improvements in average SINR by using soft estimation instead of hard estimation. The SINR varied slightly over the sequence of packets. A dense structure of multipath arrivals is observed with increased delay spread in the case of 200 m range. Shorter range shallow water channels suffer from the surface time variability, which results in faster changes of the propagation conditions than those observed in any of the long range channels. Although the transmission distance increases, better output SINRs were obtained at 1000 m than those at 500 and 200 m trials. However, it is worth emphasizing that as the transmission range increases there is a point after which the system becomes SNR limited due to transmission losses caused by the cylindrical spreading. The measured input SNR values for the investigated ranges were approximately 22.1, 20.6 and 17.7 dB for the 200, 500 and 1000 m ranges, respectively. This suggests that although SNR is reduced at longer ranges the improvement in SINR is due to the shorter delay spread, which results in reduced ISI. Additionally, the shorter range channels require longer DFE filters, which in turn result in higher noise enhancement.

Fig. 5.15 demonstrates the performance results along with the receiver parameters of some packets for two active users transmitting with equal powers over the 1000 m channel. After a small number of iterations, the algorithms converge steadily, until error-free transmissions are observed. The bit error rate versus iteration number demonstrates that the proposed iterative receivers have a rapid convergence speed. Most of the iterative gains are obtained in the first three iterations, and more than

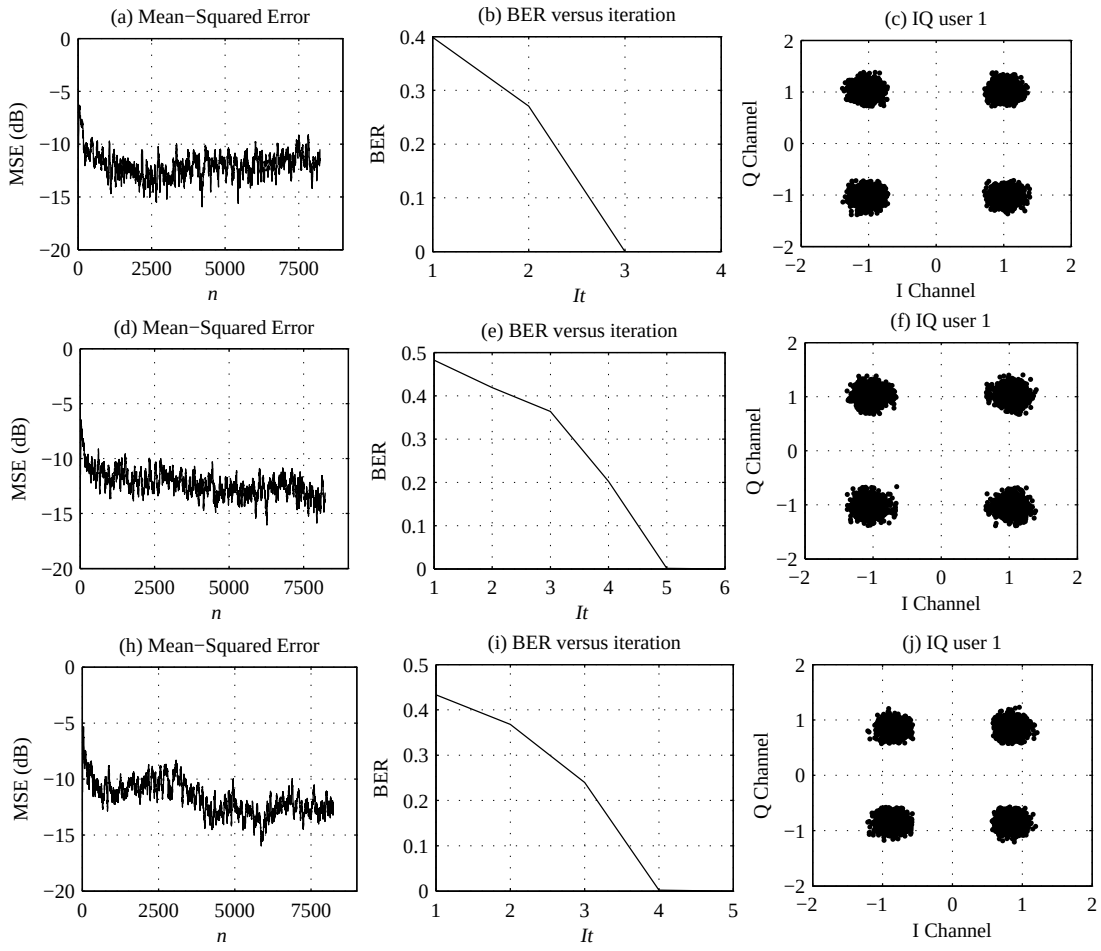

Figure 5.15: Performance results of DFE-IDMA (a - c), long code DFE-CDMA (d - f) and short code DFE-CDMA (h - j) with K=2, where (SINR (dB), M_f, M_b, μ_f, μ_b, a)=(15.5, 16, 16, 0.2, 0.001, 0.01), (15.2 , 16, 16, 0.2, 0.1, 0.1), and (14.4, 16, 16, 0.3, 0.001, 0.00001), respectively.

90% of the data packets are error-free after six iterations. The signal constellation at the equalizer outputs for user 1 is also drawn and shows that adaptive equalization successfully copes with both the ISI and phase variations. Hence, the scatter around the ideal constellation points is reduced as the number of iterations increases. This improvement implies that iterative techniques improve the reliability of the feedback information, which in turn reduces the error propagation in the DFE. Additionally, the detection strategy benefits from more reliable chip decisions which improve the MAI cancellation.

Table 5.6: Results of DFE-IC based turbo schemes with multiplexing pilot, K=4

	K=4								
	DFE-IDMA			long code DFE-CDMA			short code DFE-CDMA		
Ch. range (m)	200	500	1000	200	500	1000	200	500	1000
Av. BER - hard	0	0	2/61440	40/61440	0	0	34/61440	0	17/61440
Av. SINR - hard	10	10.6	11	9.8	10.4	10.9	9.8	10.3	9.9
Av. BER - soft	0	0	0	40/61440	0	0	33/61440	0	17/61440
Av. SINR - soft	10.2	10.6	11.1	10.1	10.4	10.9	9.9	10.5	10.9

The performance of the proposed receivers with four active users under the same conditions is illustrated in Table 5.6. The achieved output SINR decreases significantly as the number of active users increases. The degradation due to this increase is in the order of 1, 0.6 and 0.8 dB for each added user in the DFE-IDMA, long code DFE-CDMA and short code DFE-CDMA systems, respectively. As the number of active users increases, the residual MAI impairs detection, which in turn effects the amount of ISI removed, especially during the first few iterations. Inevitably, the performance of the algorithm regresses due to error propagation in the DFE. However, provided that the BER is sufficiently low, the chip estimates improve with increasing decoding iterations, due to redundancy introduced by the time-bandwidth product and channel coding. Thus, the number of errors in the decisions decreases along with the effects of error propagation. Therefore, the effects of the residual ISI and MAI can be completely removed iteratively.

A closer look at the results of the BER and SINR reveals that the performance reflects the robustness of the iterative receivers, and the DFE-IDMA performance is as good as, or slightly outperforms, the long code DFE-CDMA and short code DFE-CDMA in most configurations. This is due to the fact that in IDMA based systems, the chip level interleavers are more effective in dispersing the chips throughout the packet than their bit-level equivalents in CDMA. The MSE convergence performance and IQ constellation diagrams for user 1, and the BER diagrams versus the iteration number along with suitable receiver parameters of selected packets are demonstrated in Fig. 5.16. The number of iterations directly effects the variance of the error signal, where the error signal represents all residual contamination sources and ISI. Therefore, in this scenario, the iteration number in some packets is increased to achieve error-free transmission, and completely remove the MAI and ISI, as demonstrated in Fig. 5.16 (i).

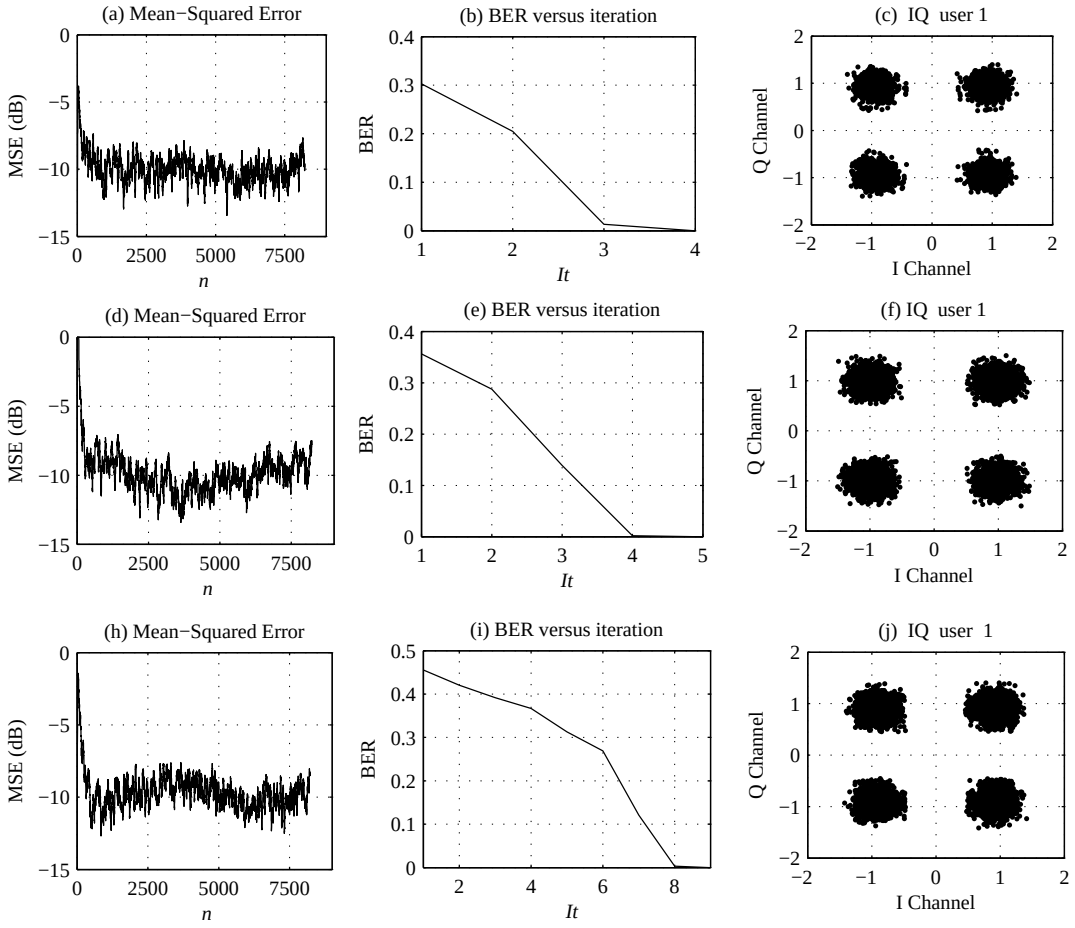

Figure 5.16: Performance results of DFE-IDMA (a - c), long code DFE-CDMA (d - f) and short code DFE-CDMA (h - j) with K=4, where (BER, SINR (dB), M_f, M_b, μ_f, μ_b, a)=(2/4096, 12.8, 8, 8, 0.2, 0.001, 0.001), (0/4096, 13.1, 8, 8, 0.15, 0.001, 0.001), and (17/4096, 12.4, 16, 16, 0.2, 0.001, 0.01), respectively.

Emphasis should also be placed on the fact that the majority of bit-errors occurred due to excessive ISI induced by the 11 ms multipath channel. The penalty in performance is approximately 0.7 and 1 dB compared with the SINR achieved with 500 and 1000 m, respectively, in almost all combinations. Evidently, the iterative detection bring more benefits to the proposed receivers, because the decoders can detect and recover the signals after every iteration and feedback more reliable estimates of the interference. Therefore, the MAI and ISI can be cancelled iteratively in order to achieve an adequate SINR required for reliable operation.

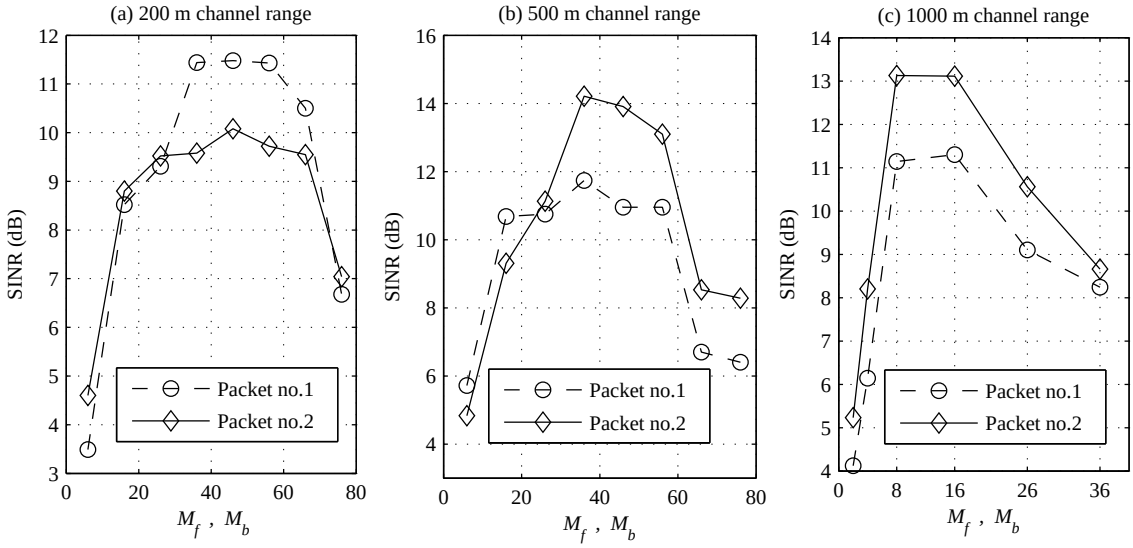

Figure 5.17: The effects of filter lengths of DFE-IDMA receiver over different channel ranges.

5.6.1.1 Transversal filter lengths and adaptive parameters

The filters' lengths are chosen to maintain the algorithm stability and the complexity increases as they cover the overall delay spread, which has an adverse effect on the convergence speed. Additionally, the noise level is not known and a larger number of taps makes the task of adaptive estimation more difficult due to the noise enhancement that leads to errors in feedback decisions. The effect of filter length versus SINR with the adaptive algorithm is illustrated in Fig. 5.17, where the number of taps M_f and M_b are assumed equal in all the investigated packets.

These figures show small filter lengths can be chosen at some expense of system performance, and the SINR is maximized when the number of taps covers the entire delay spread. However, the SINR begins to deteriorate with large number of taps. Therefore, the adaptive parameters or channel parametrization were chosen according to output SINR in all packets, which are 46, 36 and 16 taps for 200, 500 and 1000 m channel ranges, respectively. In the case of the 1000 m trials, the taps are fixed at 8 taps in some of the trials, while in some others they are fixed at 16 taps. However, despite this difference in parameters, the adaptive algorithm easily provides adequate MSE for data transmission on this channel with different channel parameters. This was due to the location of the principal arrivals of the responses and the relative

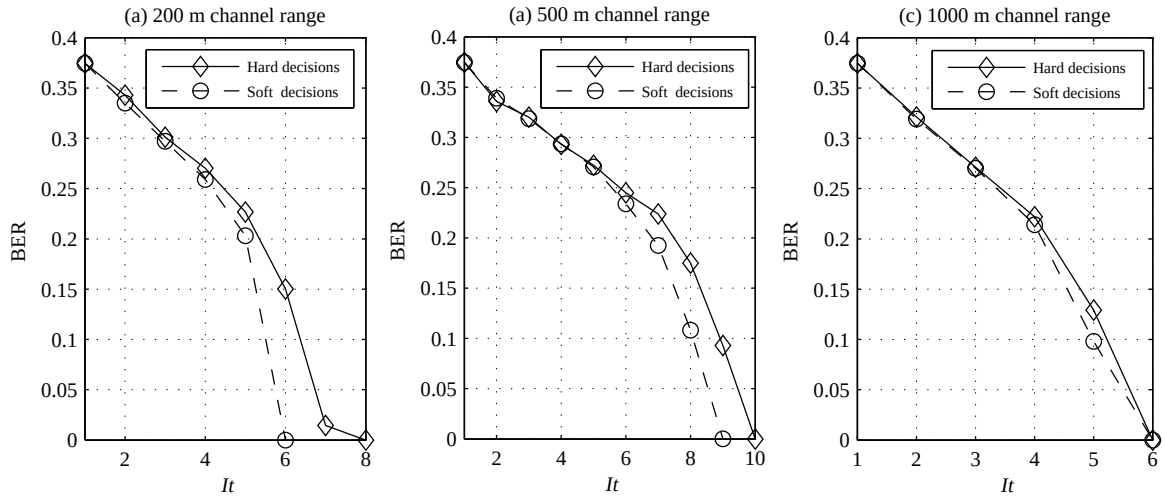

Figure 5.18: Feedback function type effects with DFE-IDMA receiver over different channel ranges.

delays of the signals, where the estimated channel responses concentrate most of their energy in a time span of about 5 ms or less. The values of μ_f and μ_b decide how far the update will take the coefficients of the FIR filters in the negative direction of the gradient. Therefore, choosing a small value will lead to a slow convergence, while very large values might misadjust the coefficients. A compromise must be selected between the MSE value of the update process and fast tracking capability of the algorithm.

5.6.1.2 Feedback function type

In general, the error in estimation is caused by the feedback decisions errors and the additive noise. The impact of the feedback function type is studied in Fig. 5.18, by applying estimation using both hard and soft decisions. The soft algorithm achieved less bit errors and has faster convergence compared with the hard estimation. This minor improvement of soft decisions has an advantage in effective updating of the DFE-IDMA receiver to track time-variant channels.

Table 5.7: Performance of DFE-IC based IDMA receiver with partial knowledge.

	K=2				K=4					
	Full knowledge		Without knowledge		Full knowledge		3 out 4		2 out 4	
Packet No.	Bit errors	SINR	Bit errors	SINR	Bit errors	SINR	Bit errors	SINR	Bit errors	SINR
1	0	12.5	0	6.9	0	10.9	0	9.9	10/2048	4.4
2	0	12.2	0	6.6	0	10.5	0	10.1	16/2048	4.4
3	0	14.2	0	7.4	0	9.8	0	9.6	55/2048	4.1
4	0	13.5	0	6.8	0	10.3	4/3072	9.7	48/2048	4.2
5	0	13.6	0	6.5	0	9.5	11/3072	9.3	71/2048	4
6	0	13.2	0	7.2	0	12.3	4/3072	9.8	74/2048	4.3
7	0	14.7	0	7.3	0	11.2	0	9.5	0	4.7
8	0	14.2	0	7.4	0	13.3	0	10.3	0	4.5
9	0	13	0	7.2	0	10	4/3072	9.7	65/2048	3.1
10	0	15	0	6.4	0	10.6	0	9.7	52/2048	4.1
11	0	11.9	0	7.1	0	10.6	0	9.5	61/2048	4.2
12	0	11.4	0	7.5	0	11.7	0	10	87/2048	3.3
13	0	13.8	0	7.5	0	10.9	0	9.8	54/2048	4.2
14	0	14.9	0	7.2	0	11.4	2/3072	10	26/2048	4.3
15	0	13.5	0	7.1	0	13.9	0	10	18/2048	4.5

5.6.2 Performance Evaluation with Partial Knowledge

For the K=2 scenario, and in the absence of knowledge of the interleaver patterns, it is shown in Table 5.7 that the proposed receiver can still achieve a performance comparable to the receiver with full knowledge of the separation patterns. Error-free transmission is achieved; however, partial interleaver pattern knowledge reduces the achieved SINR by half. Furthermore, in the case of partial knowledge and K=4, with only 3 of 4 of the active users' interleavers known by the receiver, the proposed scheme exhibits a performance comparable to that when all the patterns are known. To achieve excellent performance, more iterations in the MUD are generally needed. However, in 2 out of 4 active users known by the receiver, the performance deteriorated significantly with the increased number of unknown users' parameters. Therefore, it may justify the use of MUD downlink with known users' parameters for some applications in such environments. Since the detector treats the other signals as noise, this approach yields computationally simple structures. In contrast, MUD exploits the knowledge about the structure of interference and perform joint detection of all the users' signals. Although more complex, this approach gives performance gain in cases with high levels of MAI.

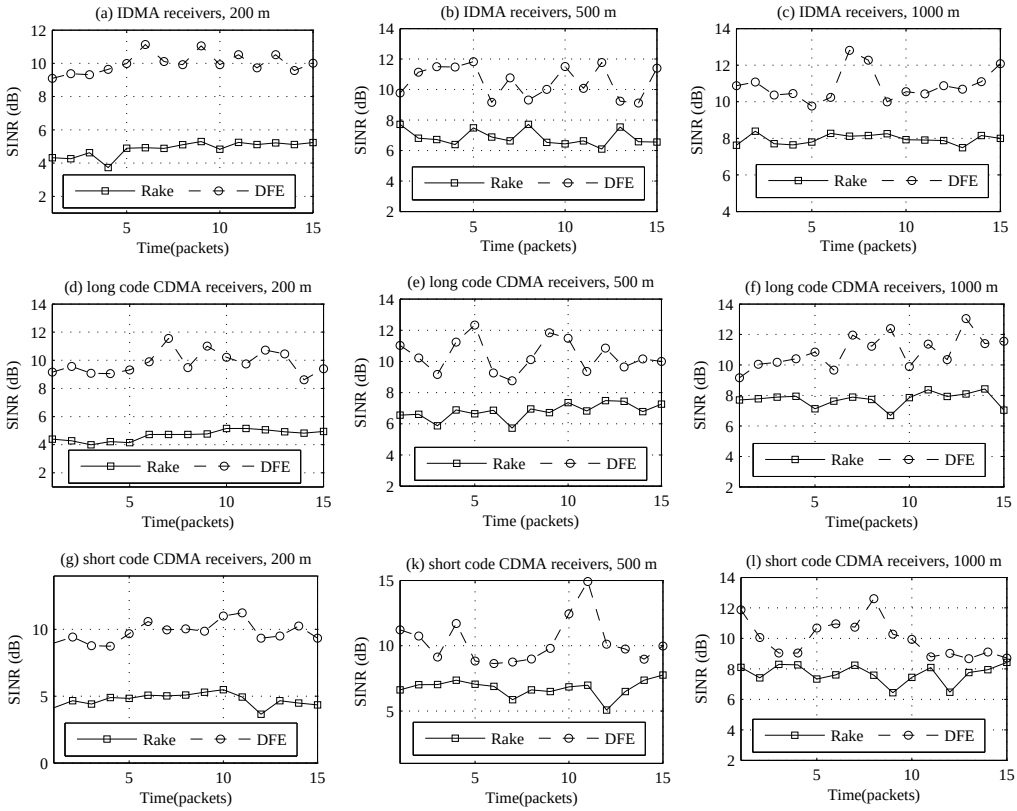

Figure 5.19: SINRs comparison of DFE-IC and Rake with CE based T-MUDs receivers over different trials, K=4.

5.6.3 Performance Comparison of IDMA/CDMA Structures

The results of CE based Rake-IDMA and Rake-CDMA receivers with K=2 and K=4 are listed in Table 5.3. The receivers successfully process the received data that has negligible Doppler spread and MAI signals to yield few or no information bit errors in the case of two active users, but the BERs and SINRs of the receivers differentiate significantly with K=4. The majority of bit errors also occurred due to the extended ISI induced by the 11 ms delay spread of the multipath channel. The receivers fail to produce better results in some packets, whereas in others, the algorithms converge to five bit errors or less. However, in the case of K=4, a reasonable performance over 500 m and 1000 m with Rake-IDMA is still achieved and shows better performance than both forms of Rake-CDMA in most packets.

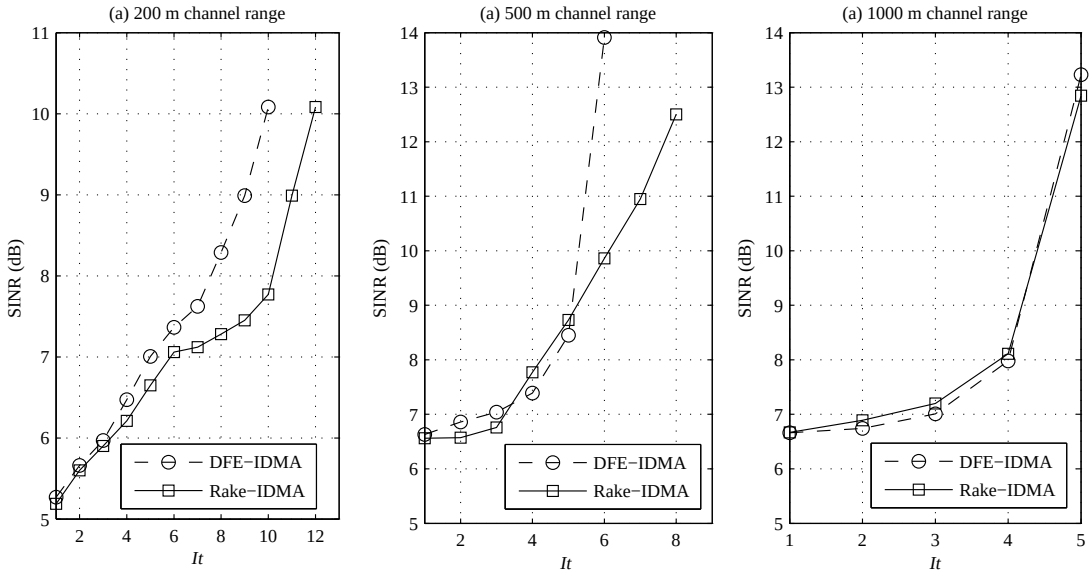

Figure 5.20: SINRs versus iteration numbers of DFE and Rake based IDMA receivers.

The BER and SINR comparison results in Tables 5.3, 5.5, 5.6 and Fig. 5.19, respectively, demonstrate that the direct adaptive DFE based IDMA/CDMA receivers can mitigate the bit errors and outperform the IDMA/CDMA receivers based on CE under different ISI and MAI conditions, due to the iterative equalization and MAI cancellation. Although, the use of adaptive CE with Rake IDMA/CDMA produces no errors with most of the packets except for a few due to very low SINR. In these packets, the receiver was not able to give reliable outputs for the single-users' decoders, due to the fact that the channel estimator relies on the feedback decisions and was not able to detect the multipath properly. Thus, these wrong components when entering the joint ISI and MAI cancellation cause the output LLRs to become unreliable. The output SINR for reliable operation depends on the system error probability as well as error-correction coding, and these figures also give an indication that these systems operate reliably at a SINR of approximately more than 6 dB.

5.6.3.1 Convergence speed and cancellation stage number

The SINR values of the same packets using adaptive DFE-IDMA and Rake-IDMA receivers are drawn in Fig. 5.20 as a function of iteration number. These figures illustrate the successful improvement of the SINR along with each pass, where the bit

Table 5.8: Performance of DFE-IC based IDMA receiver with continuous pilot

	K=3								
	DFE-IDMA			long code DFE-CDMA			short code DFE-CDMA		
Ch. Range(m)	200 m	500 m	1000 m	200 m	500 m	1000 m	200 m	500 m	1000 m
Av. BER	0/46080	0/46080	0/46080	0/46080	2/46080	0/46080	0/46080	0/46080	0/46080
Av. SNIR	10.9	11	11.3	10.3	10.4	11	10.3	10.7	11.1

errors reduce dramatically. An improvement of between 5-8 dB in SINR was observed between the first and last iteration. The plots also highlight the performance gaps and the convergence speed of the two receivers for the different channel ranges, which in turn translates to different delay spreads. The direct adaptive receiver has faster convergence than the Rake receiver based channel estimation in most investigated packets. Moreover, the algorithms need less number of iterations with the small delay spread compared to the large delay spread that needs more iterations to converge to a reliable SINR.

5.6.4 Performance Comparison using Continuous Pilots

The performance of the DFE-IDMA and DFE-CDMA receivers with three active users is illustrated in Table 5.8. The turbo DFE based IDMA/CDMA receivers with continuous training approach, produced no errors in all but one case. In this case, an error of 2 bits out of 46080 was observed for long-code DFE-CDMA in the case of the 500 m channel, where the decoder for user 3 was not able to correct these 2 bits errors. In contrast, the use of adaptive channel estimation with Rake IDMA/CDMA in 5.4, deteriorate significantly and produces errors in a few packets. However, the Rake receivers still demonstrate good performance, especially with 1000 m channel range. Fig. 5.21, demonstrate the results of packet no.15 with turbo receivers-based continuous pilot approach. The plot also shows that the phase variation can pick up a random varying component, which if not cancelled can result in non negligible symbol errors.

Further, it is not surprising to see that direct receivers have much better performance than Rake receivers and are less affected and limited by other factors, such as ISI. The results in terms of SINRs are also shown in Fig. 5.23 and Fig. 5.22, and illustrate this deterioration for the rake receivers, where the channel estimation errors increase with increasing channel variation. With a relatively small number of

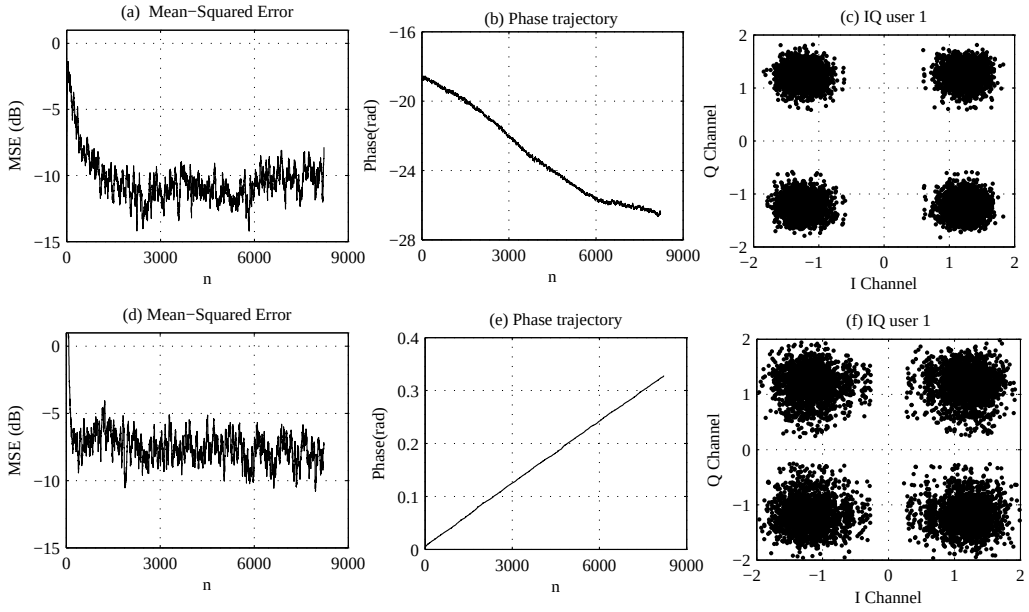

Figure 5.21: Performance results of DFE-IDMA (a-c) and Rake-IDMA (d-f) receivers with continuous pilots over 1000 m channel range, where M_f=24, M_b=24, and M= 22.

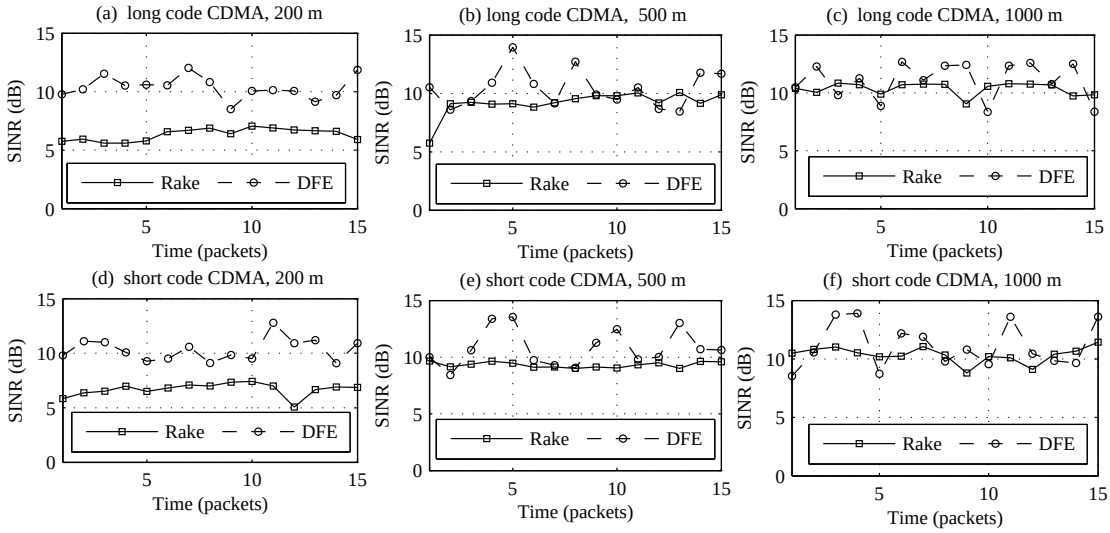

Figure 5.22: SINR comparison of DFE-CDMA and Rake-CDMA receivers using continuous pilots.

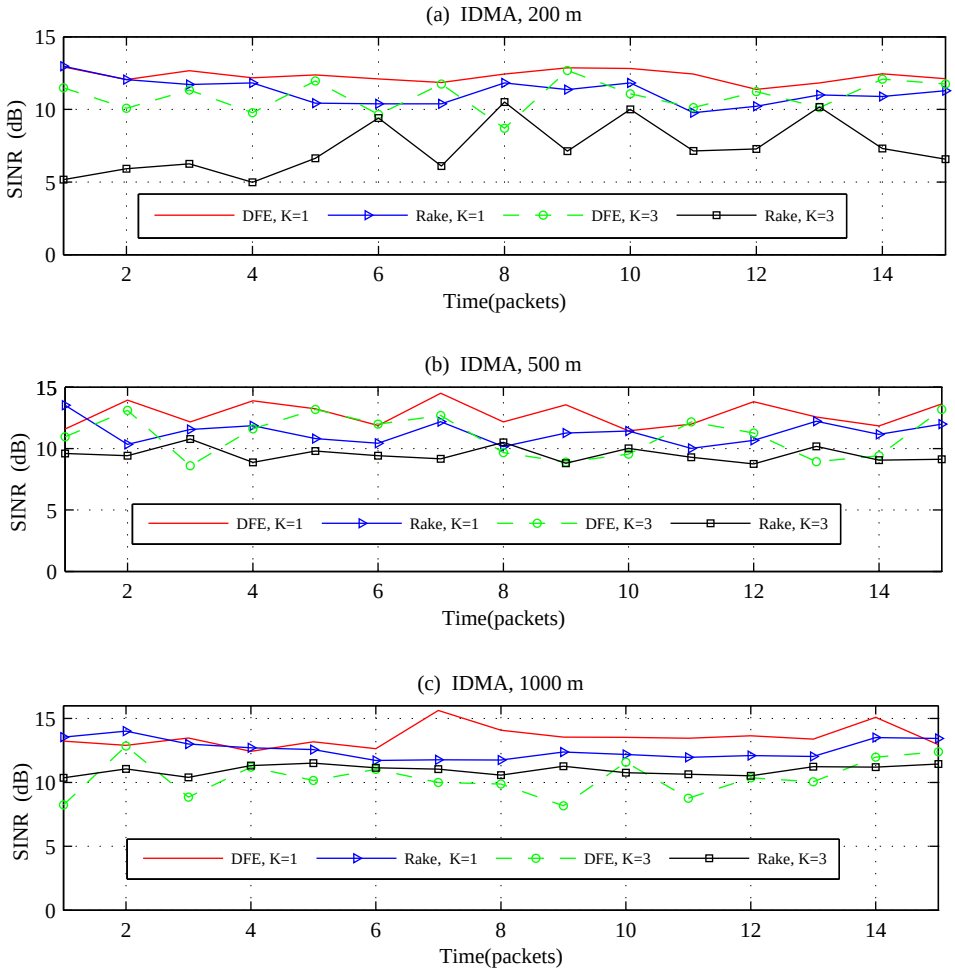

Figure 5.23: SINR comparison of DFE-IDMA and Rake-IDMA receivers using continuous pilots.

iterations, the SINRs in Fig. 5.23 with $K = 3$ converge to the $K = 1$ performance in both receivers, where the single-user bound performance depends on the channel coding and the iteration number. The results for single user scenarios are not included in the tables since the data from all receivers cause the algorithms to converge with zero bit errors after just three iterations. However, the direct adaptive receivers generally outperform the Rake receivers, and the acceptable bit errors of the DFE based IDMA/CDMA receivers suggest that the proposed scheme is a realistic means of obtaining low bit error rates. The results of the BERs and SINRs for all packets can be found in Appendix A .

5.7 Real-time Processing System Considerations

With their low cost and low power consumption, DSPs are the most suitable devices for physical layer based functions such as MUDs, CE and decoding. In general, the system constraints affect not only the physical layer, but all the layers of network architecture. Some of these obvious constraints are the transmission power, acoustic transducers and high complexity that preclude the implementation of optimal algorithms over long delay spread channels. The transmission power depends on the range and its typical values are in the order of tens of watts. The acoustic transducers transform electrical waves into sound waves and vice versa, and they have their own bandwidth limitation that limits the available bandwidth beyond that offered by the UAC.

To show that the proposed structures are actually manageable on current hardware, we turn our attention to the issues, such as the execution time as well as complexity requirements that influence the design and realizing such architectures in practice. We will also present details about the hardware structures such as DSP typically used in such systems. The UAC characteristics that drive the complexity of underwater systems include large delay spreads, the presence of Doppler spread and the frequency-dependence of propagation loss. Further, as the range and the data rate of the systems increase, the complexity of the algorithms grows beyond the capacity of current DSP hardware. However, this study constitutes the first steps towards the realization of a real-time processing platform.

5.7.1 Computational Complexity Comparison

In real-time adaptive applications, there are hardware limitations that may affect the system performance. The complexity is of extreme importance in system design, where the complex algorithm requires more hardware resources than a simple algorithm. Moreover, the high complexity may result in long processing delays as well as high energy consumption. In order to compare the computational cost of the proposed architectures, a hypothetical implementation is considered using a DSP such as the ADSP-21364 SHARC from Analog Devices that can perform the different operations in a 3 ns cycle. The comparison does not take into account the decoders, despreaders, spreaders and interleavers operation since these operations are identical

in both receivers. Table 5.9 summarizes the number of real operations per chip (a QPSK symbol), per user and per iteration for the detection process in both receivers, where one complex multiplication equals 4 real multiplications and 2 real additions. An example for sea trial data with $K = 4$, $It = 6$ with 1000 m channel range is also given. The required computational times are also given, and the read/write operations have not been considered.

The PIC has linear complexity in frame length and is independent of P, while the feedforward and feedback filter coefficients of adaptive equalization, as well as the overall complexity, are a linear function of the channel dimension and independent to some degree of the constellation size. For the Rake scheme, the total complexity involves 13104 multiplications, 8754 add./sub., and 48 hyperbolic tangent (tanh) operations. In contrast, there are approximately 1776 multiplications, 1524 add./sub. and 48 hyperbolic tangent operations for the proposed detector. Therefore, the proposed detector is the simplest detector and require less computational time, both in number of add./sub. and multiplication operations. The number of other functions is exactly the same in both detectors. Additionally, the division operations that have a high hardware complexity are fewer in the proposed receiver compared with the

Table 5.9: Complexity comparison of DFE-IC and Rake detectors

CE based Rake-IDMA detector			
Op.	Rake MUD (M=16)	Adaptive CE (M=16)	K=4, It=6
$\times$	32$\times$ $M \times K \times It$	8 $(M+1) \times It$	13104
+/-	22 $\times M \times K \times It$	$3(M+1) \times It$	8754
$\div$	$2 \times M \times K \times It$	$1 \times It$	774
tanh	2$\times$ $K \times It$	-	48
exp	-	$4 \times It$	24
Computational time=22704 $\times$ 3 ns =68.112 μs			
Adaptive DFE-IC detector			
Op.	Adaptive DFE (M_f=16, M_b=16)	PIC	K=4, It=6
$\times$	$8(M_f + M_b + 1) \times It$	$8 \times K \times It$	1776
+/-	$6(M_f + M_b + 1) \times It$	$14 \times K \times It$	1524
$\div$	$2 \times It$	$2 \times K \times It$	60
tanh	-	2$\times$ $K \times It$	48
exp	4$\times$ It	-	24
Computational time=3432 $\times$ 3 ns =10.296 μs			

original receiver. These algorithms may need more processing time to be run by the DSPs than the packets duration, and they should meet the real-time requirements to be implemented within the DSPs. However, the low computational complexity and memory requirements make our systems attractive for real time implementation.

5.7.2 ADSP-21364 Architecture Description

The analog devices of super Harvard architecture (SHARC) ADSP-2136x family processors such as ADSP-21364 are high speed special processors with a single instruction and multiple data (SIMD) computational architecture. The processors emphasize the balance among the bandwidth of I/O data, clock, and data processing ability. Consequently, the system satisfied the real-time processing requirements of underwater acoustic communication. The ADSP-21364 contains a central processing unit (CPU) with an instruction cache and executes multiple instructions in parallel, which results in fast operations. The processors have very large scale integration (VLSI) techniques that support 32-/40-bit floating-point and operate at 333 MHz instruction rate with other peripherals. The functional block diagram of ADSP-2136x in Fig. 5.24 uses two computational units to deliver a significant performance, and includes the following architectural features:

- Two processing units with arithmetic logic unit (ALU), shifter, and multiplier.
- 3 Mbit static RAM and 4 Mbit mask-programmable ROM.
- Program sequencer (PS), multiple internal buses program memory (PM) and data memory (DM).
- I/O processor that handles 32-bit DMA for the peripherals.
- 8/16-bit parallel port, six full duplex serial ports.
- Digital audio interface (DAI) that includes 8 serial interfaces, 10 interrupts, 6 flag inputs/outputs, 3 timers, 2 precision clock generators (PCG) and DTCP cipher.

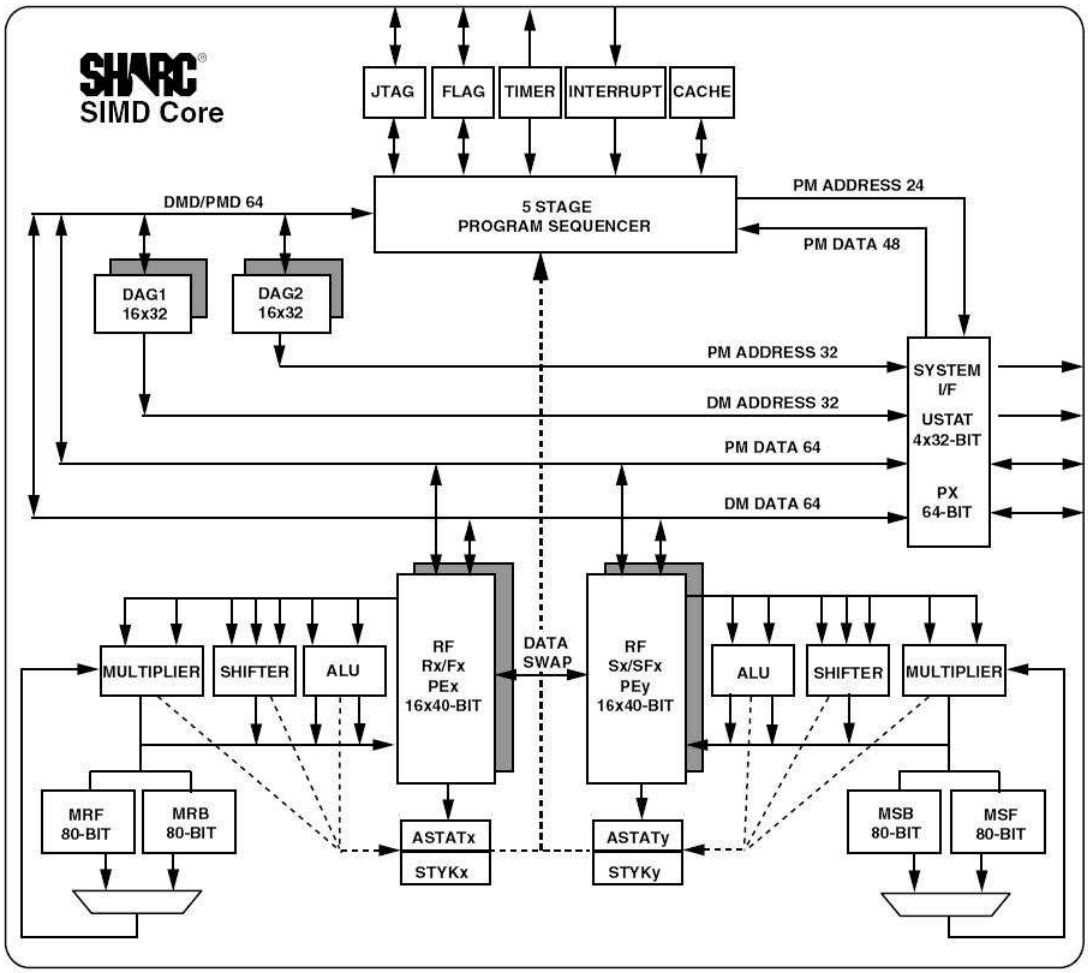

Figure 5.24: The functional block diagram of the SHARC DSPs.

In addition, there is a need at the receiver side for continuous collection of received data prior to actual processing. This collected data will have to be buffered while actual processing occurs on previously collected data samples. Hence some hardware support such as direct memory access (DMA) and parallel port (PP) are essential for efficient operation. The PP includes a 16-bit multiplex address/data buses and an address latch enable pin (ALE). The PP connects to an 8-bit SRAM memory/parallel flash memory and 8 general-purpose LEDs. See also in Appendix B the block diagrams of the system architecture and PP [99, 100].

5.8 Summary

In realistic network scenarios, the adaptive architectures presented in previous chapters are examined using experimental signals. A detailed description of the experimental parameters and scenarios, employed in order to investigate the proposed structures are given in Section 5.2. By employing different shallow UACs, the performance of these algorithms using two training methods was demonstrated for a two, three and four user multiple-access network.

These results demonstrated a remarkable improvement of the structures using adaptive DFE-IC detector as compared to the Rake MUD with separate CE. The decoupled CE is shown to be robust against severe channel fluctuation and it is limited by MAI especially with small processing gain. The direct adaptive receivers achieve lower bit error rates, while needing fewer stages than CE based Rake-IDMA to reach its steady-state level. However, the DFE-IC based IDMA/CDMA is more robust and solves the error floor problem as compared to the Rake based IDMA/CDMA in the case of sparse channels, where ISI/MAI suppression degrades considerably in Rake based receivers if the CE is not reliable. In addition, the different IDMA receivers perform somewhat better than both CDMA forms in most cases. Due to the ability to cope effectively with the dynamic nature of the UACs, the most promising results are obtained using the schemes with continuous pilots. Minor improvement is obtained using a soft algorithm instead of hard due to its ability to mitigate and correct feedback decision errors. In the presence of unknown codes, the direct adaptive schemes can still achieve good performance, but increasing the MAI from other users will limit the performance of such single-user algorithms. In such cases, the multiuser algorithm that exploits the knowledge of all the codes will be a more attractive solution for such downlink systems. However, these results were also confirmed with the simulation results, which were presented in Chapters 3 and 4, and emphasize the feasibility of reliable communications over these channels.

The computational complexity, which represents the major considerations in the implementation of any system, was evaluated along with the required computational time. The details about the DSP are also presented and these details represent the primary steps towards the realization of a real-time processing system.

CHAPTER 6

Conclusions and Future Work

6.1 Conclusions

IN this thesis, the research is entirely devoted to investigate the use of T-MUDs in single carrier multiple access shallow-water networks. The main objective was to design practical multiuser algorithms that can deal with the MAI from other acoustic modems, the extended multipath spread, as well as the rapid phase fluctuations induced by the UACs. Therefore, special communication techniques, such as spread spectrum, time filtering as well as utilization of error correction codes are required and need to be applied simultaneously. However, reliable communication in such challenging environment requires a better understanding of the channel characteristics and environmental parameters.

The multipath in UACs and its impacts on transmitted signals were considered in chapter 2. In this chapter attention was concentrated on the channel propagation model and the concepts of time dispersion and the frequency selective nature of fading. The characteristics such as path loss, ambient noise and multipath fading were also considered. In such bandlimited channels, multipath phenomena occur as a result of surface and bottom reflections, which superimpose on each other to distort the signal in amplitude and phase. The background noise is often characterized as non Gaussian. Examination of both the CIRs and the time varying nature in the investigated realistic channels highlighted that the channel is rapidly fluctuating and it has a sparse channel structure that spreads over both propagation delay and Doppler. Therefore, spread spectrum systems such as CDMA and IDMA systems will help to compensate for the resulting signal distortion, differentiate between different users and improve immunity against multipath effects.

The mathematical representation of CDMA and IDMA systems along with the concept of spread spectrum techniques were considered in chapter 2. The representation of pseudorandom sequences, correlation function, and optimization criteria were also discussed. A description of the commonly CDMA receiver structures, which utilize spreading codes to differentiate between users was given, highlighting the optimum and suboptimum detector architectures. Although the trellis-based turbo-architectures constitute attractive structures in the context of bandwidth efficient transmissions over the ISI channels, they rely on optimum detectors whose high computational complexity limits its practical implementation. We have then introduced the basic principles of the turbo IDMA scheme, which employ different chip-level

interleavers for user separation. By removing spreading and devoting entire bandwidth expansion to channel coding, IDMA can obtain additional coding gain over conventional CDMA. Because of the fact that a multiuser scenario is employed, it is important to choose weakly correlated interleavers between different users. Additionally, the optimum and Gaussian approach of the IDMA detector are considered with the important IDMA features in comparing with the existing multiple access architectures. However, the IDMA scheme allows very low cost chip detection algorithm that can be used in both synchronous and asynchronous channels.

In chapter 3, CE based IDMA and CDMA structures, are examined for different channel conditions. In this chapter, we have demonstrated that the Rake multiuser algorithm is very effective to suppress MAI with known channels. Even with small spreading factors and random interleavers, it can achieve near single user performance. The BERs of long code and short code CDMA systems are close to that of the IDMA systems and this small improvement in IDMA performance is due to the long periods of chip level interleavers. Moreover, the detection algorithm can be carried out either by SIC or PIC. SIC takes a serial approach to remove the MAI signals, while PIC estimates and simultaneously removes out all the MAI produced by the other users accessing the channel. It is observed that SIC needs less iterations than PIC to reach the same performance, and the parallel processing is the reason for considering PIC in this thesis. However, the channel coefficients' estimates are not assumed to be perfect in practice, and if the channel estimates are not reliable, these estimates will significantly reduce the ability of the detection algorithms to remove the correlation introduced by the channels.

An adaptive joint CE and phase tracking algorithm is developed in chapter 3 for IDMA and CDMA systems using two different training methods. Training sequences are usually embedded in transmitted signals to acquire the channel state and facilitate synchronization and CE. Based on the enhanced soft iterative information, the transversal filters and carrier tracking are adapted jointly at chip rate based on MMSE criterion to ensure reliable communication, especially for long delay spread channels. Two low cost adaptive algorithms, LMS and NLMS, are employed to track and correct the effects of time variations. The adaptive algorithm was significantly refined by using multiplexing pilots or continuous pilots as well as soft feedback estimates after single users' decoders.

In addition, multipath channels exhibiting Rician characteristics were used in order to examine the performance of the proposed approaches. Erroneous feedback decisions cause error propagation and limit the system performance. By employing threshold devices, it is possible to design a Rake that uses only the significant channel components. Since pilot symbols are transmitted along with data, the tracking using continuous pilot method was found to be more bandwidth efficient. However, the limited capability of most of these algorithms with time-multiplexing pilots may preclude their use in highly Doppler channels. In contrast, by exploiting the presence of a continuous pilot signal this approach has been shown to be a better technique to track fast fading channels than the conventional pilot-based approach.

Unfortunately, the rapid fluctuations and sparse structure in UACs, together with the extended overall delay spread, creates a challenging CE problem. As the channel dispersion increases, the errors in the estimated coefficients have a significant impact on the performance of coherent Rake based receivers, where performance is limited by both MAI and ISI and exhibits an error floor due to degraded CE. In such cases, the chip-level DFE based turbo structures can have better immunity against the spectral channel characteristics, and give the forward filter greater flexibility in handling ISI. In chapter 4, the DFE-IC detector is proposed using two different training methods for synchronous IDMA and CDMA systems operating over frequency selective channels. The direct adaptation detector based on MMSE criteria integrate the functions of the DFE, phase tracking and IC techniques into one structure, which requires partial or full knowledge of interfering users. By taking advantage of previous decisions of interfering users at each iteration, the receivers minimize the MSE and the contribution of channel coding improves the robustness and protects the transmitted data from the remaining errors.

The DFE-CDMA structure has been formulated based on the derivation of the adaptive DFE-IDMA receiver. The simulation results of these different receivers show that the proposed continuous training approach outperforms the conventional approach over a wide range of normalized Doppler spreads. Minor improvements are obtained by adopting soft feedback decisions instead of hard feedback decisions, which help to reduce the impacts of error propagation in the DFE. For channels where it is necessary to track the signal on a chip-by-chip basis, the results indicate that the DFE-IDMA can provide the flexibility required to improve the performance with limited training by 1-2 dB over the Rake receiver. Therefore, the joint direct forms

constitute a powerful technique with overwhelming performance gains over separate CE based receivers in fading environments. However, the major difference between the two approaches is in their ability to track the time-variation in the signal. For additional improvement, feedback ISI canceller that utilizes the estimates of both past and future chips can be used when both the pre-cursive and post-cursive ISI are significant in the CIR. Furthermore, the simplicity of these structures makes them attractive for deployment in the underwater environment.

In order to gain more insight into the convergence behaviour of such detectors, the analytical results with the aid of EXIT charts were evaluated over unknown time variant channels. The results have shown that the detected trajectory is quite close to the real simulated trajectory. The performance difference between the Rake-MUD and DFE-IC detectors with different pattern of training sequences, are also presented. However, the convergence of such detectors is not only related to its architecture and channel conditions, but also related to the system parameters. The impact of these parameters, e.g., the user number and the spreading factor, were also examined to obtain a better understanding in the design of successful T-MUDs.

In realistic network scenarios, the proposed architectures presented in previous chapters are also investigated in chapter 5 using experimental signals. The investigated scenarios are used to examine the schemes over three different channels, where the number of active users was maximally four. The results demonstrated a remarkable improvement for structures that use adaptive DFE-IC detector as compared to those that use Rake-MUD with separate CE. Direct adaptive receivers demonstrated lower bit error rates and needed fewer stages than CE based Rake-IDMA to reach its steady-state level. Therefore, the DFE-IC based IDMA/CDMA is more robust and solves the error floor problem as compared to the Rake based IDMA/CDMA in case of sparse channels. Although the Rake based receivers was shown to be also robust against severe channel fluctuation with two users, the ISI/MAI suppression was degraded considerably especially with increasing number of users.

The different IDMA receivers performed somewhat better than both CDMA forms in most scenarios. Due to the ability to cope effectively with the dynamic nature of the UACs, the most promising results were obtained using the schemes with continuous pilots. Minor improvement was obtained using soft algorithm instead of hard algorithm due to its ability to mitigate and correct feedback decision errors. The filters' lengths can become problematic for the algorithms that rely on the inver-

sion of the channel correlation matrix. Further, longer filters' lengths may not lead to better performance when the error-propagation is taken into account, thus, the filters' lengths are chosen to maintain the algorithm stability and span the longest multipath delay spread. In some cases, the direct adaptive schemes can be operated as a single-user receiver without requiring any explicit knowledge of the interfering users. However, increasing the MAI from other users will limit the performance of such single-user algorithms, where the DFE-IC cannot subtract a sufficient amount of interference to achieve good performance. In such cases, multiuser algorithm that exploits the knowledge of all the codes was proven to be more attractive for such downlink systems.

Finally, we have performed a comparative study on the proposed techniques with regard to their computational complexities. The complexities of these structures are respectively linear to the path number, and both are independent of the user number. However, DFE-IC detector is proposed as a low complexity alternative to the MAP and Rake detectors over long delay spread channels. These results also demonstrate the possibility of implementing the proposed structures on portable terminals in real-world environments, and also offer an interesting perspective for the DSP implementation and the realization of a field programmable gate arrays (FPGA) prototype.

6.2 Future Research Work

The following points can be considered in future research:

- To increase the systems' reliability at low data rates, further redundancy can be introduced using error correction codes, such as those in [6], rather than using longer spreading sequences.

- The low complexity clearly demonstrates the possibility of implementing such architectures in practice on DSP and FPGA platforms. However, this work constitutes the preliminary steps towards such hardware realization and much work is required to achieve the objective.

- Our research has concentrated on time domain techniques to remove MAI/ISI effects in single-carrier downlink systems. However, the basic algorithms are applicable for the detection schemes in frequency domain transmissions. Research in this field may also investigate the benefits of using multi-carrier architectures, and uplink multi-user communication in real underwater environments.

- It must also be noted that these experimental results were obtained when there was no significant movement in the systems. If there were intentional movement, one could expect the performance to degrade more rapidly with an increase in the spreading factor. Future trials should encompass a broader range of conditions, including transmission from moving autonomous underwater vehicles (AUVs), where more robust processing techniques are required to combat Doppler effects.

- In the majority of UACs, a single-sensor is not adequate for a reliable performance. Hence, further work should use other diversity techniques to ensure stability and convergence of the employed adaptive algorithms. Furthermore, higher modulation schemes may also be used to increase the data rate in shallow UACs exhibiting short time-delay spreads.

- By keeping only those taps whose magnitude are larger than a pre-determined threshold, the tracking algorithms can have lower complexity and smaller noise errors. Thus, future work combining sparse techniques with turbo multiuser structures may help address the difficulty of such sparse channels.

Appendices

Appendix A

A BER/SINR values of IDMA/CDMA systems

Table 1: Results of CE based T-MUDs with multiplexing pilot, K=2

	K=2								
	IDMA			long code CDMA			short code CDMA		
Ch. Range(m)	200 m	500 m	1000 m	200 m	500 m	1000 m	200 m	500 m	1000 m
Packet 1	0	0	0	0	0	0	0	0	0
Packet 1	7.8	11.2	13.2	7.8	11.3	12.3	7.3	10.6	15.9
Packet 2	0		0	0	0	0	0	0	0
Packet 2	7.2	12.4	12.9	7.8	10.5	14.9	6.5	12.1	13.4
Packet 3	0	0	0	0	0	0	0	0	0
Packet 3	7.8	10.3	16.1	8.3	10.4	12.1	8.5	10.9	14.5
Packet 4	0	0	0	0	0	0	0	0	0
Packet 4	6.8	10.3	13.3	6.1	11.7	14.7	7.3	11.5	12.3
Packet 5	0	0	0	0	4	0	0	0	0
Packet 5	6.7	11.5	13.8	8.0	10.8	13.2	6.3	11.1	14.8
Packet 6	0	0	0	0	0	0	0	0	0
Packet 6	6.9	12.3	12.5	7.7	12.6	12.8	7.3	12.6	12.6
Packet 7	0	0	0	0	0	0	4	0	0
Packet 7	7.3	11.8	12.3	6.2	11.1	11.7	7.3	11.3	15.1
Packet 8	0	0	0	0	0	0	0	0	0
Packet 8	7.3	11.5	11.7	7.0	11.7	13.0	7.6	11.5	14.2
Packet 9	0	0	0	0	0	0	0	0	0
Packet 9	7.0	11.1	14.1	6.9	13.2	15.3	7.6	12.3	13.5
Packet 10	0	0	0	19	0	0	0	0	0
Packet 10	7.6	10.1	14.7	6.7	10.2	13.9	6.5	12	11.8
Packet 11	0	0	0	0	0	0	0	0	0
Packet 11	6.6	11.5	12.3	6.8	13.0	13.6	7	11.2	11.1
Packet 12	0	0	0	0	0	0	0	0	0
Packet 12	6.0	11.5	14.2	7.2	10.6	12.2	6.2	12.1	10.4
Packet 13	0	0	0	0	0	0	0	0	0
Packet 13	7.9	13.9	12.7	6.1	11.4	14.7	6.1	10.1	10.4
Packet 14	0	0	0	0	0	0	0	0	0
Packet 14	7.8	12.2	11.8	7.4	11.8	13.8	6.2	10.1	15.6
Packet 15	0	0	0	0	0	0	32	0	0
Packet 15	7.0	10.8	13.9	6.7	10.5	14.4	7.2	10.8	12
Av. BER	0	0	0	19/30690	4/30690	0	36/30690	0	0
Av. SINR	7.2	11.5	13.3	7.1	11.3	13.6	6.9	11.2	13.1

Table 2: Results of CE based T-MUDs with multiplexing pilot, K=4

	K=4								
	IDMA			short code CDMA			long code CDMA		
Ch. Range(m)	200 m	500 m	1000 m	200 m	500 m	1000 m	200 m	500 m	1000 m
Packet 1	0	0	6	37	0	4	59	8	0
Packet 1	4.3	7.7	7.6	4.1	6.6	8.1	4.3	6.5	7.7
Packet 2	77	0	2	37	4	8	341	15	0
Packet 2	4.2	6.8	8.3	4.6	7.0	7.4	4.2	6.6	7.7
Packet 3	0	4	6	24	2	0	998	1119	8
Packet 3	4.6	6.7	7.7	4.4171	7.0	8.2	3.9	5.8	7.8
Packet 4	1038	132	12	42	0	0	130	6	2
Packet 4	3.7	6.3	7.6	4.8	7.3	8.2	4.2	6.8	7.9
Packet 5	12	0	4	10	0	138	1367	19	216
Packet 5	4.8	7.4	7.7	4.8	7.0	7.3	4.1	6.6	7.1
Packet 6	0	0	0	6	20	8	126	6	12
Packet 6	4.9	6.8	8.2	5.0	6.8	7.6	4.7	6.8	7.6
Packet 7	0	18	0	49	167	0	46	853	8
Packet 7	4.8	6.6	8.1	5.0	5.8	8.2	4.7	5.7	7.8
Packet 8	0	0	0	0	4	6	2	10	4
Packet 8	5.1	7.7	8.1	5.0	6.6	7.5	4.7	6.9	7.7
Packet 9	0	6	0	4	35	1466	8	4	932
Packet 9	5.2	6.5	8.2	5.3	6.5	6.4	4.76	6.71	6.6
Packet 10	0	6	0	8	8	0	4	4	0
Packet 10	4.8	6.4	7.9	5.4	6.8	7.4	5.1	7.3	7.8
Packet 11	2	22	8	92	8	16	0	0	0
Packet 11	5.2	6.6	7.9	4.9	6.9	8.0	5.1	6.8	8.3
Packet 12	0	704	4	1447	1586	1134	4	0	6
Packet 12	5.1	6.0	7.8	3.6	5.0	6.4	5.0	7.4	7.9
Packet 13	0	0	4	73	46	4	0	10	0
Packet 13	5.2	7.5	7.4	4.6	6.4	7.7	4.9	7.4	8.0
Packet 14	45	24	0	84	0	4	18	0	0
Packet 14	5.1	6.5	8.1	4.4	7.3	7.9	4.8	6.7	7.1
Packet 15	0	64	0	41	6	6	0	12	804
Packet 15	5.2	6.5	8.0	4.3	7.7	8.4	4.9	7.2	7.0
Av. BER	1174/61440	980/61440	46/61440	1954/61440	1886/61440	1794/61440	3124/61440	2066/61440	1992/61440
Av. SINR	4.9	6.8	7.9	4.7	6.7	7.6	4.7	6.7	7.6

Table 3: Results of DFE-IC based T-MUDs with multiplexing pilot, K=2

	K=2								
	DFE-IDMA			long code DFE-CDMA			short code DFE-CDMA		
Ch. Range(m)	200 m	500 m	1000 m	200 m	500 m	1000 m	200 m	500 m	1000 m
Packet 1	0	0	0	0	0	0	0	0	0
Packet 1	11.0	11.1	11.5	12.0	10.9	12.5	12.5	11.5	12.2
Packet 2	0	0	0	0	0	0	0	0	0
Packet 2	11.7	15.9	12.1	11.0	11.9	13.8	12.1	12.0	14.5
Packet 3	0	0	0	0	0	0	0	0	0
Packet 3	12.8	12.3	14.1	11.7	11.1	10.1	11.8	12.2	13.8
Packet 4	0	0	0	0	0	0	0	0	0
Packet 4	12.2	13.6	13.5	11.7	12.2	14.0	11.9	11.4	13.5
Packet 5	0	0	0	0	0	0	0	0	0
Packet 5	12.6	11.5	13.6	11.9	10.6	13.8	11.0	12.9	13.2
Packet 6	0	0	0	0	0	0	0	0	0
Packet 6	11.4	14.4	13.2	11.8	14.0	13.0	11.1	14.0	11.7
Packet 7	0	0	0	0	0	0	0	0	0
Packet 7	10.7	13.9	14.6	11.9	12.2	13.8	11.0 6	11.0	11.6
Packet 8	0	0	0	0	0	0	0	0	0
Packet 8	11.8	11.5	14.1	10.8	10.6	11.4	11.7	12.2	11.8
Packet 9	0	0	0	0	0	0	0	0	0
Packet 9	11.2	12.1	13.0	11.3	11.5	13.3	10.9	11.7	12.2
Packet 10	0	0	0	0	0	0	0	0	0
Packet 10	12.0	12.4	14.9	11.1	10.4	10.6	10.7	14.3	12.8
Packet 11	0	0	0	0	0	0	0	0	0
Packet 11	12.6	13.7	10.9	11.2	10.1	11.4	12.0	10.7	14.8
Packet 12	0	0	0	0	0	0	0	0	0
Packet 12	11.1	12.6	11.3	10.7	13.6	12.9	11.3	10.7	10.1
Packet 13	0	0	0	0	0	0	0	0	0
Packet 13	12.5	13.7	13.8	10.7	11.8	14.1	12.3	11.1	12.6
Packet 14	0	0	0	0	0	0	0	0	0
Packet 14	12.6	11.3	14.8	11.8	13.1	14.0	11.5	11.8	11.8
Packet 15	0	0	0	0	0	0	1	0	0
Packet 15	11.6	11.5	13.4	11.7	13.3	12.8	11.5	11.1	11.9
Av. BER	0	0	0	0	0	0	1/30690	0	0
Av. SINR	11.9	12.9	13.5	11.5	11.9	12.8	11.6	11.9	12.6

Table 4: Results of DFE-IC based T-MUDs with multiplexing pilot, K=4

	K=4								
	DFE-IDMA			long code DFE-CDMA			short code DFE-CDMA		
Ch. Range(m)	200 m	500 m	1000 m	200 m	500 m	1000 m	200 m	500 m	1000 m
Packet 1	0	0	0	4	0	0	0	0	0
Packet 1	9.6	9.3	10.9	9.1	9.4	11.4	8.9	11.1	10.7
Packet 2	0	0	0	0	0	0	2	0	0
Packet 2	9.3	13.1	10.5	9.5	10.7	10.6	8.9	10.7	10.6
Packet 3	0	0	0	0	0	0	11	0	0
Packet 3	9.2	12.7	9.4	9.1	10.5	9.5	8.8	9.0	11.8
Packet 4	0	0	0	0	0	0	20	0	0
Packet 4	9.6	14.1	10.3	10.9	10.7	9.9	8.9	11.8	11.8
Packet 5	0	0	0	0	0	0	0	0	0
Packet 5	10.5	13.9	9.4	9.9	10.8	10.4	9.2	9.6	10.9
Packet 6	0	0	0	0	0	0	0	0	0
Packet 6	10.7	9.4	12.3	10.2	9.9	9.0	9.7	11.6	11.2
Packet 7	0	0	0	0	19	0	0	0	0
Packet 7	11.0	12.9	11.1	11.4	8.7	11.5	9.2	9.8	9.8
Packet 8	0	0	0	0	0	0	0	0	0
Packet 8	10.0	9.2	13.3	10.4	10.7	9.3	10.8	11.5	11.2
Packet 9	0	0	0	0	0	0	0	0	0
Packet 9	11.0	11.1	10.0	11.4	9.9	10.5	9.7	9.6	10.5
Packet 10	0	0	0	0	0	0	0	0	0
Packet 10	9.7	11.0	10.5	9.4	11.7	10.0	10.2	9.3	9.5
Packet 11	0	0	0	0	0	0	0	0	0
Packet 11	10.0	13. 0	10.5	9.5	11.3	12.1	11.7	13.9	12.7
Packet 12	0	0	0	0	0	0	0	0	0
Packet 12	9.7	12.3	11.7	11.4	10.2	12.3	11.3	9.1	10.6
Packet 13	0	0	0	0	0	0	0	0	0
Packet 13	10.6	9.2	10.8	10.5	9.8	12.4	9.6	10.4	9.4
Packet 14	0	0	0	36	0	0	0	0	17
Packet 14	10.3	9.12	11.4	8.6	10.4	11.3	10.1	9.4	8.6
Packet 15	0	0	0	0	0	0	0	0	0
Packet 15	10.1	11.2	13.7	9.3	10.1	11.2	10.5	10.0	12.7
Av. BER	0	0	0	40/61440	0	0	33/61440	0	17/61440
Av. SINR	10.2	10.6	11.1	10.1	10.4	10.9	9.9	10.5	10.9

Table 5: Results of CE based T-MUDs with continuous pilot, K=3

	K=3								
	IDMA			long code CDMA			short code CDMA		
Ch. Range(m)	200 m	500 m	1000 m	200 m	500 m	1000 m	200 m	500 m	1000 m
Packet 1	4	4	0	27	6	0	0	0	0
Packet 1	5.1	9.5	10.3	5.7	5.7	10.3	5.8	9.6	10.4
Packet 2	78	0	0	97	0	0	0	4	0
Packet 2	5.9	9.4	11.0	5.9	9.1	10.0	6.3	9.1	10.8
Packet 3	12	0	0	522	66	0	0	0	0
Packet 3	6.2	10.7	10.3	5.6	9.2	10.8	6.5	9.3	11.0
Packet 4	694	14	0	159	0	0	0	0	0
Packet 4	4.9	8.8	11.3	5.6	9.0	10.7	6.9	9.6	10.5
Packet 5	8	0	0	841	0	50	0	0	17
Packet 5	6.6	9.7	11.5	5.7	9.1	9.9	6.5	9.4	10.1
Packet 6	0	0	0	27	4	0	0	16	0
Packet 6	9.4	9.4	11.1	6.5	8.8	10.7	6.8	9.1	10.2
Packet 7	0	2	0	4	0	0	0	117	0
Packet 7	6.1	9.1	11.0	6.7	9.2	10.7	7.0	9.1	11.0
Packet 8	0	0	0	0	0	0	0	0	0
Packet 8	10.5	10.5	10.5	6.8	9.5	10.7	7	9.0	10.3
Packet 9	0	6	0	0	0	57	0	10	263
Packet 9	7.1	8.8	11.2	6.4	9.8	9.0	7.3	9.1	8.8
Packet 10	0	0	0	0	2	0	0	0	0
Packet 10	10.0	10.0	10.7	7.0	9.8	10.5	7.4	9.0	10.2
Packet 11	0	0	0	0	0	0	0	0	0
Packet 11	7.1	9.3	10.6	6.9	10.0	10.8	6.9	9.3	10.1
Packet 12	6	35	0	0	0	0	859	0	27
Packet 12	7.2	8.7	10.5	6.7	9.1	10.7	5.0	9.5	9.10
Packet 13	0	0	0	0	4	0	0	2	0
Packet 13	10.1	10.1	11.2	6.6	10.0	10.6	6.6	9.0	10.4
Packet 14	6	8	0	4	2	0	0	0	0
Packet 14	7.3	9.0	11.1	6.6	9.1	9.7	6.9	9.6	10.6
Packet 15	0	6	0	0	0	252	0	2	0
Packet 15	6.5	9.1	11.4	5.9	9.8	9.8	6.8	9.5	11.4
Av. BER	808/46080	75/46080	0	1681/46080	84/46080	359/46080	859/46080	151/46080	307/46080
Av. SINR	7.4	9.8	10.9	6.3	9.8	9.3	6.6	9.3	9.2

Table 6: Results of DFE-IC based T-MUDs with continuous pilot, K=3

	K=3								
	DFE-IDMA			long code DFE-CDMA			short code DFE-CDMA		
Ch. Range(m)	200 m	500 m	1000 m	200 m	500 m	1000 m	200 m	500 m	1000 m
Packet 1	0	0	0	0	0	0	0	0	0
Packet 1	11.4	10.9	8.2	9.7	10.5	10.4	9.8	9.9	8.5
Packet 2	0	0	0	0	0	0	0	0	0
Packet 2	10.0	13.1	12.8	10.2	8.6	12.2	11.1	8.4	10.5
Packet 3	0	0	0	0	0	0	0	0	0
Packet 3	11.3	8.6	8.8	11.5	9.3	9.8	11.0	10.6	13.8
Packet 4	0	0	0	0	0	0	0	0	0
Packet 4	9.7	11.6	11.2	10.5	10.9	11.2	10.0	13.3	13.8
Packet 5	0	0	0	0	0	0	0	0	0
Packet 5	11.9	13.1	10.1	10.5	13.9	8.8	9.2	13.5	8.7
Packet 6	0	0	0	0	0	0	0	0	0
Packet 6	9.6	11.8	11.0	10.5	10.8	12.6	9.5	9.7	12.1
Packet 7	0	0	0	0	2 bits	0	0	0	0
Packet 7	11.7	12.6	9.9	12.0	9.1	11.1	10.5	9.2	11.8
Packet 8	0	0	0	0	0	0	0	0	0
Packet 8	8.7	9.6	9.8	10.8	12.7	12.3	9.1	9.0	9.7
Packet 9	0	0	0	0	0	0	0	0	0
Packet 9	12.6	8.9	8.1	8.5	9.9	12.4	9.8	11.2	10.8
Packet 10	0	0	0	0	0	0	0	0	0
Packet 10	11.0	9.5	11.5	10.0	9.4	8.3	9.5	12.4	9.5
Packet 11	0	0	0	0	0	0	0	0	0
Packet 11	10.1	12.1	8.7	10.1	10.5	12.3	12.7	9.8	13.6
Packet 12	0	0	0	0	0	0	0	0	0
Packet 12	11.2	11.2	10.3	10.0	8.6	12.5	10.9	10.0	10.4
Packet 13	0	0	0	0	0	0	0	0	0
Packet 13	10.1	8.9	10.0	9.1	8.4	10.7	11.1	13.0	9.8
Packet 14	0	0	0	0	0	0	0	0	0
Packet 14	12.0	9.4	11.9	9.7	11.7	12.5	9.0	10.7	9.6
Packet 15	0	0	0	0	0	0	0	0	0
Packet 15	11.7	13.1	12.4	11.8	11.6	8.3	10.9	10.6	13.6
Av. BER	0	0	0	0	2/46080	0	0	0	0
Av. SINR	10.9	11	11.3	10.3	10.4	11.0	10.3	10.7	11.1

Appendix B

B Block diagrams of the system architecture and parallel port

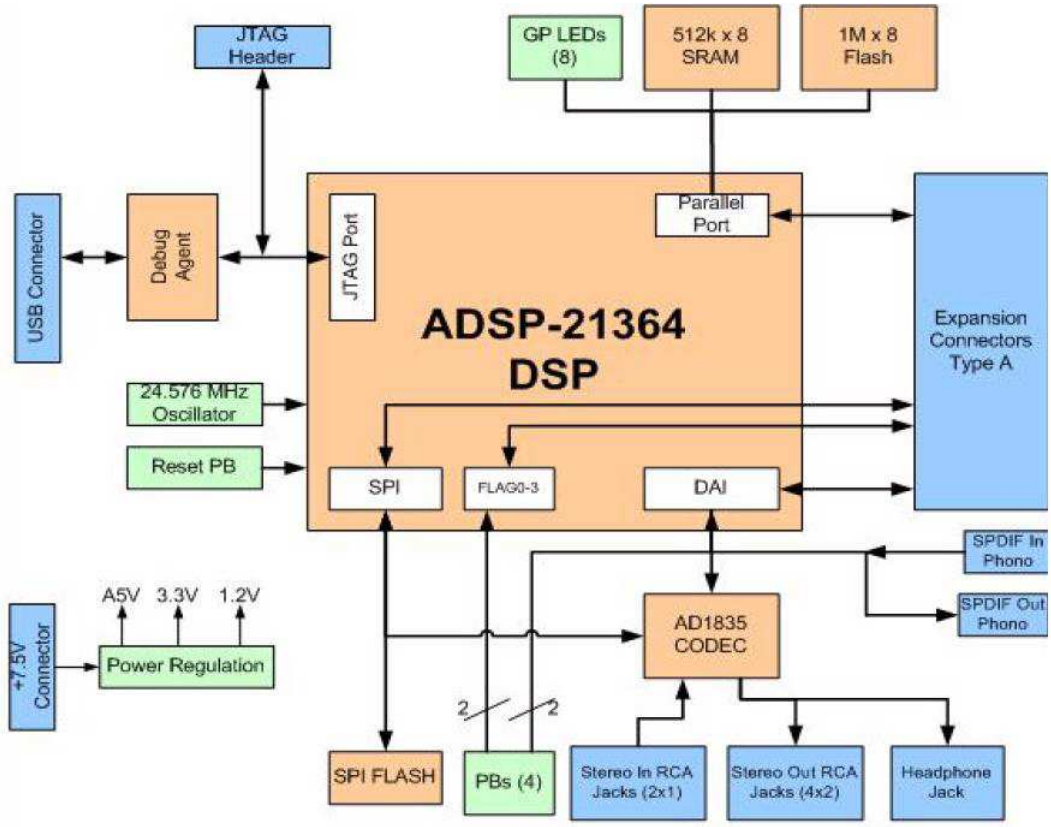

Figure 1: The functional block diagram of the SHARC DSPs.

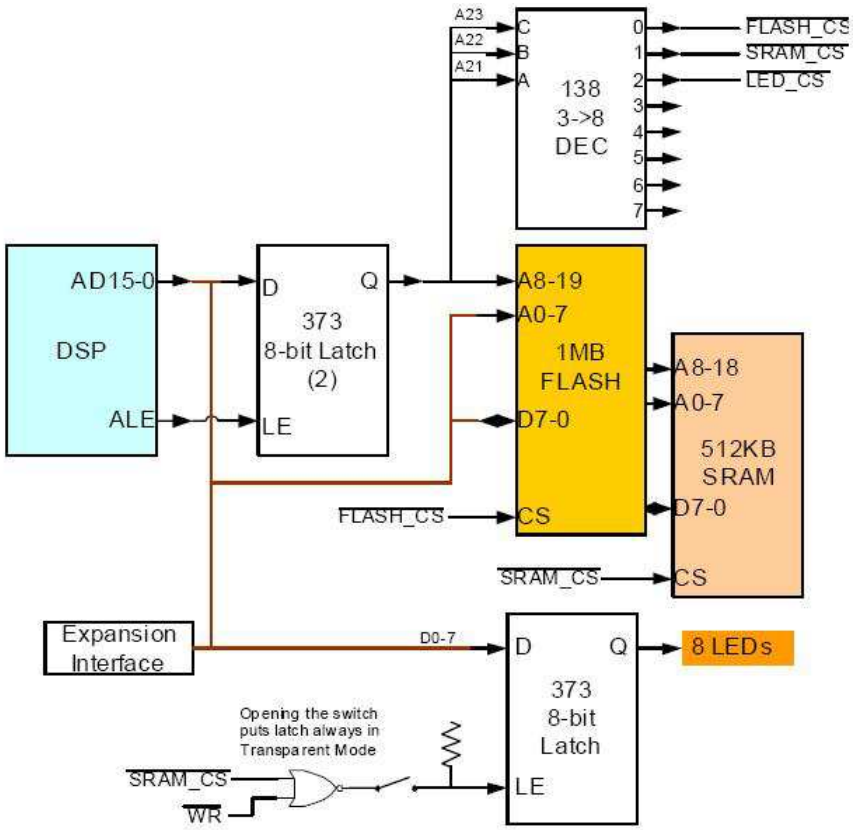

Figure 2: Parallel port of ADSP-21364 processor.

References

[1] M. Stojanovic, J. A. Catipovic, and J. G. Proakis, "Phase-coherent digital communications for underwater acoustic channels," *IEEE J. Ocean Eng.*, vol. 19, pp. 100–111, Jan. 1994.

[2] J. Preisig and D. Brady, "Adaptive equalization for underwater wireless communications," in *Proc. IEEE ICASSP Conf.*, Apr 1996, pp. 1077–1076.

[3] M. Stojanovic and L. Freitag, "Multichannel detection for wideband underwater acoustic CDMA communications," *IEEE J. Ocean Eng.*, vol. 31, pp. 685–695, Jul. 2006.

[4] E. M. Sozer, M. Stojanovic, and J. G. Proakis, "Underwater acoustic networks," *IEEE J. Ocean Eng.*, vol. 25, pp. 72–83, Jan 2000.

[5] M. Stojanovic and L. Freitag, "Hypothesis-feedback equalization for direct-sequence spread-spectrum underwater communications," in *Proc. MTS/IEEE Oceans Conf. and Exhibition*, Sep 2000, pp. 123–129.

[6] P. Frenger, P. Orten, and T. Ottosson, "Code-spread CDMA using maximum free distance low-rate convolutional codes," *IEEE Trans. Wir. Comm.*, vol. 48, pp. 135–144, Jan 2000.

[7] R. H. Mahadevappa and J. G. Proakis, "Mitigating multiple access interference and intersymbol interference in uncoded CDMA systems with chip-level interleaving," *IEEE Trans. Wir. Comm.*, vol. 1, pp. 781–792, Oct 2002.

[8] L. Ping, L. Liu, K. Y. Wu, and W. K. Leung, "Interleave-division multiple-access," *IEEE Trans. Wir. Comm.*, vol. 5, Apr 2006.

[9] X. Wang and H. V. Poor, "Iterative (turbo) soft interference cancellation and decoding for coded CDMA," *IEEE Trans. Comm.*, vol. 47, pp. 1046–1061, Jul 1999.

[10] H. Dapeng and P. A. Hoeher, "Iterative estimation and cancellation of clipping noise for multi-layer IDMA systems," in *7th Inter. Conf. on Source and Channel Coding (SCC)*, Jan 2008, pp. 1–6.

[11] R. Otnes and M. Tuchler, "Iterative channel estimation for turbo equalization of time-varying frequency-selective channels," *IEEE Trans. Wir. Comm.*, vol. 3, p. 19181923, Nov. 2001.

[12] R. Otnes and T. H. Eggen, "Underwater acoustic communications:long-term test of turbo equalization in shallow water," *IEEE J. Ocean Eng.*, vol. 33, p. 321334, Jan. 2008.

[13] C. Frank and E. Visotsky, "Adaptive interference suppression for direct sequence CDMA systems with long spreading codes," in *Proc. Allerton Comm., Control, and Computing Conf.*, Sep 1998.

[14] F. Petre, M. Moonen, M. Engels, B. Gyselinckx, and H. D. Man, "Pilot aided adaptive chip equalizer receiver for interference suppression in DS-CDMA forward link," in *Proc. IEEE Vehicular Tech. Conf.*, Sep 2000, pp. 303–308.

[15] J. Garcia-Frias and J. Villasenor, "Combined turbo detection and decoding for unknown ISI channels," *IEEE Trans. Comm.*, vol. 51, pp. 79– 85, Jan 2003.

[16] S. Song, A. Singer, and K. Sung, "Soft input channel estimation for turbo equalization," *IEEE Trans. on Signal Processing,*, vol. 52, pp. 2885– 2894, Oct 2004.

[17] T. H. Eggen, A. B. Baggeroer, and J. C. Preisig, "Communication over doppler spread channels, part I: Channel and receiver presentation," *IEEE J. Ocean Eng.*, vol. 25, pp. 62–72, Aug 2000.

[18] T. H. Eggen, J. C. Preisig, and A. B. Baggeroer, "Communication over doppler spread channels, part II: Receiver characterization and practical results," *IEEE J. Ocean Eng.*, vol. 26, pp. 612–622, Aug 2001.

[19] W. Li and J. C. Preisig, "Estimation of rapidly time-varying sparse channels," *IEEE J. Ocean Eng.*, vol. 32, pp. 927–939, Oct 2007.

[20] E. Strom and S. Miller., "Iterative demodulation and channel estimation of orthogonal signalling formats in asynchronous DS-CDMA systems," *IEICE Trans. on Electronics*, vol. E85-C, pp. 442–451, Oct 2002.

[21] J. Choi, "Multipath CDMA channel estimation by jointly utilising pilot and traffic channels," in *IEE Proc. on Comm.*, Sep 1999, pp. 312–318.

[22] H. Zhu, B. Farhang-Boroujeny, and C. Schlegel, "Pilot embedding for joint channel estimation and data detection in MIMO communication systems," *IEEE Comm. Letters,*, vol. 7, pp. 30– 32, Jan 2003.

[23] H. Schoeneich and P. A. Hoeher, "Iterative pilot-layer aided channel estimation with emphasis on interleave-division multiple access systems," *EURASIP J. on Applied Signal Processing*, vol. 7, pp. 1–15, Jan 2006.

[24] P. A. Hoeher and H. Schoeneich, "Semi-blind pilot-layer aided channel estimation with emphasis on interleave-division multiple access systems," in *Proc. IEEE GLOBECOM*, Dec 2005, pp. 3513–3517.

[25] X. Zhou, Z. Shi, and M. Reed, "Iterative channel estimation for IDMA systems in time-varying channels," in *IEEE Global Telecomm. (GLOBECOM) Conf.*, Nov 2007, pp. 4020–4024.

[26] S. Tomasin and N. Benvenuto, "Frequency domain interference cancellation and nonlinear equalization for CDMA systems," *IEEE Trans. Wir. Comm.*, vol. 4, pp. 2329–2339, Sep 2005.

[27] M. Baissas and A. Sayeed, "Pilot-based estimation of time-varying multipath channels for coherent CDMA receivers," *IEEE Signal Proc. Trans.*, vol. 50, pp. 2037–2049, Aug 2002.

[28] F. Blackmon, E. Sozer, M. Stojanovic, and J. Proakis, "Performance comparison of Rake and hypothesis feedback direct sequence spread spectrum techniques for underwater communication applications," in *Oceans'02 MTS/IEEE Conf.*, Oct 2002, pp. 594– 603.

[29] M. Abdulrahman, A. Sheikh, and D. Falconer, "Decision feedback equalization for CDMA in indoor wireless communications," *IEEE J. Sel. Areas Comm.*, vol. 12, pp. 698–706, May 1994.

[30] M. Stojanovic and L. Freitag, "MMSE acquisition of DSSS acoustic communications signals," in *Proc. of MTS/IEEE Oceans 04*, 2004.

[31] H. Jianguo, H. Jing, and S. Wei, "A multiuser chip-rate equalization algorithm for CDMA underwater communication systems," in *IET Wir., Mobile and Sensor Networks Conf.*, Dec 2007, pp. 1009–1012.

[32] M. Stojanovic and L. Freitag, "Hypothesis-feedback equalization for direct-sequence spread-spectrum underwater communications," in *Proc. IEEE OCEANS*, 2004.

[33] S. ten Brink, "Convergence of iterative decoding," *Electron. Lett.*, vol. 35, pp. 1117– 1118, Jun 1999.

[34] M. Tuchler, R. Koetter, and A. Singer, "Turbo equalization: Principles and new results," *IEEE Trans. on Comm.*, vol. 50, pp. 754–767, May 2002.

[35] R. Otnes and M. Tchler, "EXIT chart analysis applied to adaptive turbo equalization," in *Proc. IEEE 5th Nordic Signal Processing Symp.*, Oct 2002.

[36] K. Li and X. Wang, "EXIT chart analysis of turbo multiuser detection," *IEEE Trans. Wir. Comm.*, vol. 4, pp. 300– 311, Jan 2005.

[37] M. Chitre, S. hahabudeen, L. Freitag, and M. Stojanovic, "Recent advances in underwater acoustic communications and networking," in *Proc. IEEE Oceans Conf.*, Sep 2008, pp. 15–18.

[38] J. Catipovic, M. Johnson, and D. Adams, "Noise cancelling performance of an adaptive receiver for underwater communications," in *Proc. Autonomous Underwater Vehicle Tech. AUV '94. Sym.*, July 1994, pp. 171–178.

[39] W. C. Jun, T. J. Riedl, K. Kyeongyeon, A. Singer, and J. Preisig, "Practical application of turbo equalization to underwater acoustic communications," in *Proc. IEEE 7th Inter. Sym. on Wir. Comm. Systems (ISWCS)*, Sep 2010, pp. 601–605.

[40] C. Shah, C. Tsimenidis, B. Sharif, and J. Neasham, "Low-complexity iterative receiver structure for time-varying frequency-selective shallow underwater acoustic channels using BICM-ID: Design and experimental results," *IEEE J. Ocean. Eng.*, vol. 36, pp. 406–421, July 2011.

[41] H. K. Yeo, B. S. Sharif, A. E. Adams, and O. R. Hinton, "Implementation of multiuser detection strategies for coherent underwater acoustic communication," *IEEE J. Ocean. Eng.*, vol. 27, pp. 17–27, Jan 2002.

[42] Z. Zvonar, D. Brady, and J. Catipovic, "Adaptive detection for shallow-water acoustic telemetry with cochannel interference," *IEEE J. Ocean Eng.*, vol. 21, pp. 528–536, 1996.

[43] G. Loubet, V. Capellano, and R. Filipiak, "Underwater spread spectrum communications," in *Proc. IEEE Oceans Conf.*, Sep 1997, pp. 574–579.

[44] L. Linton, P. Conder, and M. Faulkner, "Multiuser communications for underwater acoustic networks using MIMO-OFDM-IDMA," in *Proc. Inter. Conf. on Signal Processing and Comm. Sys. (ICSPCS)*, Dec 2008, pp. 1–8.

[45] E. Hardouin and C. Laot, "Iterative channel equalization for the multicode DS-CDMA downlink," in *Proc. 57th IEEE Veh. Tech. Conf. VTC*, April 2003, pp. 1857–1861.

[46] S. Aliesawi, C. Tsimenidis, B. Sharif, and M. Johnston, "Iterative multiuser detection for underwater acoustic channels," *IEEE J. Ocean Eng.*, vol. 36, pp. 728–744, Oct 2011.

[47] ——, "Adaptive channel estimation for synchronous coded IDMA and CDMA underwater communication systems," *American J. of Eng. and App. Sciences*, vol. 5(1), pp. 15–24, Feb 2012.

[48] ——, "Efficient channel estimation for chip multiuser detection on underwater acoustic channels," in *Proc. IEEE 7th Inter. Symp. on Comm. Sys. Networks and Digital Signal Processing (CSNDSP)*, July 2010, pp. 173–177.

[49] S. Aliesawi, C. Tsimenidis, B. Sharif, M. Johnston, and O. Hinton, "Adaptive multiuser detection with decision feedback equalization based IDMA systems on underwater acoustic channels," in *Proc. European Conf. on Underwater Acoustics (ECUA2011)*, July 2010, pp. 1–8.

[50] S. Aliesawi, C. Tsimenidis, B. Sharif, and M. Johnston, "Performance comparison of IDMA receivers for underwater acoustic channels," in *Proc. IEEE 7th Inter. Symp. on Wir. Comm. Sys. (ISWCS)*, Sep 2010, pp. 596–600.

[51] ——, "Soft Rake and DFE based IDMA systems for underwater acoustic channels," in *Proc. Sensor Signal Processing for Defence (SSPD2010)*, Sep 2010, pp. 1–5.

[52] ——, "Continuous pilot based adaptive estimation for IDMA systems on underwater acoustic channels," in *Proc. IEEE 2011 Inter. Conf. on Acoustic, Speech and Signal processing (ICASSP)*, May 2011, pp. 3476–3479.

[53] S. Aliesawi, C. Tsimenidis, and B. Sharif, "Turbo multiuser detectors for IDMA-based underwater communications," in *Proc. IEEE 7th Inter. Workshop on Sys., Signal Processing and their Applications (WOSSPA)*, May 2011, pp. 339–342.

[54] S. Aliesawi, C. Tsimenidis, B. Sharif, and M. Johnston, "Different adaptive CDMA forms with continuous pilot over long-spread fading channels," in *Proc. 4th Inter. Conf. on Underwater Acoustic Measurements (UAM)*, June 2011, pp. 1391–1396.

[55] ——, "Performance assessment and EXIT chart analysis of IDMA-based underwater communications," in *Proc. IEEE/OES of OCEANS 2011*, June 2011, pp. 596–600.

[56] J. C. Preisig and G. B.Deane, "Surface wave focusing and acoustic communications in the surf zone," *J. of Acoustical Society of America*, vol. 116(3), pp. 2067–2080, Sep 2004.

[57] A. F. Harris and M. Zorzi, "Modeling the underwater acoustic channel in NS2," in *Proc. 2nd Inter. Conf. on Performance evaluation methodologies and tools*, 2007, pp. 18:1–18:8.

[58] R. Urick, *Principles of Underwater Sound*. McGraw Hill, 3rd edition, 1983.

[59] M. Stojanovic and J. Preisig, "Underwater acoustic communication channels: propagation models and statistical characterization," *IEEE Commun. Mag.*, vol. 47, pp. 84–89, Jan 2009.

[60] J. G. Proakis, *Digital Communications*. McGraw Hill, Fourth edition, 2001.

[61] D. B. Kilfoyle and A. Baggeroer, "The state of the art in underwater acoustic telemetry," *IEEE J. Ocean Eng.*, vol. 25, No. 1, pp. 4–27, Jan 2000.

[62] B. S. Sharif, J. Neasham, O. Hinton, and A. E. Adams, "A computationally efficient doppler compensation system for underwater acoustic communications," *IEEE J. Ocean Eng.*, vol. 25, No. 1, pp. 52–61, Jan 2000.

[63] M. Stojanovic, J. Proarkis, J. Rice, and M. Green, "Spread spectrum underwater acoustic telemetry," in *Proc. IEEE Oceans Conf.*, Oct 1998, pp. 650–654.

[64] N. Nasri, A. Kachouri, L. Andrieux, and M. Samet, "Design considerations for wireless underwater communication transceiver," in *Proc. IEEE Inter. Conf. on Signals, Circuits and Systems*, Nov 2008, pp. 1–5.

[65] M. L. Moher, "An iterative multiuser decoder for near-capacity communications," *IEEE Trans. Comm.*, vol. 46, pp. 870–880, Jul 1998.

[66] S. Verdu, *Multiuser Detection*. Cambridge, U.K.: Cambridge Univ. Press, 1998.

[67] Z. Shidong, L. Yunzhou, Z. Ming, X. Xibin, W. Jing, and Y. Yan, "Novel techniques to improve downlink multiple access capacity for beyond 3G," *IEEE Comm. Mag.*, vol. 43, pp. 61–69, Jan 2005.

[68] I. Pupeza, A. Kavcic, and L. Ping., "Efficient generation of interleavers for IDMA," in *IEEE Proc. ICC Conf. on Comm.*, June 2006, pp. 1508–1513.

[69] C. Zhang and J. Hu, "2-dimension interleaver design for IDMA systems," in *Proc. IEEE Conf. on Circuits and Sys. for Comm.*, May 2008, pp. 372–376.

[70] H. Wu, L. Ping, and A. Perotti, "User-specific chip-level interleaver design for IDMA systems," *IEE Electron. Letter*, vol. 42, pp. 233–234, Feb 2006.

[71] L. Ping, L. Liu, and W. K. Leung, "A simple approach to near optimal multiuser detection: Interleave-division multiple-access," in *IEEE Proc. Wir. Comm. and Net. Conf. (WCNC2003)*, Mar 2003, pp. 391–396.

[72] P. Robertson, E. Villebrun, and P. Hoeher, "A comparison of optimal and sub-optimal map decoding algorithms operating in the log domain," in *IEEE Proc. ICC*, Jun 1995, pp. 1009–1013.

[73] Q. Huang, K. Ko, P. Wang, L. Ping, and S. Chan, "Interleave-division multiple-access based broadband wireless networks," in *IEEE Infor. Theory Workshop*, Oct 2006, pp. 502–506.

[74] C.C.Tsimedidis, "Adaptive array receiver algorithms for DS/CDMA communications through double-spread fading channels," *Newcastle University Ph.D. thesis*, Sep 1998.

[75] L. Ping, L. Liu, K. Wu, and W. Leung, "Interleave division multiple (IDMA) communication systems," in *Proc. 3rd Inter. Symp. on Turbo Codes Related Topics*, Sep 2003, pp. 173–180.

[76] L. Liahai, "Interleave division multiple access," in *Ph.D. thesis, City University of Hong Kong*, Dec 2005.

[77] S. Moshavi, "Multi-user detection for DS-CDMA communications," *IEEE comm. Mag.*, vol. 34, pp. 124–136, Oct 1996.

[78] D.Divsalar, M. Simon, and D. Raphaeli, "Improved parallel interference cancellation for CDMA," *IEEE Trans. Comm.*, vol. 46, pp. 258–268, Feb 1998.

[79] B. Widrow, J. McCool, and M. Ball, "The complex LMS algorithm," in *Proc. IEEE*, Apr 1975, pp. 719– 720.

[80] B. Widrow, J. McCool, M. Larimore, and C. J. Johnson, "Stationary and non-stationary learning characteristics of the LMS adaptive filter," in *Proc. IEEE*, Aug 1976, pp. 1151– 1162.

[81] S. Haykin, *Adaptive Filter Theory*. Englewood Cliffs, NJ: Prentice Hall, 1996.

[82] M. Stojanovic and Z.Zvonar, "Multichannel processing of broad-band multiuser communication signals in shallow water acoustic channels," *IEEE J. Ocean Eng.*, vol. 21, pp. 156–166, Apr 1996.

[83] N. Oliver, C. R. Mark, and S. Zhenning, "Performance analysis of a generic system model for uncoded IDMA using serial and parallel interference cancellation," *European Trans. on Telecomm.*, vol. 19, pp. 511–522, Jan 2008.

[84] C. Laot, A. Glavieux, and J. Labat, "Turbo equalization: adaptive equalization and channel decoding jointly optimized," *IEEE J. on Sel. Areas in Comm.*, vol. 19, pp. 1744–1752, Sep 2001.

[85] R. Otnes, "Improved receivers for digital high frequency communications: Iterative channel estimation, equalization, and decoding (adaptive turbo equalization)," *Ph.D. thesis, Norwegian University Science and Technology, Trondheim, Norway*, Dec 2002.

[86] G. S. M. Kerpen, "Data-aided equalization using receivers with a restricted decoding-delay," *Ph.D. thesis, Eindhoven University of Technology, Netherlands*, Oct 1987.

[87] L. Ping, "Interleave-division multiple access and chip-by-chip iterative multi-user detection," *IEEE Radio Comm. Mag.*, vol. 43, pp. S19–S23, Jun 2005.

[88] X. X. J. Hu, "A simplified downlink transmission and receiving scheme for IDMA," in *Inter. Conf. on Comm., Circuits and Sys. , ICCCAS 2008*, May 2008, pp. 157–161.

[89] L. R. Bahl, J. Cocke, F. jelinek, and J. Raviv, "Optimal decoding of linear codes for minimizing symbol error rate," *IEEE Trans. on Info Theory*, vol. 20, pp. 284–287, Mar 1974.

[90] K. Kusume and G. Bauch, "A simple complexity reduction strategy for interleave division multiple access," in *Proc., 64th IEEE Veh. Tech. Conf. (VTC'06)*, Montreal, Canada, Sep 2006, pp. 1–5.

[91] L. Mailaender and J. Proakis, "Linear-aided decision-feedback equalization for the CDMA downlink," in *Signals, Sys. and Computers Conf.*, Nov 2003, pp. 131– 135.

[92] A. Margetts and P. Schniter, "Chip-rate adaptive two-stage receiver for scrambled multirate CDMA downlink," in *Signals, Sys. and Computers Conf.*, Nov 2003, pp. 465– 469.

[93] J. Rossler, L. Lampe, W. Gerstacker, and J. Huber, "Decision-feedback equalization for CDMA downlink," in *IEEE Veh. Tech. Conf.*, Nov 2002, pp. 816–820.

[94] Y. Jingnong and Y. Li, "A decision-feedback equalizer with tentative chip feedback for the downlink of wideband CDMA," in *IEEE Inter. Conf. on Comm. ICC 2002*, Nov 2002, pp. 119–123.

[95] L. W. K. Raymond, "Concatenated error control codes and their applications in telecommunication systems," *Ph.D. thesis, City University of Hong Kong*, Jul 2004.

[96] M. Stojanovic and L. Freitag, "Multiuser undersea acoustic communications in the presence of multipath propagation," in *IEEE Oceans Conf.*, Montreal, Canada, Nov 2001, pp. 2165–2169.

[97] K. Li and X. Wang, "Convergence behavior of iteratively decoded parallel concatenated codes," *IEEE Trans. Comm.*, vol. 49, pp. 1727–1737, Oct 2001.

[98] M. Tuchler and J. Hagenauer, "EXIT charts of irregular codes," in *Proc. CISS, Princeton University*, NJ, USA, Mar 2002, pp. 748–753.

[99] A. D. Inc., "Data sheet of SHARC processor," Tech. Rep., March 2011. [Online]. Available: http://www.analog.com/en/processors-dsp/sharc/processors/index.html

[100] ——, "ADSP-21364 EZ-KIT lite evaluation system manual," Tech. Rep., July 2007. [Online]. Available: http://www.analog.com/en/processors-dsp/sharc/processors/index.html